

TECHNICAL REPORT STANDARD PAGE

1. Report No. FHWA/LA.04/385		2. Government Accession No.	3. Recipient's Catalog No.
4. Title and Subtitle ASSESSMENT OF IN-SITU TEST TECHNOLOGY FOR CONSTRUCTION CONTROL OF BASE COURSES AND EMBANKMENTS		5. Report Date May 2004	
		6. Performing Organization Code	
7. Author(s) Murad Y. Abu-Farsakh, Ph.D., P.E., Khalid Alshibli, Ph.D., P.E, Munir Nazzal, and Ekrem Seyman		8. Performing Organization Report No. 385	
9. Performing Organization Name and Address Louisiana Transportation Research Center 4101 Gourrier Avenue Baton Rouge, LA 70808		10. Work Unit No.	
		11. Contract or Grant No. 02-1GT	
12. Sponsoring Agency Name and Address Louisiana Transportation Research Center 4101 Gourrier Avenue Baton Rouge, LA 70808		13. Type of Report and Period Covered Final Report July 2001 – December 2003	
		14. Sponsoring Agency Code	
15. Supplementary Notes Conducted in Cooperation with the U.S. Department of Transportation, Federal Highway Administration			
16. Abstract <p>With the coming move from an empirical to mechanistic-empirical pavement design, it is essential to improve the quality control/quality assurance (Q_C/Q_A) procedures of compacted materials from a density-based criterion to a stiffness/strength-based criterion. The non-destructive in-situ tests such as the Geogauge, Dynamic Cone Penetrometer (DCP), and Light Falling Weight Deflectometer (LFWD) can be effective tools for assessing of subsurface conditions and evaluating the stiffness of pavement materials and embankments. This report evaluates the potential of these three devices to reliably measure the stiffness characteristics of highway materials for possible application in the Q_C/Q_A procedures during and after the construction of pavement layers and embankments. To achieve this, field and laboratory testing programs were conducted. The laboratory program included construction of different sections inside two boxes (5×3×2.5 ft.) located at the Geosynthetic Engineering Research Laboratory (GERL) at the Louisiana Transportation Research Center (LTRC). The field tests were conducted on highway sections selected from various projects in Louisiana. In addition, six test sections and three trench sections were constructed and tested at the LTRC Pavement Research Facility (PRF) site. The field and laboratory tests included Geogauge, LFWD, and DCP tests in conjunction with two standard tests such as the Plate Load Test (PLT) and Falling Weight Deflectometer (FWD) test. The California Bearing Ratio (CBR) laboratory tests were also conducted on similar samples collected during the field and laboratory tests. A statistical analysis revealed good correlations between the measurements obtained from the three investigated devices and those obtained from the standard tests, thus demonstrating that the investigated devices can reliably measure the in-situ stiffness of highway materials, subgrades and embankments.</p>			
17. Key Words Geogauge, DCP, LFWD, FWD, PLT, Elastic modulus, CBR, Laboratory tests, Field tests, Compacted soils, Subgrades, Base courses.		18. Distribution Statement Unrestricted. This document is available through the National Technical Information Service, Springfield, VA 21161.	
19. Security Classif. (of this report) Unclassified	20. Security Classif. (of this page) Unclassified	21. No. of Pages 126	22. Price

**ASSESSMENT OF IN-SITU TEST TECHNOLOGY FOR CONSTRUCTION
CONTROL OF BASE COURSES AND EMBANKMENTS**

by

Murad Y. Abu-Farsakh, Ph.D., P.E.

**Louisiana Transportation Research Center
4101 Gourrier Avenue
Baton Rouge, LA 70808**

Khalid Alshibli, Ph.D., P.E.

**Department of Civil Engineering
Louisiana State University and Southern University
Baton Rouge, LA**

Munir D. Nazzal, E.I.

**Department of Civil Engineering
Louisiana State University
Baton Rouge, LA**

and

Ekrem Seyman, E.I.

**Department of Civil Engineering
Louisiana State University
Baton Rouge, LA**

**LTRC Project No. 02-1GT
State Project No. 736-02-0995**

Conducted for

**Louisiana Department of Transportation and Development
Louisiana Transportation Research Center**

The contents of this report reflect the views of the author/principal investigator who is responsible for the facts and the accuracy of the data presented herein. The contents do not necessarily reflect the views or policies of the Louisiana Department of Transportation and Development or the Louisiana Transportation Research Center. This report does not constitute a standard, specification, or regulation.

May, 2004

ABSTRACT

With the coming move from an empirical to mechanistic-empirical pavement design, it is essential to improve the quality control/quality assurance (QC/QA) procedures for compacted materials from a density-based criterion to a stiffness/strength-based criterion. The non-destructive in-situ tests such as the Geogauge, Dynamic Cone Penetrometer (DCP), and Light Falling Weight Deflectometer (LFWD) can be effective tools for assessing of subsurface conditions and evaluating the stiffness of pavement materials and embankments. This report evaluates the potential of these three devices to reliably measure the stiffness characteristics of highway materials for possible application in the QC/QA procedures during and after the construction of pavement layers and embankments. To achieve this, field and laboratory testing programs were conducted. The laboratory program included construction of different sections inside two boxes (5 × 3 × 2.5 ft.) located at the Geosynthetic Engineering Research Laboratory (GERL) at the Louisiana Transportation Research Center (LTRC). The field tests were conducted on highway sections selected from various projects in Louisiana. In addition, six test sections and three trench sections were constructed and tested at the LTRC Pavement Research Facility (PRF) site. The field and laboratory tests included Geogauge, LFWD, and DCP tests in conjunction with two standard tests such as the Plate Load Test (PLT) and Falling Weight Deflectometer (FWD) test. The California Bearing Ratio (CBR) laboratory tests were also conducted on similar samples collected during the field and laboratory tests. A statistical analysis revealed good correlations between the measurements obtained from the three investigated devices and those obtained from the standard tests, thus demonstrating that the investigated devices can reliably measure the in-situ stiffness of highway materials, subgrades and embankments.

ACKNOWLEDGMENTS

This research project was funded by the Louisiana Transportation Research Center (LTRC Project No. 02-1GT) and the Louisiana Department of Transportation and Development (State Project No. 736-02-0995). The comments and suggestions of Mark Morvant, Pavement and Geotechnical Administrator, are gratefully acknowledged. The authors would also like to thank Zhongjie Zhang and Gavin Gautreau for providing valuable help in this study.

IMPLEMENTATION STATEMENT

The results of this study indicated that the Geogauge, Light Falling Weight Deflectometer (LFWD) and the Dynamic Cone Penetrometer (DCP) devices can be used to reliably measure the in-situ stiffness modulus of pavement layers, subgrades, and embankments. These devices can be implemented in future mechanistic pavement design. However, the use of these devices in the Q_C/Q_A procedures during the construction of compacted materials is not ready for implementation because the concept of using stiffness as acceptance criteria is not yet established. The stiffness of a compacted layer is sensitive to the moisture content during compaction, drying of the material, and strength gain with time for cement and lime-treated soils. The current construction procedure requires compacting at the optimum moisture content \pm two percent as obtained from the laboratory standard Proctor test. However, the results of this study indicated that the variation of stiffness within this range was greater than the variation in the dry density. Consequently, with the current construction procedures, the use of stiffness as acceptance criteria is not recommended at this time. Further study to investigate the effect of moisture content variation on the stiffness measurements of these devices is needed before implementation. This should include laboratory and field tests to establish a moisture-density and strength/stiffness profiles for materials expected to be used for construction.

The investigated devices have some limitations when measuring the in-situ stiffness for different compacted materials. For example, it was observed that the potential cracks of cement-treated and lime-treated soils affected the Geogauge measurements. However, in practice, acceptance of these soils is based on measurements conducted immediately after construction (i.e., before cracks develop). Therefore, future implementation of the Geogauge on these soils should focus on correlating its measurements with unconfined compressive strength of the soil with time. The LFWD showed wide scatter and poor repeatability when testing weak subgrade layers; therefore, it is not recommended for use in weak soils. In addition, the LFWD's depth of influence was estimated to be 11 to 12 inches, which can be greater than the thickness of compacted layer. Thus, the LFWD measurement would not reflect the true modulus for the tested layer, so the LFWD modulus would have to be back-calculated. Therefore, it is recommended to use more than one geophone sensors in the LFWD. The DCP has proven to be an excellent and reliable device to evaluate the strength/stiffness of tested materials. It is inexpensive, easy to use, and can provide a continuous profile of stiffness modulus with depth. Therefore, we strongly recommend

using this device to assess the compacted highway materials as a first step for future implementation in the Q_C/Q_A procedure.

Based on the results of this study, we recommend that the Louisiana Department of Transportation and Development (DOTD) implement these devices in two phases:

1) Phase I:

- a. Start verification of the DCP device for the quality acceptance of stone bases such that $PR < 10$ mm/blow, where PR is the penetration ratio.
- b. Start conducting field measurements using the investigated devices (particularly the DCP) along with dry density/water content measurements using the nuclear density gauge. Continue the comparison between the measurements of these devices and other in-situ measurements, such as the FWD, until enough confidence is gained. The collected data will be used to verify the models developed in this study. This phase will also serve as a training experience for DOTD engineers and technicians, ensuring a smooth statewide implementation during Phase II. A parallel study should be conducted to establish the moisture-density and strength/stiffness relations for different construction materials.

2) Phase II:

Based on the results of Phase I, specific measurement ranges should be recommended for various soils used to construct base course and embankments in Louisiana.

TABLE OF CONTENTS

ABSTRACT	iii
ACKNOWLEDGMENTS	vii
IMPLEMENTATION STATEMENT	vi
TABLE OF CONTENTS	ix
LIST OF TABLES	xi
LIST OF FIGURES	xiii
INTRODUCTION	1
OBJECTIVE	3
SCOPE	5
METHODOLOGY	7
Background	7
Soil Stiffness Gauge (Geogauge).....	7
Dynamic Cone Penetrometer (DCP).....	9
Light Falling Weight Deflectometer (LFWD).....	14
Falling Weight Deflectometer (FWD).....	17
Static Plate Load Test (PLT)	20
California Bearing Ratio (CBR)	22
Testing Program.....	24
Laboratory Tests	24
Field Tests.....	40
ANALYSIS OF RESULTS	73
Analysis of Laboratory Test Results.....	73
Analysis of the Cement-soil.....	73
Moisture Effect Test Results.....	75
Analysis of Field Test Results	82
Analysis of Base Test Sections at PRF Site.....	82
Trench Test Sections.....	86
Repeatability of Geogauge and LFWD for Field Tests	92
Moduli Correlations.....	94
Geogauge Correlations	94
LFWD Correlations	99
DCP Correlations.....	106
CONCLUSIONS.....	115
Geogauge	115
LFWD	116
DCP.....	117
RECOMMENDATIONS	119
REFERENCES	121
APPENDIX.....	125

LIST OF TABLES

Table 1	Poisson Ratios for different materials [4].....	8
Table 2	Geogauge and FWD suggested values to characterize base layer.....	9
Table 3	Values of B [19].....	13
Table 4	Limiting DCP penetration rates by MNDOT [23].....	14
Table 5	Testing program for the laboratory investigation.....	25
Table 6	Gradations (percent passing) and classifications for coarse grained materials.....	26
Table 7	Classification of the fine grained materials used in the laboratory investigation.....	27
Table 8	Dry density and moisture content measurement of US 190.....	42
Table 9	Dry density and moisture content measurements at highway LA 182.....	45
Table 10	Geogauge test results.....	57
Table 11	Descriptive Statistics of the Geogauge Results.....	58
Table 12	LFWD test results.....	59
Table 13	Descriptive statistics of the LFWD results.....	60
Table 14	DCP test results.....	61
Table 15	Plate load test and CBR test results.....	62
Table 16	Summary of test results on highway sections.....	63
Table 17	Geogauge, LFWD, and nuclear density gauge test results for PRF clayey silt section.....	64
Table 18	Summary of DCP result for three layers after 6 passes.....	64
Table 19	Geogauge, LFWD, and nuclear gauge test results with number of passes for cement-soil section (1).....	64
Table 20	Test results with number of passes for cement-soil section (1).....	65
Table 21	Geogauge and LFWD test results with time for cement-soil section (1).....	65
Table 22	DCP test results with time for cement-soil section (1).....	65
Table 23	DCP test results with number of passes for cement-soil section (2).....	66
Table 24	Test results with number of passes for cement-soil section (2).....	66
Table 25	Geogauge and LFWD test results with time for cement-soil section (2).....	66
Table 26	DCP test results with time for cement-soil section (2).....	67
Table 27	DCP test results after six passes for lime-treated soil section.....	67
Table 28	Geogauge, LFWD, and nuclear gauge test results with number of passes for lime-treated soil section.....	67
Table 29	Geogauge, LFWD test results with time for lime-treated soil section.....	68
Table 30	DCP Test results with time for lime-treated soil section.....	68
Table 31	Geogauge, LFWD, and nuclear gauge test results with number of passes for crushed limestone section.....	68
Table 32	DCP results after construction of crushed limestone section.....	69
Table 33	DCP test results after six passes for BCS section.....	69
Table 34	Geogauge, LFWD, and nuclear gauge test results with number of passes for BCS section.....	69
Table 35	Geogauge and LFWD with time for BCS section.....	69
Table 36	DCP Test results with time for BCS section.....	70

Table 37	Geogauge, LFWD, DCP, and nuclear gauge test results for crushed limestone trench	70
Table 38	Geogauge, LFWD, DCP and nuclear gauge test results for sand trench	71
Table 39	Geogauge, LFWD, DCP, and nuclear gauge test results for RAP trench	71
Table 40	Results for test on clayey silt soil	75
Table 41	Results for tests on sandy lean clay soil	76

LIST OF FIGURES

Figure 1	Geogauge device	8
Figure 2	Dynamic Cone Penetrometer (DCP)	11
Figure 3	Prima 100 Light Falling Weight Deflectometer	16
Figure 4	Screen of Prima 100 software	16
Figure 5	Dynatest model 8000 (FWD) (LTRC 2000)	18
Figure 6	Definition of modulus from PLT	20
Figure 7	Proctor curves for (a) clayey silt, and (b) clay soils	28
Figure 8	One of the two LTRC test boxes used for test case preparation	29
Figure 9	(a) Crusher and pulverizer, and (b) mixing the pulverized soil with water	30
Figure 10	The Geogauge device and the use of sand for proper seating	32
Figure 11	Layout of the Geogauge and the Light Falling Weight Deflectometer tests	32
Figure 12	(a) LFWD device, and (b) DCP device	34
Figure 13	Layout of the DCP test, PLT and the nuclear density gauge readings	35
Figure 14	Sample profiles of DCP tests	35
Figure 15	Plate load test setup	36
Figure 16	Typical Plate load test results	36
Figure 17	Determination of CBR for desired dry unit weight	38
Figure 18	Test box in which the experiments were conducted	39
Figure 19	Mold constructed within soil in test box	39
Figure 20	Layout of field test measurements	41
Figure 21	Gradation for the crushed limestone tested at US 190	41
Figure 22	Layout and profile for sections at US highway 190	42
Figure 23	Cross-section of tests at highway LA 182	44
Figure 24	Cross-section PRF site Sections	46
Figure 25	Proctor curve for clayey silt soil used in PRF sections	47
Figure 26	Different section constructed at PRF Site	47
Figure 27	Conducting tests on cement-soil and crushed limestone sections at PRF site	48
Figure 28	Construction of PRF sections	48
Figure 29	Gradation of tested material at the crushed limestone section	49
Figure 30	Gradation of BCS	50
Figure 31	Layout and cross section for PRF trench sections	51
Figure 32	Construction of trenches at PRF site	52
Figure 33	Compaction of trenches at PRF site	52
Figure 34	Testing RAP and sand trenches at PRF site	52
Figure 35	Gradation of crushed limestone	53
Figure 36	Gradation of sand	53
Figure 37	Gradation of RAP	54
Figure 38	United machine used to conduct CBR test	54
Figure 39	E_G with time for cement-soil	74
Figure 40	DCP average PR (8 inch) with time for cement-soil	74
Figure 41	E_{LFWD} with time for cement-soil	75

Figure 42	Geogauge stiffness modulus and dry unit weight curves (clayey silt soil)	77
Figure 43	Geogauge stiffness modulus and dry unit weight curves (sandy lean clay).....	77
Figure 44	Geogauge stiffness modulus curve for BCS layer versus thickness	79
Figure 45	LFWD stiffness modulus curve for BCS layer versus thickness	79
Figure 46	Geogauge stiffness modulus curve for sand layer versus thickness.....	80
Figure 47	Geogauge stiffness modulus curve for clay layer versus thickness	80
Figure 48	LFWD stiffness modulus curve for clay layer versus thickness	81
Figure 49	Geogauge modulus variation with number of passes	83
Figure 50	Geogauge modulus variation with number of passes	83
Figure 51	Geogauge modulus variations with time	84
Figure 52	Rainfall record during testing time.....	84
Figure 53	E_{LFWD} variation with number of passes	85
Figure 54	E_{LFWD} variation with time	86
Figure 55	DCP-PR with time for cement soil section (1).....	87
Figure 56	DCP-PR with time for cement soil section (2).....	88
Figure 57	DCP-PR with time for lime-treated soil section.....	88
Figure 58	DCP-PR with time for BCS section	89
Figure 59	E_G and dry unit weight for different trenches.....	89
Figure 60	E_{LFWD} and dry unit weight for different trenches	90
Figure 61	DCP-PR profiles for crushed limestone trench sections	90
Figure 62	DCP-PR profiles for RAP trench sections	91
Figure 63	DCP-PR profiles for sand trench sections.....	91
Figure 64	C_v variation with LFWD modulus.....	93
Figure 65	Correlation between E_G and the $E_{PLT(i)}$ (laboratory test).....	95
Figure 66	Correlation between E_G and the $E_{PLT(R2)}$ (laboratory test)	95
Figure 67	Correlation between E_G and the $E_{PLT(i)}$ (field test).....	96
Figure 68	Correlation between E_G and the $E_{PLT(R2)}$ (field test)	96
Figure 69	Comparison between laboratory and field for $E_G - E_{PLT(i)}$ correlation.....	97
Figure 70	Comparison between laboratory and field for $E_G - E_{PLT(R2)}$ correlation	97
Figure 71	Correlation between E_G and the M_{FWD}	98
Figure 72	Correlation between E_G and CBR (laboratory test)	99
Figure 73	Correlation between E_G and CBR (field test).....	100
Figure 74	Correlation between E_{LFWD} and the $E_{PLT(i)}$ (laboratory test)	100
Figure 75	Correlation between E_G and the $E_{PLT(i)}$ (laboratory test).....	101
Figure 76	Correlation between E_{LFWD} and the $E_{PLT(i)}$ (field test)	102
Figure 77	Correlation between E_{LFWD} and the $E_{PLT(R2)}$ (field test)	102
Figure 78	Comparison between laboratory and field for $E_G - E_{PLT(i)}$ correlation.....	103
Figure 79	Comparison between laboratory and field for $E_G - E_{PLT(R2)}$ correlation	104
Figure 80	M_{FWD} versus E_{LFWD} correlation, and comparison to Fleming et al. (2000)	105
Figure 81	Correlation between (E_{LFWD}) and CBR (%) (laboratory test)	105
Figure 82	Correlation between (E_{LFWD}) and CBR (%) (field test).....	106
Figure 83	Correlation between DCP- PR and $E_{PLT(i)}$ (laboratory test)	107
Figure 84	Correlation between DCP- PR and $E_{PLT(R2)}$ (laboratory test)	108

Figure 85	Correlation between DCP- <i>PR</i> and $E_{PLT(i)}$ (field test).....	109
Figure 86	Correlation between DCP- <i>PR</i> and $E_{PLT(R2)}$ (field test).....	109
Figure 87	Comparison between laboratory and field for DCP- <i>PR</i> - $E_{PLT(i)}$ correlation	110
Figure 88	Comparison between laboratory and field for DCP- <i>PR</i> - $E_{PLT(R2)}$ correlation	110
Figure 89	Correlation between DCP- <i>PR</i> and M_{FWD}	111
Figure 90	Correlation between DCP- <i>PR</i> and <i>CBR</i> (laboratory test)	113
Figure 91	Correlation between DCP- <i>PR</i> and <i>CBR</i> (field test).....	113
Figure 92	Comparison between laboratory and field for DCP- <i>PR</i> - $E_{PLT(R2)}$ correlation	114

INTRODUCTION

Soil compaction is one of the most critical components in the construction of roads, airfields, embankments, and foundations. The durability and stability of a structure are related to the achievement of proper soil compaction. Therefore, compaction control of soils used in highway construction is necessary to improve their engineering properties. The current Louisiana state quality acceptance criteria for the construction of pavement base layers and other geo-materials is based mainly on achieving adequate field density (or compaction) relative to a maximum dry density obtained in the laboratory by using either standard or modified proctor tests. However, the design of these materials in a given project is based on engineering parameters such as strength and/or stiffness. It is anticipated in any project to have a durable material that can perform satisfactorily in the field throughout its expected design life. The missing link between the design process and field quality control makes it difficult to implement performance-based specifications or warranty-based construction criteria. Therefore, the construction quality control/quality assurance procedures should be based on criteria that closely correlate to the parameters used in the design to ensure that the required performance levels are achieved. A fundamental performance parameter for constructed highway layers is the elastic stiffness modulus of the materials. Currently, there are different non-destructive test devices that are reported to measure in-situ elastic stiffness modulus for the pavement material under test. These devices include the Geogauge, Light Falling Weight Deflectometer (LFWD), and Dynamic Cone Penetrometer (DCP).

In this study, field and laboratory testing programs evaluated the three testing devices to reliably measure the in-situ elastic modulus. The laboratory testing program included constructing and testing different test samples with a variety of materials inside two test boxes (5×3×2.5 ft.) located at the Geosynthetic Engineer Research Laboratory (GERL) laboratory. The testing material included: silt clay, clayey soil, cement-treated soils, crushed limestone, Recycled Asphalt Pavement, and sand. The field testing program included testing various highway sections selected from various projects in Louisiana. In addition, six soil sections and three trench sections were constructed and tested at the LTRC Pavement Research Facility (PRF) site for testing. The laboratory and field tests included Geogauge, LFWD, and DCP tests in conjunction with standard tests such as the Plate Load Test (PLT) and Falling Weight Deflectometer (FWD) test (for field tests only). In addition, California Bearing Ratio (CBR) laboratory tests were conducted on the tested laboratory samples and samples collected from

sections constructed in the field. A statistical analysis was then conducted on the collected data to correlate the measurements obtained from the three investigated devices and the measurements obtained from the standard tests (PLT and FWD, and CBR).

OBJECTIVES OF RESEARCH

The main objective of this research was to assess the use of non-destructive in-situ tests (DCP, LFWD, and Geogauge) to evaluate the strength/stiffness characteristics of highway materials for application in the quality control/quality assurance (QC/QA) procedures during construction of pavement layers (base, subbase, and subgrade) and embankments. The objectives can be summarized as follows:

1. Evaluate the strength/stiffness properties of embankment soils using the Geogauge, LFWD, DCP, FWD, and PLT tests.
2. Evaluate the strength/stiffness properties of crushed stone base course using Geogauge, LFWD, DCP, FWD, and PLT tests.
3. Evaluate the strength/stiffness properties of cement and lime-treated base and subbase layers using Geogauge, LFWD, DCP, FWD, and PLT tests.
4. Develop correlations between measurements obtained using the Geogauge, LFWD, and DCP with moduli obtained by the PLT and FWD.
5. Determine the repeatability of the Geogauge and LFWD devices when testing different pavement layers and embankments.
6. Determine the influence depth of the Geogauge and LFWD devices for future application in QC/QA during construction of pavement layers and embankments.
7. Recommend procedures for the use of in-situ stiffness as acceptance criteria for controlling construction of pavement layers and embankments.

SCOPE

This research effort focused on evaluating the ability of the Geogauge, Light Falling Weight Deflectometer (LFD) and Dynamic Cone Penetrometer (DCP) devices to reliably measure the in-situ stiffness of base course layers and embankments for potential use in the construction Q_C/Q_A procedures. Two well-established tests, the plate load test (PLT) and Falling Weight Deflectometer (FWD), were selected to measure the reference stiffness needed for statistical analysis and correlations. This project applied the three investigated devices on a wide range of soils in the laboratory and in the field. The laboratory tests were conducted inside two boxes of 5 x 3 x 2.5 ft. dimensions using a wide range of soils: silty clay, clayey silt, sand, crushed limestone, soil cement, and sandy gravel with clay. Obtaining the target density and moisture content values was difficult due to compaction in small boxes. However, the measurements of all devices were taken under the same condition. Field investigation included constructing and testing six test sections and three trench sections at the PRF site in addition to three other highway sections. Test parameters included soil type, density, and California bearing ratio (CBR). This research study emphasized evaluating the devices, not evaluating the materials. The effects of moisture sensitivity on the materials' stiffness were not part of this investigation.

METHODOLOGY

Background

This section presents a review of all test devices that were used in this study. This summary includes existing correlations for soil measurement acquired by the test devices under evaluation (i.e., Geogauge, LFWD, and DCP).

Soil Stiffness Gauge (Geogauge)

The stiffness gauge technology was originally developed by the defense industry for detecting land mines. The collaboration between Bolts, Beranek, and Newman of Cambridge, MA; CNA consulting Engineers of Minneapolis, MN; and Humboldt (FHWA research program) resulted in the introduction of the Humboldt Stiffness Gauge, known as the Geogauge (figure 1) to the transportation industry [1]. The Geogauge measures the in-place stiffness of compacted soil at the rate of about one test per 1.3 minutes. It weighs about 10 kilograms (22 lbs.), is 280 mm (11 in.) in diameter and 254 mm (10 in.) tall. It has an annular ring that contacts the soil with an outside diameter of 114 mm (4.50 in.), an inside diameter of 89 mm (3.50 in.), and a thickness of 13 mm (0.5 in.) [2]. The Geogauge has a shaker that generates a very small dynamic force at 25 specific frequencies ranging from 100 to 196 Hz. This produces a very small deflection, δ , which is measured by a geophone sensor within the body of the gauge. The principle of Geogauge operation is described in the Appendix. The Geogauge stiffness, H_{SG} , is based on the average of 25 stiffness values obtained at 25 different frequencies. The Geogauge stiffness, H_{SG} , can then be converted to soil elastic modulus, E_G , using the equation proposed by CNA Consulting Engineers:

$$E_G = H_{SG} \frac{(1 - \nu^2)}{1.77R} \quad (1)$$

Where E_G = the elastic stiffness modulus in MPa, H_{SG} = the Geogauge stiffness reading in MN/m, ν = Poisson's ratio and R = the radius of the Geogauge foot (57.15 mm = 2.25 in.).

In this study, Poisson's ratio was selected from the values shown in table 1 to calculate Geogauge stiffness modulus for the tested soils. For a Poisson's ratio of 0.35, a factor of approximately 8.67 can convert the Geogauge stiffness (in MN/m) to a stiffness modulus (in MPa). The Geogauge manufacturer (Humboldt) recommends that it should be used only up to 23 MN/m because the Geogauge may lose accuracy when measuring stiffnesses greater than 23 MN/m [3].



Figure 1

Geogauge Device

Table 1

(Poisson Ratios for Different materials [4])

Material	Range	Typical value
Portland cement concrete	0.15-0.2	0.15
Untreated granular materials	0.3-0.4	0.35
Cement-treated granular materials	0.1-0.2	0.15
Cement-treated fine-grained soils	0.15-.035	0.25
Lime stabilized materials	0.1-0.25	0.2
Lime-flyash mixtures	0.1-0.15	0.15
Dense Sand	0.2-0.4	0.35
Fine-grained soils	0.3-0.45	0.4
Saturated soft soils	0.4-0.5	0.45

Geogauge Stiffness Modulus Correlation with Moduli of other In-situ Tests

In their study, Chen et al. reported that the base moduli measured with the FWD are higher than those measured with the Geogauge [5]. Chen et al. also suggested a general relationship between the Geogauge stiffness and the FWD back-calculated modulus, M_{FWD} as follows [3]:

$$M_{FWD} = 37.65 H_{SG} - 261.96 \quad (2)$$

Where M_{FWD} is expressed in MPa, and H_{SG} is the Geogauge stiffness reading expressed in MN/m.

They also suggested that the quality of base layers can be classified by FWD or Geogauge results as listed in table 2. A Direct-Seismic Pavement Analyzer (D-SPA) was also used by Chen et al. to measure the corresponding shear wave velocities (V_s) for different quality bases as shown in Table 2 [3].

Table 2
Geogauge and FWD suggested values to characterize base layer

Base Quality	E_G (MPa)	V_s (m/sec)	M_{FWD} (MPa)
Weak	<87	<250	<140
Good	156-209	300-350	310-450
Excellent	>261	>400	>700

To the best knowledge of the authors, there are no published studies correlating Geogauge measurements to the plate load test, except by the CNA Consulting Engineers study that conducted a number of field tests to compare the modulus from the Quasi-Static Plate Load Test (QSPLT) to the Geogauge stiffness modulus. The results of this study are presented in equations 3 through 5. These results suggest that values of the reloading elastic modulus obtained from (QSPLT) are similar in magnitude to the Geogauge stiffness modulus. On the contrary, the Geogauge modulus is nearly seven times higher than the initial loading modulus. In addition, the results indicate that Geogauge stiffness modulus correlates better with the initial modulus than with the other two moduli [6].

$$E_{(QPLT)r} = 0.8962(E_G) + 25.9 \quad \text{with} \quad R^2 = 0.23 \quad (3)$$

$$E_{(QPLT)u} = 0.6158(E_G) + 10.3 \quad \text{with} \quad R^2 = 0.27 \quad (4)$$

$$E_{(QPLT)i} = 0.3388(E_G) + 84.7 \quad \text{with} \quad R^2 = 0.66 \quad (5)$$

Where $E_{(QPLT)r}$, $E_{(QPLT)u}$, and $E_{(QPLT)i}$ are the reloading, unloading, and initial elastic moduli, respectively, in MPa obtained from quasi-static plate load test.

Dynamic Cone Penetrometer (DCP)

The DCP was initially developed in South Africa for in-situ evaluation of pavements [7]. Since then, it has been used in South Africa, the United Kingdom, Australia, New Zealand, and several states in the United States, such as California, Florida, Illinois, Minnesota, Kansas, Mississippi, and Texas for site characterization of pavement layers and subgrades. The U.S. Corps of Engineers has also used the DCP. The DCP has proven to be an effective tool for assessing in-

situ strength/stiffness of pavement and subgrade, and it can be used for Q_C/Q_A in highway construction.

The DCP is simple and economical; it requires minimum maintenance, easy to access sites, and provides continuous measurements of the in-situ strength/stiffness of pavement section and the underlying subgrade layers without the need for digging the existing pavement as in the CBR test [8]. The DCP consists of an upper fixed 575 mm travel rod with an 8 kg falling weight, a lower rod containing an anvil, and a replaceable cone with an apex angle of 60° and 20 mm diameter (figure 2). The test is conducted by dropping the weight from 575 mm height and recording the number of blows versus depth. Then the penetration rate (PR) is then calculated. The DCP ratio is defined by the slope of the curve relating the number of blows to the depth of penetration (in mm/blow) at a given linear depth segment.

The DCP can verify both the level and uniformity of compaction, which makes it an excellent tool for quality control of pavement construction. Moreover, it can be used to determine the tested layer thickness [8]. Livneh et al. demonstrated that the results from penetration tests correlate well with the in-situ CBR values [9]. They also indicated that the layer thickness obtained from DCP tests matches with that obtained in the test pits. Chen et al. also indicated that the DCP can be a useful tool when the FWD back-calculated resilient moduli is not accurate, such as when the asphalt concrete layer thickness is less than 75 mm or when bedrock is shallow [8].

During the past decade, the DCP test has been correlated to many engineering properties such as the CBR, shear strength of granular materials, and most recently, the subgrade Resilient modulus (M_R), Elastic Modulus (E_s), and soil classification. In addition, Minnesota Department of Transportation (MnDOT) conducted many studies attempting to determine if a reasonable correlation exists between the DCP PR and in-place compaction density. Most results of DCP testing on cohesive and selected granular materials showed too much variability to practically apply a correlation for density. However, these studies demonstrated that properly compacted granular base materials exhibit very uniform PR values.

Existing Correlation between DCP and CBR

To assess the structural properties of the pavement subgrade, the DCP values are usually correlated with the *CBR* value [7], [10]. Different correlations were suggested between the DCP-

PR in (mm/blow) and CBR values. Kelyn [7] conducted DCP tests on 2,000 samples of pavement materials in standard molds directly following CBR determination. Based on his results the following correlation was recommended:

$$\text{Log } CBR = 2.62 - 1.27 \log PR \quad (6)$$

Based on a field study, Smith and Pratt suggested the following correlation [11]:

$$\text{Log } CBR = 2.56 - 1.15 \log PR \quad (7)$$

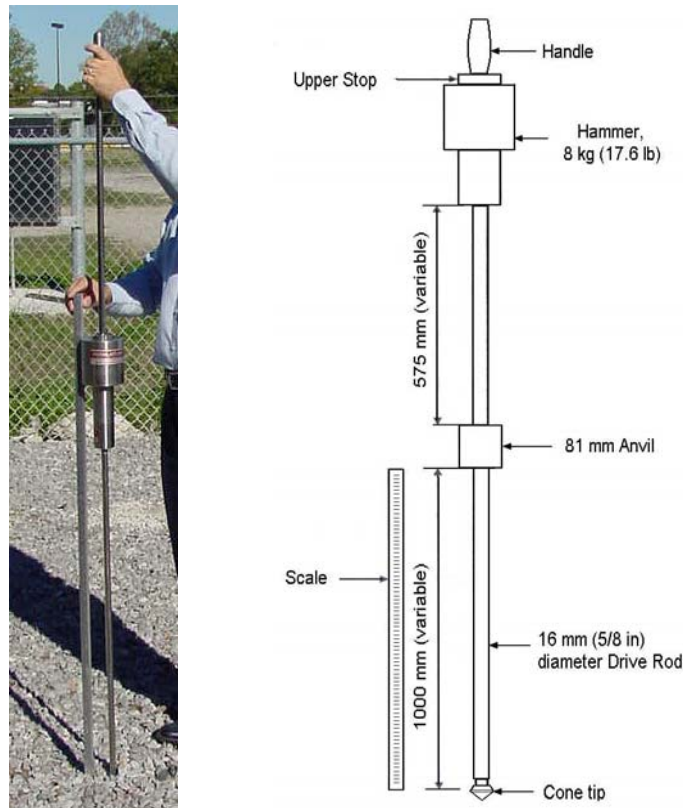


Figure 2
Dynamic Cone Penetrometer (DCP)

Livneh and Ishia conducted a correlation between the DCP- PR and the in-situ CBR values using a wide range of undisturbed and compacted fine-grained soil samples, with and without saturation [10]. Compacted granular soils were tested in flexible molds with variable controlled lateral pressures. The following relationship was obtained between CBR and DCP- PR :

$$\text{Log } CBR = 2.2 - 0.71 (\log PR)^{1.5} \quad (8)$$

Harrison also suggested the following correlations for different soils [12]:

$$\text{Log } CBR = 2.56 - 1.16 \log PR \quad \text{for clayey-like soil of } PR > 10 \text{ (mm/blow)} \quad (9)$$

$$\text{Log } CBR = 2.70 - 1.12 \log PR \quad \text{for granular soil of } PR < 10 \text{ (mm/blow)} \quad (10)$$

For a wide range of granular and cohesive materials, the U.S. Army Corps of Engineers found the relation described in equation 11 [13]; this equation was also adopted by many researchers [14],[15], [8].

$$\text{Log } CBR = 2.465 - 1.12 (\log PR) \quad \text{or} \quad CBR = 292/PR^{1.12} \quad (11)$$

MnDOT also adopted equation 11. They found that the effects of soil moisture content and dry density influence both *CBR* and DCP values in a similar way; therefore, they are considered negligible for the correlation.

Existing Correlations between DCP and Different Moduli

The subgrade resilient modulus, which is used in design methods based on structural analysis, can be determined either indirectly from relation between subgrade modulus (E_s) and *CBR* or can be predicted directly from the DCP results. The 1993 AASHTO Guide for Design of Pavement Structures has adopted equation 12 for calculating subgrade resilient modulus (M_R), which was proposed by Huekelom and Klomp ([16]:

$$M_R \text{ (psi)} = 1500 * CBR \quad \text{or} \quad M_R \text{ (MPa)} = 10.34 * CBR \quad (12)$$

The resilient moduli from which this correlation was developed ranged from 750 to 3000 times the *CBR*. Also, the formula is limited to fine-grained soils with a soaked *CBR* of 10 or less [8]. Chen et al. [8] indicated that using equation 11 to compute *CBR* and then using equation 13 to compute modulus values from DCP tests yielded comparable results with those from FWD. Powell et al. [17] suggested another relationship between subgrade resilient modulus and *CBR* as shown in equation 13.

$$M_R \text{ (psi)} = 2550 \times CBR^{0.64} \quad \text{or} \quad M_R \text{ (Mpa)} = 17.58 \times CBR^{0.64} \quad (13)$$

Other equations related the DCP *PR* with the subgrade modulus directly. Pen suggested the two relationships between the subgrade's elastic modulus (E_s) in MPa and *PR* in mm/blow as defined in equations 14 and 15 [18].

$$\text{Log } (E_s) = 3.25 - 0.89 \text{ Log } (PR) \quad (14)$$

$$\text{Log } (E_s) = 3.652 - 1.17 \text{ Log } (PR) \quad (15)$$

Chua presented a new theoretical approach to model and interpret the results of the DCP with cone apex angle of 60 [19]. A one-dimensional model for penetration analysis of a rigid projectile into ideally locking material was used to back calculate the elastic modulus of the target medium. Chua developed theoretical relationships between DCP-*PR* and elastic modulus, E_s , which are a function of the principal stress differences at failure ($2 \tau_o$) as follow [19]:

$$\text{Log } (E_s) = B - 0.4 \log (PR) \quad (16)$$

Where E_s is MPa, and B is a constant value depending on the value of $2 \tau_o$ (see Table 3). The results of a regression analysis conducted by Chen et al. between the FWD back-calculated resilient modulus (M_{FWD} in MPa) and the DCP-*PR* resulted in the following model [20]:

$$M_{FWD} = 338 (PR)^{-0.39} \quad (\text{for } 10 \text{ mm/blow} < PR < 60 \text{ mm/blow}) \quad (17)$$

Table 3
Values of B [19]

Soil Type	$2 \tau_o$	B
Plastic clay	25	2.22
Clayey soil	50	2.44
Silty soil	75	2.53
Sandy soil	150	2.63

De Beer also proposed a correlation between the elastic modulus (E_s) and DCP-*PR*, which has a form similar to the CBR relation, and is shown in the following equation [21]:

$$\text{Log } (E_s) = 3.05 - 1.07 \text{ Log } (PR) \quad (18)$$

Based on a regression analysis, Konard and Lachance suggested a relationship between the *PR* of a large DCP with a 51 mm diameter cone and the elastic modulus of unbound aggregates and natural granular soils back-calculated from plate load tests (E_{PLT}), and it is as follows [22]:

$$\text{Log } (E_{PLT}) = (-0.88405) \text{ Log } (PR) + 2.90625 \quad (19)$$

Where E_{PLT} is expressed in MPa.

Current Application of DCP in Pavement Assessment

Currently many DOTs and federal agencies use the DCP to assess the strength and uniformity of highway structures [15]. One of the first states to use the DCP, MnDOT has been conducting research on the DCP since 1991. In order to use the DCP as a more effective tool for rehabilitation studies and compaction evaluation, MnDOT suggested defining limiting *PR* values for each particular subgrade soil and base type. After conducting more than 700 DCP tests on Minnesota Road Research (MN/ROAD) project, they were able to recommend the *PR* values listed in table 4 for use when analyzing DCP test results. These recommended values are based on assuming adequate confinement near the testing surface. The recommended values do not cover all types of materials; by conducting similar research, table 4 can be extended to include other classes of base courses.

Table 4
Limiting DCP penetration rates by MnDOT [23]

Material Type	Limiting PR (mm/blow)
Silty/clay subgrade	< 25
Select Granular Subgrade	< 7
Class 3 Special gradation granular base materials	< 5

MnDOT has also specified two different applications of DCP testing in its pavement assessment procedures. One application involves using the DCP as a quality control device during the backfill compaction of pavement edge drain trenches. A DCP-PR of 3 in./blow or less indicates satisfactory compaction according to MnDOT Subsurface Drain Installation Specifications. This application was proven to be reliable and effective in improving the compaction levels of edge drain trenches. The second application of DCP testing, specified by MnDOT, involves its use in the quality control of granular base layer compaction. Other non-specified applications of the DCP by MnDOT have included investigating soft subcut areas, determining the condition of the base and subgrade materials under full depth bituminous cracks, and monitoring the effectiveness of subgrade flyash stabilization [23].

Light Falling Weight Deflectometer (LFWD)

The LFWD is a portable FWD that has been developed in Germany as an alternative in-situ testing device to the plate load test. Three main types of LFWDs have been used in previous studies: the German Dynamic Plate (GDP), the Transport Research Laboratory (prototype) Foundation Tester (TFT), and the Prima 100 LFWD. All types exhibit many similarities in their mechanics of operation although there are some differences in design and mode of operation, which lead to variations in the measured results. Generally, the LFWD consists of a loading device that produces a defined load pulse, a loading plate, and one center geophone sensor (electric deflection-data device) to measure the center surface deflection.

The Prima 100 LFWD was used in this study (figure 3). It was developed and marketed by Carl Bro Pavement Consultants (previously Phønix), Denmark. It weighs 26 kg (57.2 lbs.) and has a 10 kg (22 lb.) falling weight that impacts a spring to produce a load pulse of 15-20 milliseconds. For safe operation, the drop weight is supported with a transportation-lock pin and guide rod with stabilizer. The Prima 100 has a load range of 1-15 kN (i.e. up to 450 kPa with its 200 mm diameter loading plate). It measures both force and deflection, utilizing a velocity transducer with a deflection range of 22 mm [24].

During any test operation, the center deflection (δ_c) of the loading plate will be measured and used to estimate the LFWD elastic stiffness modulus (E_{LFWD}) using PC software and display it on the screen as shown in figure 4. The expression used to calculate E_{LFWD} is similar to the one used to calculate the surface modulus of a layered media assuming a uniform Poisson's ratio (ν) and constant loading on an elastic half space (Boussineq elastic half space). This expression is described by equation 20.

$$E_{LFWD} = \frac{2(1 - \nu^2)\sigma \times R}{\delta_c} \quad (20)$$

Where σ = the applied stress, and R = the plate radius.

A complete analysis of the LFWD field data can provide an estimate of the linear-elastic response of the pavement section and its supporting layer [24].



Figure 3
Prima 100 Light Falling Weight Deflectometer

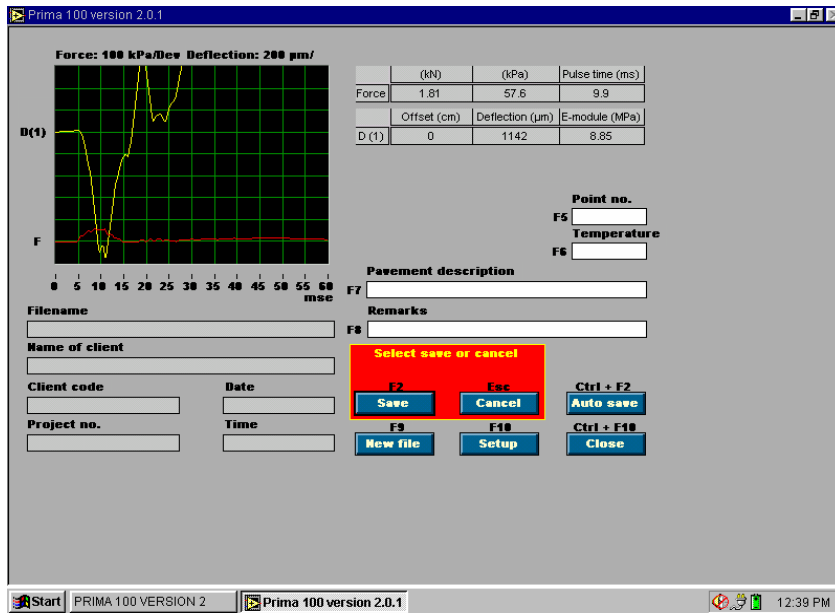


Figure 4
Screen of Prima 100 software

Existing Correlation between LFWD Moduli and Other In-Situ Test Moduli

The German Code for the design of flexible pavement structures recommends equation 21 to relate the stiffness moduli calculated from the plate load test and the German Dynamic Plate test (GDP) (one type of the LFWD that was previously described) [25].

$$E_{PLT(R2)} = 600 - \frac{300}{300 - E_{LFWD}} \quad (21)$$

Where $E_{PLT(R2)}$ is the German reloading elastic modulus in MPa obtained by the PLT test.

Fleming et al. demonstrated a correlative ratio between the deformation moduli of the GDP and the FWD of about 0.5 [26]. However, Fleming reported that his extensive field-stiffness measurements on in-situ construction sites showed a relatively consistent correlation of 0.6 between the stiffness moduli of the GDP and FWD [27]. Livneh and Goldberg suggested that the GDP (LFWD) stiffness moduli is about 0.3-0.4 times the conventional FWD moduli [25]. Fleming et al conducted field tests to correlate the moduli of three main types of LFWD (TFT, GDP, Prima 100) with that of the FWD. Their results showed that the M_{FWD} correlated well with moduli obtained from prima 100; equation 22 shows an example correlation.

$$M_{FWD} = 1.031 E_{LFWD} \text{ (Prima 100)} \quad (22)$$

However, they found that the correlation coefficients with the other LFWD types were as follows: $FWD = 1.05$ to $2.22 E_{GDP}$, $FWD = 0.76$ to $1.32 E_{TFT}$.

Kamiura et al. studied the relationship between LFWD- Prima 100 and plate load tests for subgrade materials which contains volcanic soil, and silty sand, and mechanically stabilized crushed stone [28]. They suggested the following correlation based on their results:

$$\text{Log} (k_{LFWD}/k_{30}) = 0.0031 \log (k_{LFWD}) + 1.12 \quad (23)$$

Where k_{LFWD} is the ratio of stress on the loading plate of the LFWD to the measured deflection at this stress, and k_{30} is the ratio of stress on the plate with a diameter of 300 mm for a PLT to the measured deflection at this stress.

Kamiura et al. indicated that the (k_{LFWD}/k_{30}) ratio is affected by the grain size of the tested material, where this ratio increases with increasing grain size [28]. Fleming reported that a number of factors influence the measured stiffness of LFWD, including differences in mass, transducer type and software analysis [27].

Falling Weight Deflectometer (FWD)

The FWD system used in this study is the trailer-mounted Dynatest model 8002E (figure 5). It consists of a drop weight mounted on a vertical shaft, and it can be towed by most conventional vehicles. The drop weight is hydraulically lifted to predetermined heights ranging from 50 to 510 mm. The weight is usually dropped onto a 300 mm or a 450 mm diameter loading plate resting on a 5.6 mm thick rubber buffer, which is usually used to improve the uniformity of loading stress distribution over the whole loading plate area [29].

The impact of the falling weight is capable of producing impact loads approximately half-sinusoidal wave, and a loading time between 25 and 40 ms applies impulse loading to a circular plate in contact with the pavement surface. Usually the load ranges from 6.7 kN to 155.7 kN depending on the magnitude of the dropping mass and the height of the drop. The applied load is recorded by a load cell. The FWD also has seven geophones that register the peak deflections due to an applied load. The geophones are positioned at 0; 305; 457; 610; 914; 1219; and 1,524 mm away from the center of the loading plate.

FWD Moduli Back-calculation

The analysis performed on any FWD data is aimed at determining the resilient modulus of each layer in a pavement section and the depth of the underlying bedrock layer. This analysis is usually referred to as the FWD back-calculation process. To perform the analysis, the properties such as the elastic modulus and Poisson's ratio should be known for the materials in each layer. In addition, the thickness of each pavement layer is also required in this analysis [30].

The back-calculation procedure involves calculation of theoretical deflections under the applied load using assumed pavement moduli. These theoretical deflections are compared with measured deflections and the assumed moduli are then adjusted in an iterative procedure until there is no significant difference between the theoretically calculated and the measured deflections. The moduli determined in this method represent the pavement response to load and can be used to calculate stresses or strains in the pavement structure. Examples of current back-calculation programs currently in use include the MODULUS, ELMOD and EVERCALC programs. The ELMOD 4.0 program was used in this study.

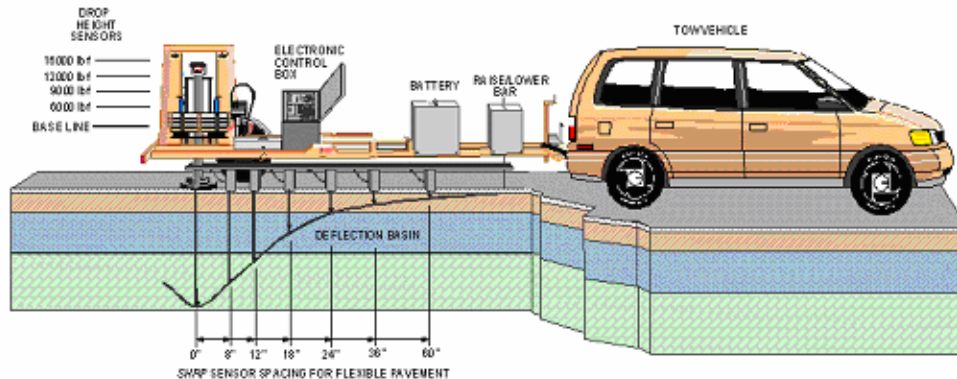


Figure 5
Dynatest model 8000 (FWD) (LTRC 2000)

Application of FWD

The FWD provided periodic non-destructive evaluation of the structural capacity of different pavement sections. It has been a good non-destructive test for pavement structure assessment mainly because of its speed, better simulation of traffic loading, and results that can directly be applied in structural design [24]. Now, there are more than 300 FWDs worldwide in operation for routine non-destructive testing and research purposes. Most testing is performed on completed pavement structures. Less experience has been gained with the use of the FWD on road bases, subbases and subgrades [31]. Furthermore, FWD data may be questionable, such as when the AC thickness is less than 3 in., or when shallow bedrock is encountered. These two situations often cause a misinterpretation of FWD data [8].

Current FWD research, suggests that it can be used in quality control during construction of pavement layers. Zaghoul and Saeed suggested an empirical approach to set FWD target deflections [32]. In this approach, trial sections are constructed and FWD tests are performed at locations showing acceptable density levels to determine the required target deflections. Zaghoul and Saeed also suggested that the Qc/Qa procedures include dividing pavement sections into homogenous segments, conducting FWD tests on each layer, and conducting statistical tests on measured deflections to evaluate construction quality and identify weak points. Furthermore, Rogers et al. performed tests using FWD to determine the relation between the stiffness and the dry density of a base course layer [33]. Their test results showed that

although the stiffness increased during the initial compaction passes, adequate stiffness development took place only when the density was close to its maximum value at the optimum moisture content. Based on this result, they suggested that there is no evident correlation between dry density and the stiffness measured by FWD.

Although the FWD is classified as a suitable device for stiffness measurements, it is sometimes considered unnecessarily complicated for base and subbase testing [27]. In addition, the use of the FWD to evaluate the pavement structure during the construction of subgrades, subbases, and base layers is faced with some problems. For example, pavement layers that are under construction are not as accessible to FWDs as layers for completed roads. Another drawback of using FWD for monitoring the load-carrying capacity of a pavement structure under construction is that the uneven surface causes tilting of the deflection sensors. Tilting in excess of a certain value leads to inaccurate deflection measurements that can not be used in back calculation [31].

Static Plate Load Test (PLT)

The PLT has been a useful site investigation tool for many years and has been used for proof testing pavement structure layers in many European countries. Currently, it is used for both rigid and flexible pavements. The test consists of loading a circular plate that is in contact with the layer to be tested and measuring the deflections under load increments. The plates used for roads are usually 30.5 cm (12 in.) in diameter. The load is transmitted to the plates by a hydraulic jack, acting against heavy mobile equipment as a reaction plate.

The PLT can be conducted using different procedures depending on the information desired. In all cases, a load-deformation curve following the general relationship shown in figure 6 will be obtained. The load must be sustained on the plate until all measured settlement has diminished so that the true deflection for each load increment is obtained. The time required for settlement is determined by plotting a time-deformation curve while the test is in progress, and identifying where this curve essentially becomes horizontal. Generally, a load increment is applied when the rate of deformation has approached about 0.001 in./min. [34]. The method of performing PLT test on soils and flexible pavement is described by ASTM D1195-93 [35]. In this method, the PLT test should continue until a peak load is reached or until the ratio of load increment to settlement increment reaches a minimum, steady magnitude.

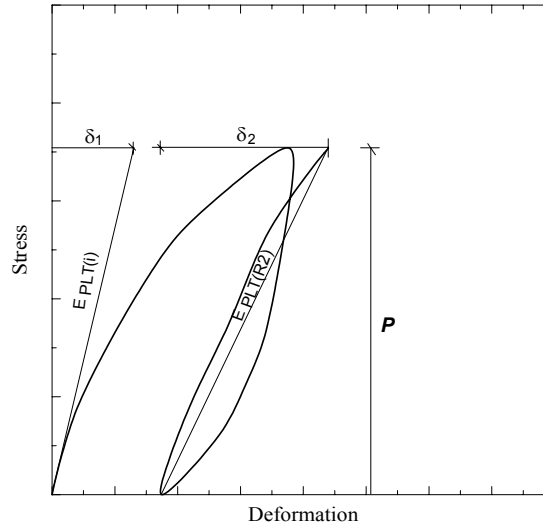


Figure 6
Definition of modulus from PLT

The influence depth of the PLT is about two times its diameter [36]. Since the tested layers' thicknesses usually ranged from 6 to 12 in., the influence zone of PLT (12 in. diameter) reached the underlying layer. Therefore, the modulus obtained from PLT reflects the composite modulus rather than the true modulus of the tested layer. In this study, the Odemark method, referred to as the Method of Equivalent Thickness (MET), was used to back-calculate the PLT moduli on multi-layer systems [37]. In this method, layers of different stiffnesses are first transformed to an equivalent layer of same stiffness, such that Boussinesq's equations for homogeneous elastic half-space media can be used to predict stresses and deflections. For example, for a two layered system with E_1 and E_2 as the stiffness moduli of the first and second layers, the following equation is used to transform the first layer into an equivalent layer with stiffness modulus E_2 [30]:

$$h_e = f \times h_1 \times \sqrt[3]{\frac{E_1}{E_2}} \quad (24)$$

Where h_e is the equivalent thickness of layer one, h_1 is thickness of layer one, and f is an adjustment factor, taken to be 0.9 for a two-layer system, and 1.0 for a multi-layer system.

Since FWD is capable of testing multi-layer systems due to the presence of several geophone sensors, this study assumed that the E_1/E_2 ratios for PLT and FWD are the same for the two-layer system.

Moduli from Plate Load Test

As in the case for other stress-strain tests, different elasticity moduli can be obtained from the PLT. Soil elasticity moduli can be defined as: (1) the initial tangent modulus; (2) the tangent modulus at a given stress level; (3) reloading and unloading modulus and; (4) the secant modulus at a given stress level. In this study, the initial tangent modulus was determined for all plate load tests. To determine the initial modulus ($E_{PLT(i)}$), a line was drawn tangent to the initial segment of the stress-strain curve; then an arbitrary point was chosen on this line and the stress and deflection corresponding to this point was used to determine the initial modulus. Figure 6 describes the deflection and stress used for determining $E_{PLT(i)}$ from δ_I and p . German Code for the design of flexible pavement structures specifies performing in-situ plate-bearing tests on constructed pavement layers. For the second cycle of the regular plate-bearing test, the German code defines a reloading stiffness modulus called $E_{PLT(R2)}$ using the following equation [25]:

$$E_{R2} = \frac{2p(1-\nu^2)}{\pi R \delta} \quad (25)$$

Where p =applied load by the end of the second cycle, and δ = deflection under the second loading cycle of the plate. In this study, the reloading elastic modulus ($E_{PLT(R2)}$) defined by the German code was also used.

California Bearing Ratio (CBR)

The *CBR* test is a simple test that is commonly used to indicate the strength of subgrade soils, subbases, and base course materials in highways and airfield pavement systems. The test is used primarily to empirically determine the required thicknesses of flexible pavements. Although it is usually performed on remolded (compacted) specimens, it may be conducted on undisturbed soils in the field. Remolded specimens may be compacted to their maximum unit weights at their optimum moisture contents if the *CBR* is desired at 100 percent maximum dry unit weight and optimum moisture content. The *CBR* tests can also be performed at the desired unit weights and moisture contents. Soil specimens are tested by soaking them in water for 96 hours to simulate very poor soil conditions.

The *CBR* is defined as the ratio (expressed as a percentage) obtained by dividing the penetration stress required to cause a piston with a diameter of 49 mm (1.95 in.) to penetrate 0.10 in. into the soil by a standard penetration stress of 1,000 psi [38]. This standard penetration stress is roughly what is required to cause the same piston to penetrate 0.10 in. into a mass of crushed

rock, so the *CBR* may be thought of as the strength of the soil relative to that of crushed rock. If the bearing ratio based on a penetration stress required to penetrate 0.20 in. with a corresponding standard penetration stress of 1,500 psi is greater than the one for a 0.10-in. penetration, the test should be repeated. If the result is still similar, the ratio based on the 0.20-in. penetration should be reported as the *CBR* value.

According to the procedure described in ASTM D1883-99, if the *CBR* is desired at an optimum water content and some percentage of maximum dry unit weight, three specimens should be prepared and tested from the soil to within ± 0.5 percent of the optimum water content [39]. A different compaction effort should be used for each specimen so that the dry unit weights of these specimens vary above and below the desired value. The *CBRs* for three specimens should then be plotted against their corresponding dry unit weight, and the *CBR* for the desired dry unit weight can be interpolated.

Testing Program

The testing program included both laboratory and field testing on a wide range of compacted geo-materials. The laboratory tests were conducted on different sections prepared inside two boxes (5 x 3 x 3 ft.) located at the Geosynthetic Engineering Research Laboratory (GERL) at the Louisiana Transportation Research Center (LTRC). The field tests were conducted on highway sections selected from different projects in Louisiana and on test sections constructed at the LTRC Pavement Research Facility (PRF) site. This section describes the field and laboratory testing programs in detail.

Laboratory Tests

Materials. Different types of soils were prepared and tested at different compaction levels and moisture contents. Materials used in this research included typical Louisiana soils (silty and clayey type soils) used in highway and embankment construction. Other materials included sand, cement-stabilized soil, crushed limestone, gravel, and Recycled Asphalt Pavement (RAP). Provided by LTRC personnel, the test materials were transported mainly from the Pavement Research Facility (PRF) stockpiles. Table 5 summarizes the experimental program for the laboratory work.

The results of sieve analysis for the coarse-grained materials are summarized in table 6. The optimum moisture content, maximum dry density and classifications for these materials are also presented in table 6. The analysis found gravel to be very poorly graded with 96 percent of particles retained on sieve No.4 (4.75mm). To compact and test this material, the gravel was modified by adding clay that was readily available in the laboratory. The modified gravel was 40 percent clay and 60 percent original gravel. The sieve analysis for the modified material, which meets the specifications of the sand clay gravel base course, is also included in table 6. Another modified material, due to difficulty in compaction, was the limestone. Although the limestone was classified as well-graded, the prepared specimen was non-uniform and had zero stiffness readings according to the Geogauge measurements. Fine particles accumulated at the top after compaction, possibly due to inadequate cohesion of the material, water content, or the method of compaction. The limestone was again modified by adding clay soil, which was readily available. The modified material consisted of 10 percent clay and 90 percent limestone. The mechanical analysis of the modified material is included in table 6. Physical properties and soil classifications for fine-grained materials are presented in table 7. The standard Proctor curves for fine grained materials are also shown in figure 7.

Table 5**Testing program for the laboratory investigation**

SAMPLE ID	Time (day)	Water Content (%)	Dry Density (t/m³)	GG	LFWD	DCP	PLT
Clay-1		11.0	1.800	7	3	2	1
Clay-2		12.5	1.911	7	3	2	1
Clay-3		14.6	1.697	7	4	2	1
Clay-4		13.9	1.894	7	4	2	1
Clay-5		9.5	1.548	7	4	2	1
Clay-6		9.4	1.722	7	5	2	1
Clay-7		13.3	1.779	7	7	2	1
Clay-8		9.8	1.516	6	4	1	1
Clay-9		11.8	1.728	6	4	1	1
2% cement + Clay	0	15.4	1.653	7	6	1	1
	4			5	4	-	-
	7			7	6	1	-
	11			6	5	-	-
	13			7	6	1	1
4% cement + Clay	1	14.5	1.743	10	7	2	1
	6			6	6	1	-
	14			7	7	1	1
	20			6	5	1	-
Sand clay gravel		7.6	1.984	6	6	2	1
Crushed Limestone-1		6.1	1.970	5	4	2	1
Crushed Limestone-2		3.2	2.000	5	3	2	1
Recycled Asphalt Pav		13.3	1.749	5	4	2	1
Clayey Silt-1 (opt.)		19.0	1.644	5	4	1	1
Clayey Silt-2 (dry)		15.4	1.625	5	5	2	1
Clayey Silt-3 (wet)		20.1	1.626	5	5	2	1
Sand-1		2.0	1.807	7	4	2	1
Sand-2		2.5	1.660	9	6	2	1
Sand-3		2.2	1.648	5	5	2	1

Table 6
Gradations (percent passing) and classifications for coarse grained materials

Sieve #	Sand Clay Gravel	Crushed Limestone-1	Crushed Limestone-2	Recycled Asphalt Pavement	Sand
2 1/2	100	100	100	100	100
2	100	100	100	96.56	100
1 1/2	100	100	100	95.98	100
1 1/4	100	98.44	98.87	94.29	100
1	97.1	94.26	96.62	92.68	100
3/4	87	83.80	87.95	89.12	100
5/8	76.1	78.45	82.23	85.87	100
1/2	64.6	72.21	75.99	80.81	100
3/8	49.6	65.60	67.5	71.37	100
No.4	41.8	52.70	50.4	51.81	99.05
No.8	40.03	33.70	36.33	36.54	95.82
No.16	39.87	30.63	33.46	33.97	89.41
No.20	39.45	24.47	26.31	27.14	-
No.30	38.24	20.28	19.61	19.3	68.54
No.40	37.2	18.52	17.06	13.91	-
No.50	36.3	17.11	15.03	9.75	10.49
No.80	35.54	16.44	13.39	4.98	-
No.100	33.91	15.30	12.49	3.13	0.56
No.200	24.96	12.90	10.61	0.45	0.17
C _U	-	25.7	150.0	21.0	1.7
C _C	-	2.3	2.9	0.4	0.98
AASHTO	A-2-6	A-1-a	A-1-a	A-1-a	A-3
USCS	GC	GC	GW	GP	SP
w _{opt} (%)	7.4	5.9	3.2	8.6	4.2
γ _{max} (pcf)	-	138.7	124.8	117.1	107.9

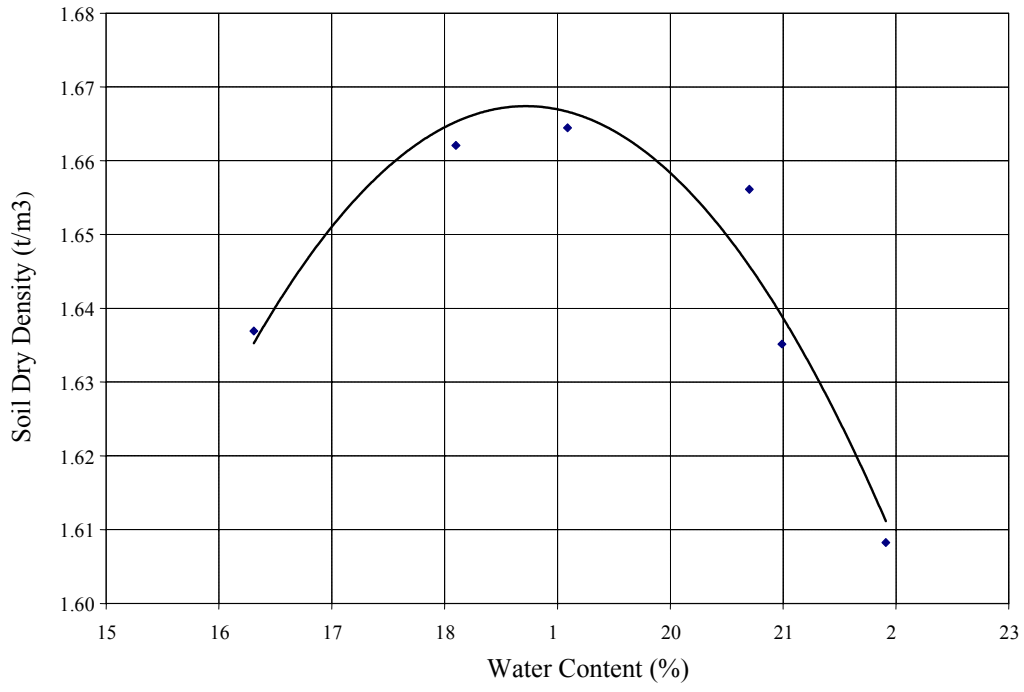
Preparation of Samples. - Samples were prepared and tested at the LTRC laboratory using two test boxes that were 5 ft. long x 3 ft. wide x 3 ft. deep (figure 8). All samples were prepared on top of a 12 in. compacted clay layer, which served as a subgrade layer and remained inside the box during the whole testing program. All samples were compacted to a total depth of 16 in. in two lifts, which is an adequate depth to accomplish the influence zone of the test devices. The procedure for test layer preparation was different for fine-grained soils (clay and clayey silt) as compared to the coarse grained materials.

Table 7
Classification of the fine-grained materials used in the laboratory investigation

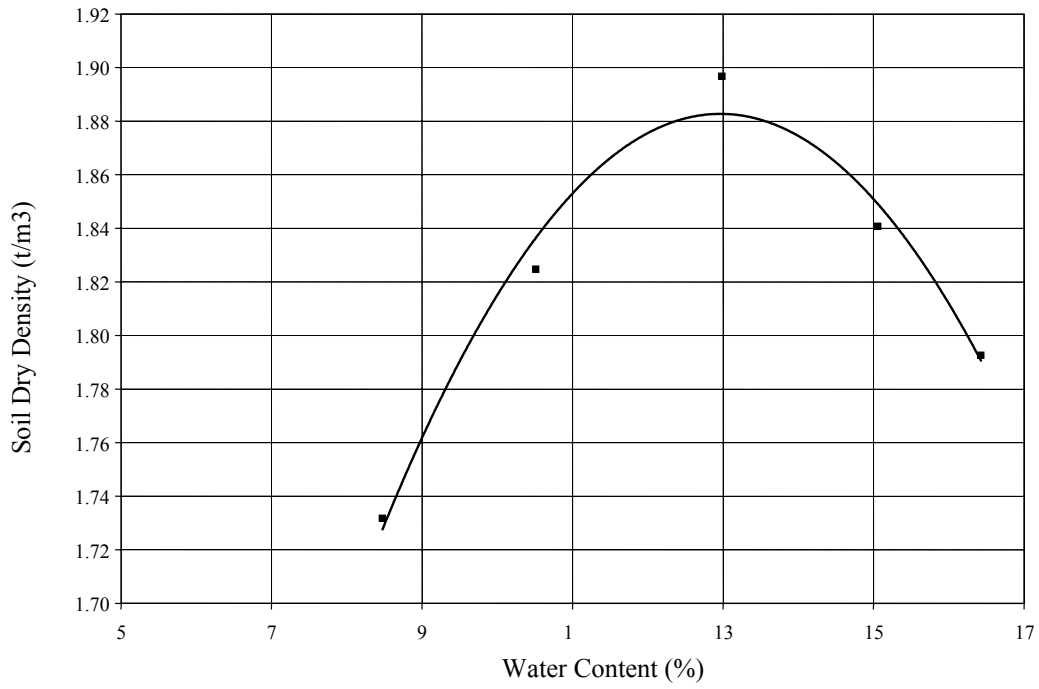
Soil ID	Liquid limit	Plasticity Index	Sand %	Silt %	Clay %	γ_{max} (t/m ³)	W_{opt} (%)	AASHTO	USCS
Clayey Silt	27	15	9	72	19	1.667	18.6	A-4	CL-ML
Clay	31	15	35	37	28	1.888	13.1	A-6	CL

Preparation of Fine Grained Materials. - Clay (PI=15) and clayey silt (PI=6) soils from the PRF site stockpiles were tested at different moisture contents and densities (table 5). The optimum moisture content was determined first for each soil using the standard proctor test. The optimum moisture content was found to be 13.1 percent for clay soil and 18.6 percent for clayey silt soil (table 7, figure 7). One test layer for each soil type was prepared at the optimum moisture content and maximum dry density. The other test layers were prepared and tested, either at the dry-of or at the wet-of optimum moisture contents. Clay soil layers were tested at nine different moisture contents with varying densities while the clayey silt soil layers were tested at three different moisture contents as shown in table 5.

In order to obtain the desired moisture content of the test cases, clay and silty clay soils were first dried in the oven. Then the dry soil was crushed, pulverized, and mixed with water by hand to ensure that a homogeneous soil layer was prepared at the desired moisture content (figure 9). A similar procedure was followed to prepare the cement-treated soil base layers, except for adding cement to the pulverized clay prior to mixing with water.



(a)



(b)

Figure 7

Proctor curves for (a) clayey silt, and (b) clay soils

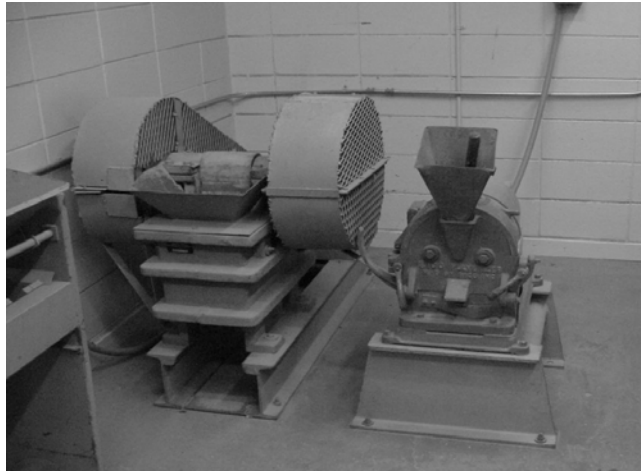


Figure 8

One of the two LTRC test boxes used for test case preparation

Cement-stabilized soil layers were prepared at two different cement ratios (2 percent and 4 percent by weight) and tested over a period of time (1 day, 1 week, 2 weeks, and 3 weeks). Since the DCP, the nuclear density gauge, and especially the PLT cause local destruction to the cement-soil layers, they were performed bi-weekly. The different devices measured strength/stiffness behavior of cement-soil layers with time.

Preparation of Coarse Grained Materials. The moisture content of granular materials has less effect on their strength than fine-grained soil. Therefore, the coarse-grained test layers, including crushed limestone, sand clay gravel, Recycled Asphalt Pavement, and sand, were prepared without modifying their in situ moisture contents. These materials were directly filled into the test boxes and mixed while pouring to ensure that the samples had uniform moisture content. Similar to other samples, the granular materials (coarse-grained soils) were compacted in two 8-in.-thick layers. The nuclear density gauge measured the density and moisture content. The moisture contents were within ± 2 percent from the optimum.



(a)



(b)

Figure 9

(a) Crusher and pulverizer, and (b) mixing the pulverized soil with water

Preparation and Testing. It was important to have moisture content and uniform compaction effort in the box since several readings were taken at different locations of the layer. However, it was not easy to have the same compaction effort in the box, which causes a variation in the results for the test layers. Two different compactors were used to compact the soils in the boxes. The small compactor (Bosch) was easy to operate but was not adequate to achieve the desired density. Another disadvantage was that its small plate size required more time to compact the samples and it was difficult for operators to maintain an even surface. The Wacker Packer compactor was more powerful with a larger plate, but it was not easy to control compaction with and it needed a strong and experienced operator. Soil and base layers were compacted in two 8 in. thick lifts. To reduce the effect of a possibly non-homogeneous sample, readings were concentrated around the center of the box. Conducting the tests around the center of the box was also advised as a result of a previous boundary conditions study conducted at LTRC. Based on that study, the minimum distance between the edge of the LFWD loading plate and the side of the box was about 6 in. The distance of the Geogauge and the DCP tests from the boundary of the test box were more than 7 in. for all tests in this project.

Test sequence was important since some of the tests were minimally invasive, such as the DCP and nuclear density gauge. The DCP and the nuclear gauge create a hole for each tested layer in the sample, which left less room for conducting the Geogauge and LFWD tests. The LFWD is also a non-destructive testing device, but the testing procedure involves dropping a 10 kg weight freely onto the loading plate, which might cause additional sample compaction. The testing program in the boxes was designed to start with the Geogauge measurements, followed by the LFWD tests, the DCP test, nuclear gauge readings, and PLT.

For each sample, Geogauge stiffness modulus (E_G) readings were taken at several locations (table 5) concentrated at the center of the box. At least two reliable readings were taken for each location. A proper seating of each Geogauge measurement was achieved as suggested by the manufacturer and all readings were recorded with a sketch of the location of data points (figure 10). The layout of lab tests is presented in figure 11.

LFWD readings were taken after completing the Geogauge tests. For each layer, the LFWD measurements were taken at several locations (table 5, figure 12a) at the same spots as the Geogauge readings (figure 11). As recommended by the manufacturer, at least three readings were taken at the same location to provide a single modulus value. The first one or two readings



Figure 10

The Geogauge device and the use of sand for proper seating

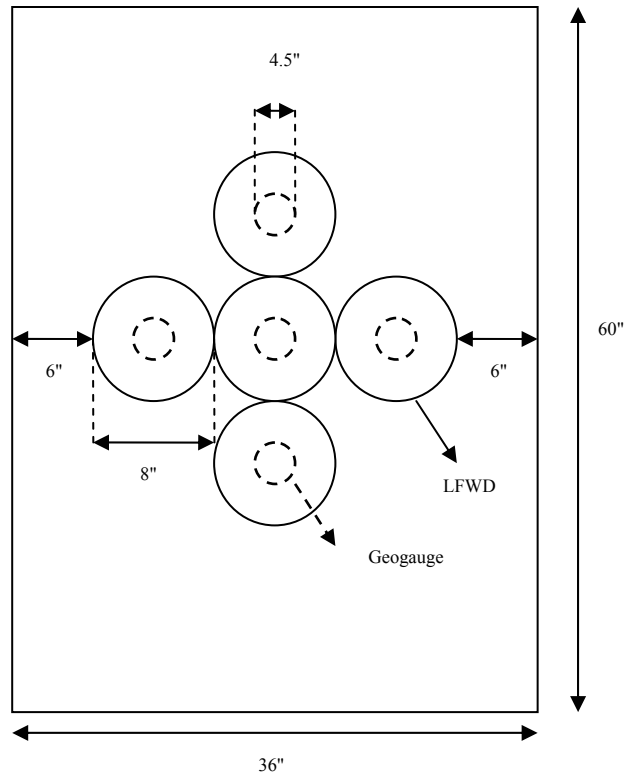


Figure 11

Layout of the Geogauge and the Light Falling Weight Deflectometer tests

were not included in any calculation since they were intended to remove any bedding errors and to ensure the plate's full contact with the surface. The displayed dynamic modulus (E_{LFWD}) values for each test were recorded with a sketch of testing locations.

Due to their destructive nature, DCP tests were also conducted after completing both the Geogauge and LFWD tests. Tests involved raising and dropping the hammer to drive the cone through the tested materials (figure 12b). The cone's penetration depths of the cone were recorded after each blow or every two blows, depending on the resistance of the tested material. In this investigation, DCP penetrations of up to 16 inches depth were recorded.

Two DCP tests were performed for most of the prepared layers. In order to minimally disturb the samples, one DCP test was conducted at each time for cement-soil and Blended Calcium Sulfate (BCS) layers. The two points were selected from the front and back halves of the soil surface, away from the middle of the sample since the plate load tests had to be conducted at the center of the box, as shown in figure 13. An example profile of DCP test results is illustrated in figure 14, which shows that the two DCP readings are very repeatable. It also suggests that the sample has uniform strength at different locations with the same depth. The average penetration rate for the sample was 13 mm/blow. However the test results indicated a relatively weaker layer from 250 mm to 325 mm depth (~ 20 mm/blow), which is still within the limiting DCP penetration rates for clay/silt subgrades as suggested by MnDOT.

The PLT was also used to evaluate the strength of constructed sections. The results of the plate load test apply to a depth of about 1.5-2.0 times the diameter of the plate on compressible soils. Round plates with 8-10 in. diameters were used for the project. The 10 in. diameter plate was preferred in order to have enough loading increments, especially for cases where the test layer could not handle high stresses.

The PLT was used as a reference test to obtain the strength characteristics of the layers. One test for each test case was conducted. A loading frame that was designed to fit to the boxes was used as a support for the test. A bearing plate and hydraulic jack were carefully placed at the center of the samples under the loading frame (figure 15). The hydraulic jack has a resolution of 0.5 tons. Dial gauges that are capable of recording a maximum deformation of 1 in. with a resolution of 0.001 in. were used in the PLT. The ASTM-D1196 standard method was followed to perform the



(a)



(b)

Figure 12

(a) LFWD device, and (b) DCP device

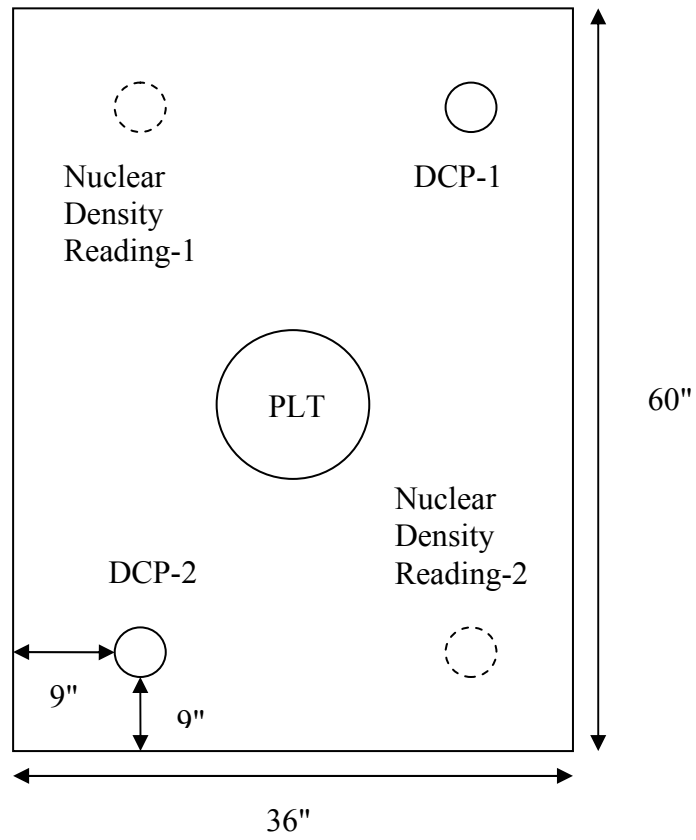


Figure 13

Layout of the DCP test, PLT, and the nuclear density gauge readings

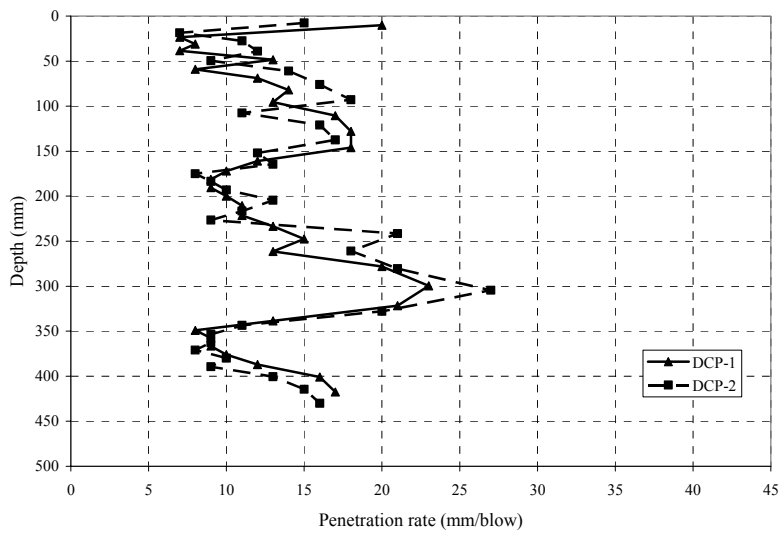


Figure 14

Sample profiles of DCP tests



Figure 15
Plate Load Test setup

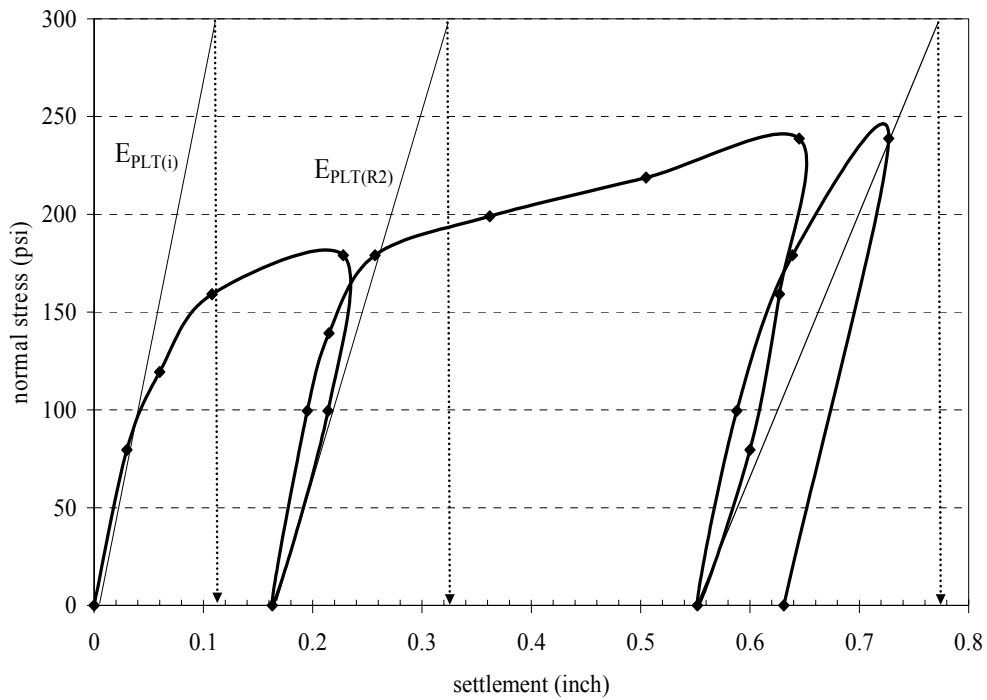


Figure 16
Typical Plate Load Test results

test. Plate diameter, applied load increments and the corresponding deflections were recorded for each load increment. Each sample was loaded up to failure or until the load capacity of the loading frame had been reached. Each sample was unloaded and reloaded at least once to be able to determine the reloading modulus of the samples in addition to the initial loading modulus (figure 16).

The Troxler nuclear density gauge was used to determine both the density and moisture content of the tested layers. Due to the disturbance caused by inserting the probe, nuclear density readings were taken after the completion of other tests. Density and moisture contents of the tested layers were recorded for 4-, 8- and 12- in. depths from the surface. Two sets of readings were taken from the front and back halves of the test boxes.

CBR samples representing the materials tested in the boxes were prepared according to the moisture content measured using the nuclear density gauge following the ASTM D1883 method. Standard molds of 6-in. diameter and 7-in. height were used for preparation. Because of the difficulty in making the exact density level, at least four samples with different compaction levels were prepared with the same required moisture content. Specimens were compacted at five layers. An automatic compactor with a 5-lb. hammer was used. The typical numbers of blows per layer were 10, 25, 56, and 75. After the dry density was obtained for each CBR sample, unsoaked CBR values were obtained for each compaction level and plotted versus the molded dry density values. The CBR value corresponding to the specific dry density of the represented material was then obtained by interpolation (figure 17).

Laboratory Investigation of Influence Depth and Moisture Content Effects. A series of tests were performed in two test boxes located at the LTRC Geosynthetic Engineering Research Lab (GERL) for the parametric study. The parametric study was divided into two parts. The objective of the first part was to investigate the relation between the Geogauge stiffness modulus and both the dry density and the moisture content for cohesive soils, and the objective of the second part was to determine the influence zone of the Geogauge and LFWD.

Experiment Setup. The two test boxes in which the tests were conducted were 900 mm (36 in.) wide, 1,824 mm (72 in.) long, and 900 mm (36 in.) deep (see figure 18). A clay layer was placed and compacted at the bottom of the first box, while a BCS layer was placed and compacted in the other box, using dynamic compactor.

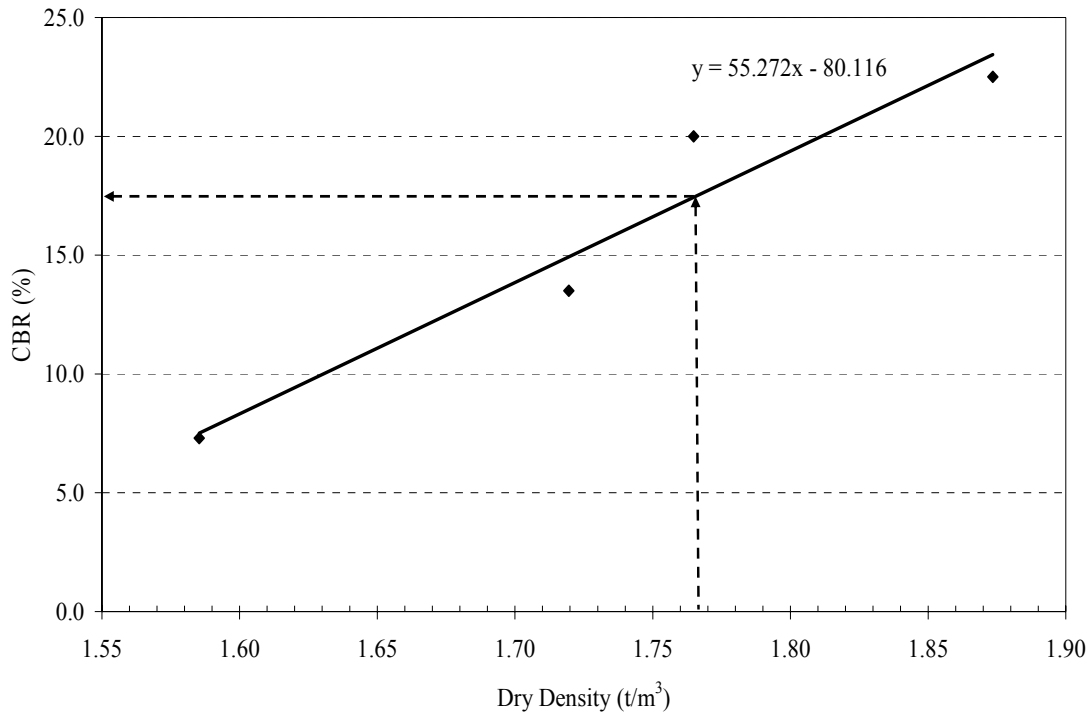


Figure 17
Determination of CBR for desired dry unit weight

Tests Procedure. For each experiment, a cylindrical mold with 300 mm (12 in.) diameter was first placed at the center of the box. Then 300 mm (12 in.) thick layer of soil was placed around this mold and compacted with a dynamic compactor. The cylindrical mold was then removed, which resulted in a cylindrical cavity of a 300 mm (12 in.) diameter surrounded by the soil to be tested (see figure 19). This procedure was done to simulate similar soil boundary condition effects.

For the first part, the tested material was placed inside the cylindrical mold and compacted in six 38 mm (1.5 in.) layers. The layers were compacted using a standard hammer dropped through its 18-in. drop height, 81 times per layer to achieve a compaction effort similar to that in the standard proctor test (12,400 ft.lb/ft³). After completing the sixth layer compaction, four Geogauge measurements were taken at the center of the compacted mold. The density was then measured using the nuclear gauge while two samples were taken from the soil mold to measure its moisture content.

To evaluate the influence depth, the tested material was placed in the cylindrical mold and compacted in 30 to 75 mm (1 to 3 in.) thick layers up to a 300 mm (12 in.) thickness. Each layer was well compacted with a standard hammer. Upon completing the compaction of each layer, Geogauge and LFWD measurements were made at the center of the compacted soil. It should be noted that in order to clearly define the zone of influence for the LFWD and Geogauge, stiff soil was built on top of soft soil, and soft soil was built on top of stiff soil in these experiments. For example, BCS was placed on top of the softer clay layer, while clay soil and sand were placed separately on top of the stiff BCS layer.



Figure 18

Test box in which the experiments were conducted



Figure 19

Mold constructed within soil in test box

Test Materials. For the first experimental part, two types of cohesive soils were selected. The first soil was the clayey silt soil used to construct the section at the PRF site. The second cohesive soil was a sandy lean clay that had LL=37 and PI=22, and was classified as A6 and CL, according to the American Association of State Highway and Transportation (AASHTO) classification system and Unified Soil Classification System (USCS), respectively. In addition, the standard proctor test indicated that the soil had a maximum density of 18.4 kN/m³ (117.2 lb/ft³) and an optimum moisture content of 13.9 percent. Experiments for the second part were conducted on the PRF soil in addition to the sand and BCS that were used to construct the PRF trench backfill.

Field Testing

This study also included conducting field tests on several highway sections in different projects within the state of Louisiana. In addition, six test sections and three trenches were constructed and tested at the LADOTD Pavement Research Facility (PRF) site. In each field test, five Geogauge measurements, five LFWD measurements, and two DCP measurements were taken. The PLT and FWD tests were also conducted on each test section for use as reference measurement. The dry unit weight and moisture content were obtained using the nuclear density gauge. Figure 20 describes the layout of the field tests. It should be indicated that the reported DCP-PR represents the average penetration rate along the thickness of the tested layer. The following sections describe in detail the field tests conducted in this study.

US Highway 190. Tests were conducted at three different stations (12+530, 12+650, and 15+800) on highway US 190. In all tests, a 200 mm (8 in.) thick crushed limestone base course section built on top of a 200 mm (8 in.) lime-treated subbase layer was tested. The crushed limestone had the gradation shown in figure 21 and was classified as A-1-a, and GW-GC, according to the AASHTO classification system and the USCS, respectively. Figure 22 shows the layout and profile of the tested section. Table 8 presents the results of dry density and moisture content using the nuclear density gauge.

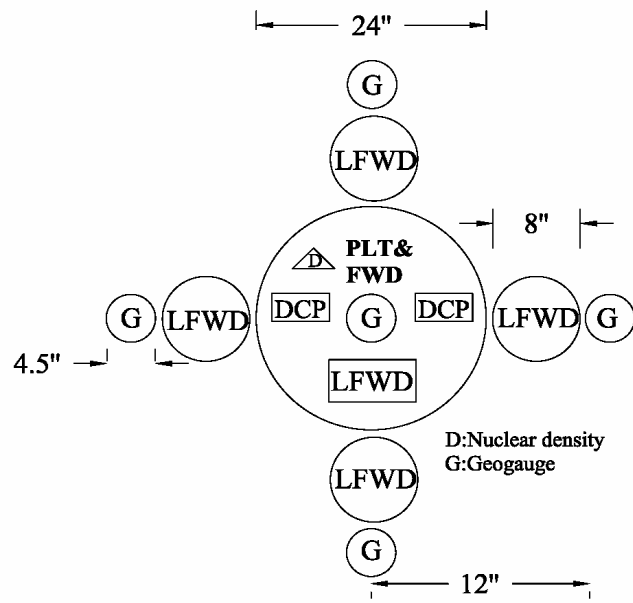


Figure 20
Layout of field test measurements

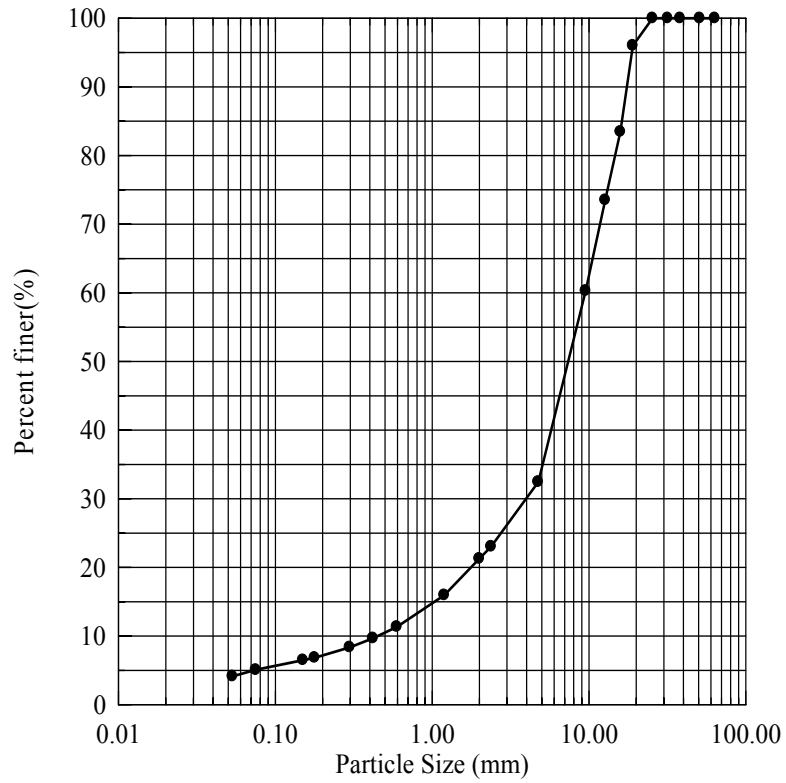


Figure 21
Gradation for the crushed limestone tested at US 190

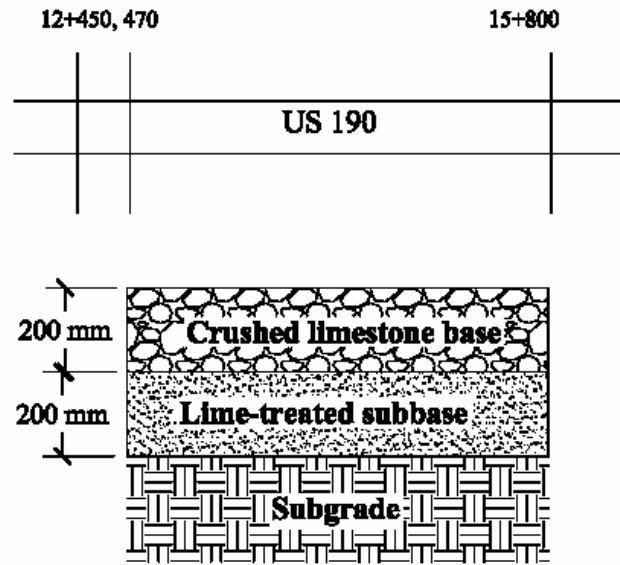


Figure 22
Layout and profile for sections at highway US 190

Table 8
Dry density and moisture content measurement of US 190

Station	γ_d kN/m ³	mc %
12+530	18.9	7.8
12+650	18.9	8.85

Louisiana State Highway 182. While the pavement section on Louisiana State Highway 182 was reconstructed, four sections were selected and tested including subgrade, lime-treated and cement-treated subbases, and cement-treated base sections. The layout and profile of the sections tested is presented in figure 23. In the first section, the subgrade layer located at station 47+10 was tested before and after the soil was treated by mixing it with 10 percent lime by volume. The subgrade soil was classified as A6 and CL, according to the AASHTO classification system and USCS, respectively.

In addition, the optimum moisture content and the maximum dry unit weight obtained in the standard proctor test for the subgrade soil were 16.57 kN/m³ (105.5 lb/ft³) and 16.4 percent,

respectively. The second section was a 300 mm (12 in.) thick cement stabilized subbase that was tested at stations 319+00 and 319+10. This section was constructed by mixing the soil with 4 percent of cement by volume. The soil in this section was classified as A4 and CL-ML according to the AASHTO classification system and USCS, respectively. The soil also had an optimum moisture content of 10.7 percent, and a maximum dry unit weight of 19.6 kN/m^3 (124.8 lb/ft^3), as measured in the standard proctor tests. The third section was 254 mm (10 in.) thick cement stabilized base and was tested one day after construction at station 173+68. This section was built on top of a 300 mm (12 in.) thick lime-treated subbase, and it was constructed by mixing the soil with 6 percent of cement by volume. In the fourth test section, a 300 mm (12 in.) thick lime-treated subbase was tested at stations 503+90, 504+00, and 504+10. This section was constructed by mixing the soil with 10 percent of lime by volume. The soil in this section was classified as A4 and CL, according to the AASHTO classification system and USCS, respectively. The standard proctor curve indicated that the soil had an optimum moisture content of 10.4 percent, and a maximum dry unit weight of 19.1 kN/m^3 (121.3 lb/ft^3). The dry density and moisture content measurements are presented in tables 9.

US Highway 61. Field tests were conducted during the compaction of a 300 mm (12 in.) thick subbase layer at US highway 61. A rubber tire roller was used in the compaction process. A test section was selected and tested after the first and fourth roller pass, using the Geogauge, LFWD, DCP and FWD. The PLT was conducted only after the fourth pass. The tested subbase layer consisted of unstabilized soil classified as A4 and CL-LM, according to the AASHTO classification system and USCS, respectively. The standard proctor test results indicated that the maximum dry unit weight and optimum moisture content for this soil were 17.5 kN/m^3 (111.4 lb/ft^3) and 17.1 percent, respectively. The dry unit weight and moisture content was measured after the fourth roller pass and they were 16 kN/m^3 and 15.63 percent, respectively.

The constructed layers in each section had an overall thickness of 300 mm (12 in.) and were compacted using a smooth wheel roller. The Geogauge, LFWD, DCP, and dry unit weight measurements were conducted during the compaction process of each section, while the FWD and PLT were conducted after the completion of compaction (figure 27). In addition, all tests (except for the nuclear density gauge) were conducted with time on sections constructed from materials that gain strength with time (cement-soil, lime-treated soil, and BCS sections). The following sections describe the tests.

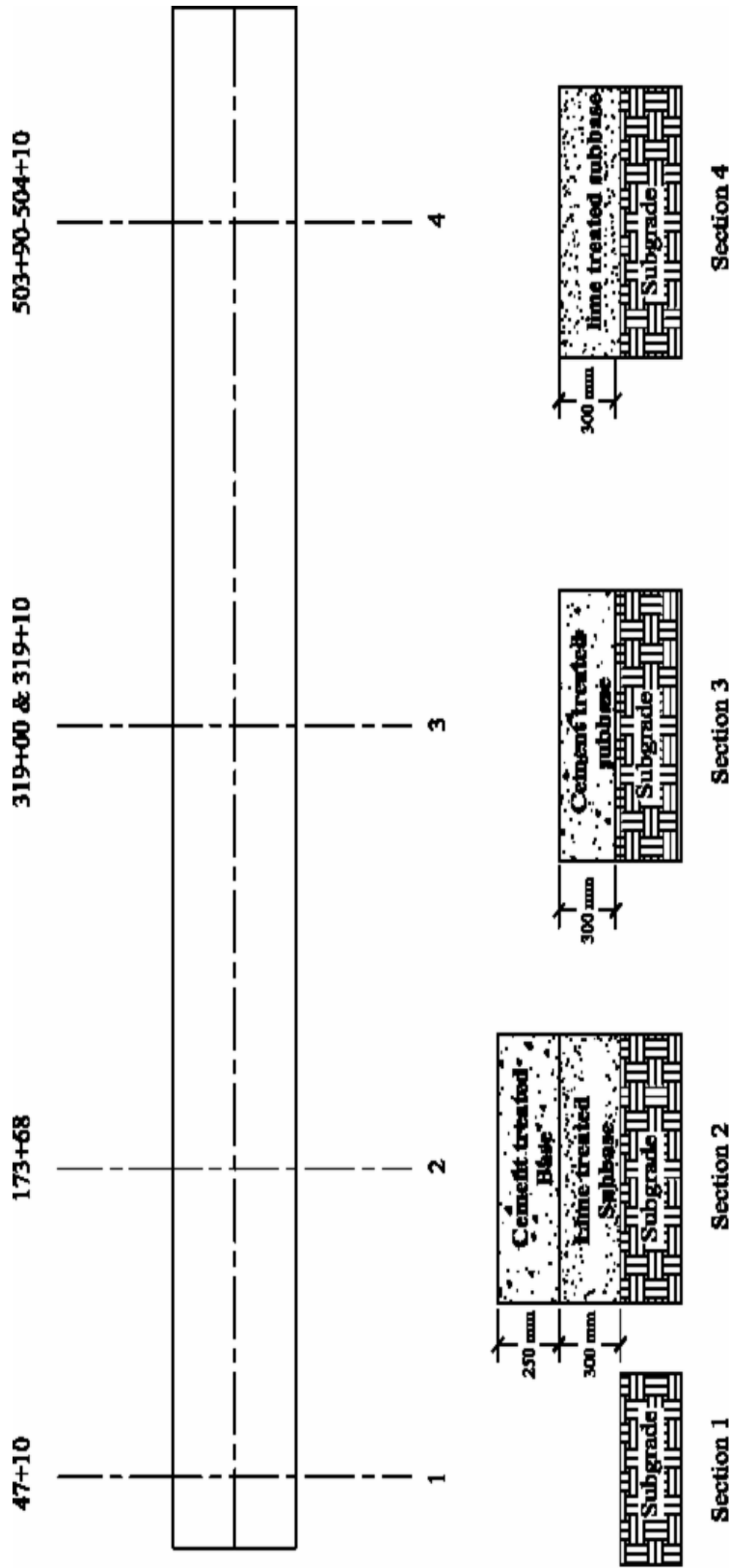


Figure 23 Cross-section of tests at highway LA 182

Table 9
Dry density and moisture content measurements at highway LA 182

Section	Station	γ_d (kN/m ³)	mc %
Untreated Subgrade	47+10	15.9	21.20
Lime-treated subgrade	47+10	--	--
Cement-treated base course	173+68	17.8	10.70
Cement-treated subbase	319.00	16.4	12.90
	319+10	16.3	12.80
Lime-treated Subbase	503+90	17.0	9.50
	504+00	17.5	10.20
	504+10	--	--

Test Sections at LADOTD Accelerated Loading Facility (PRF): Six sections were constructed at the LADOTD Accelerated Loading Facility (PRF) site to simulate base and subbase layers in pavement sections. These sections included one clayey silt soil, two cement-treated soils, one lime-treated soil, one Blended Calcium Sulfate (BCS), and one crushed limestone. Figure 24 describes the layout and profile of the six test sections constructed at the PRF site. Because the subgrade was weak, it was compacted well and was treated with lime in some sections. The clayey silt soil, the two cement-soils, and the lime-treated sections were constructed from soil available at the PRF site. The soil had 72 percent silt, 19 percent clay and a PI=15; it was classified as A4 and CL-ML, according to the AASHTO classification system and USCS, respectively. The soil had a maximum dry unit weight of 16.3 kN/m³ (104 lb/ft³) and optimum moisture content of 18.5 percent, measured in the standard proctor test (figure 25). The moisture content of the soil was taken directly before construction, which averaged 18.9 percent, close to the optimum moisture content for this soil. All sections were approximately 3 m × 3 m (10 ft. × 10 ft.); except for the BCS section that was 1.8 m × 3 m (10 ft. × 10 ft.) (figure 26).

Clayey Silt Soil Section. This section consisted of three sub-layers, each of which had a thickness of 100 mm (4 in.). The first and second layers were compacted by four roller passes. However, the third layer was compacted by six roller passes. The Geogauge, LFWD, and nuclear density tests were conducted at different passes during the construction, while the DCP, PLT, and FWD tests were conducted only after the sixth roller pass of the third sub-layer.

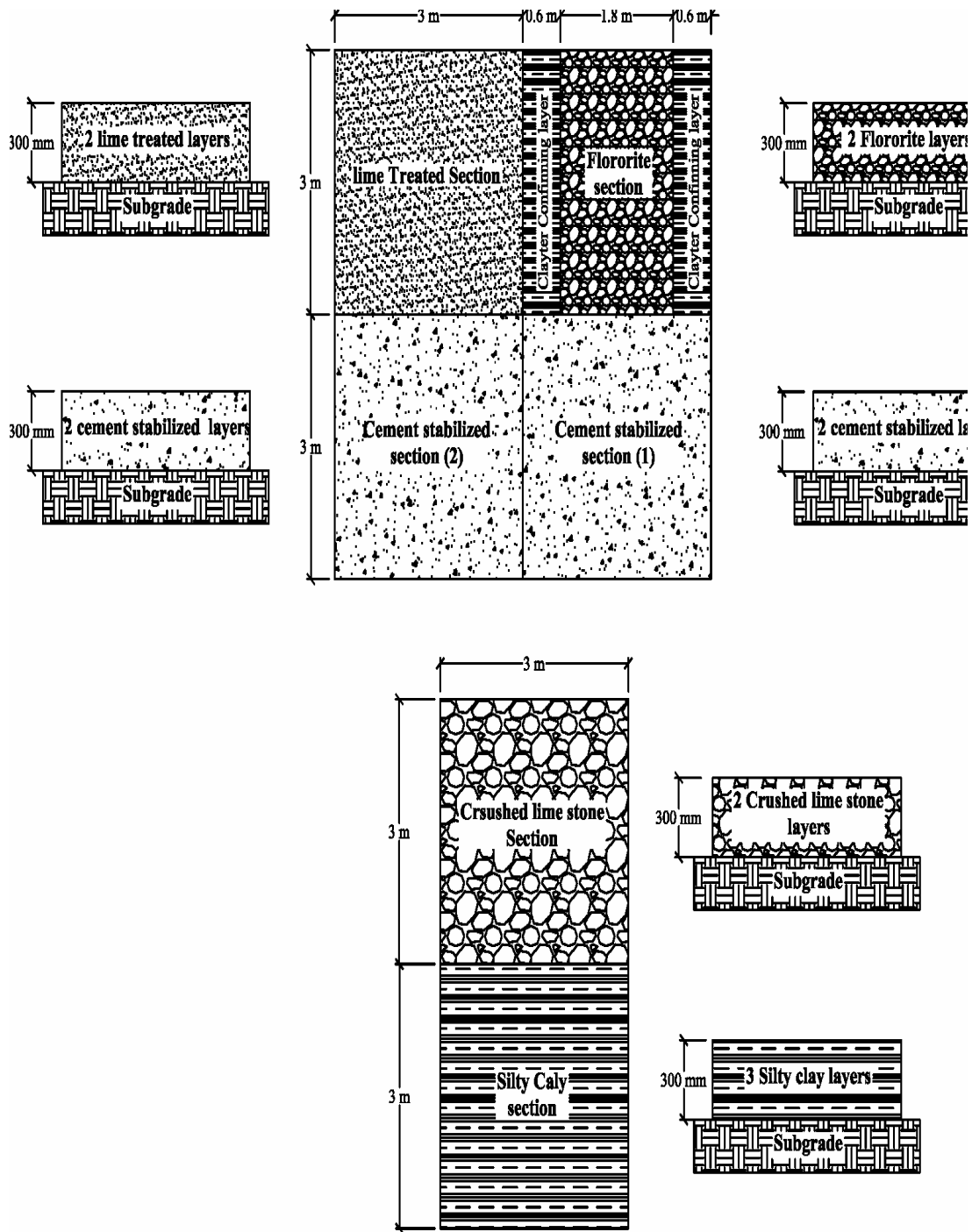


Figure 24

Cross-section PRF site Sections

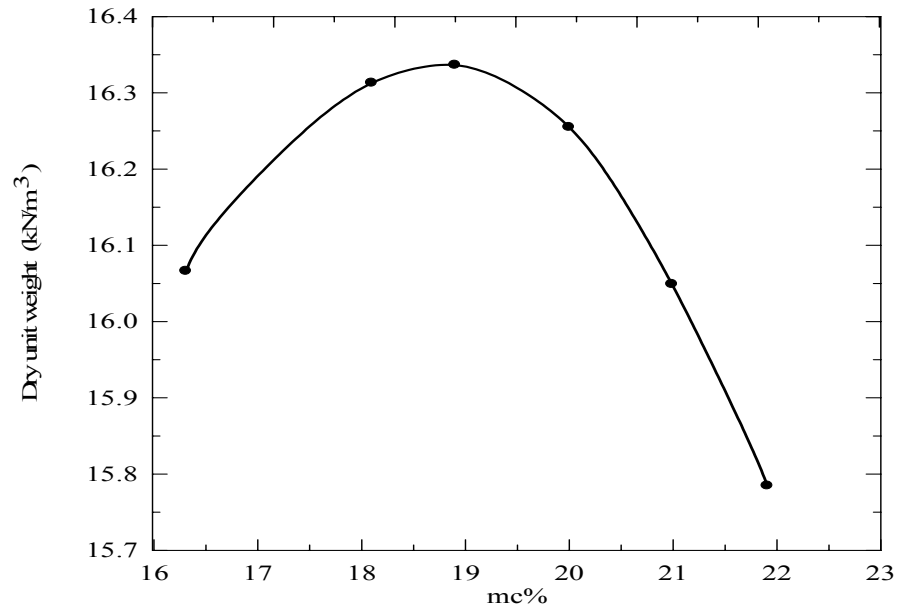


Figure 25

Proctor curve for clayey silt soil used in PRF sections



Figure 26

Different sections constructed at PRF Site

Cement-Soil Section (1). This section consisted of two 150 mm (6 in.) sub-layers of cement-treated soil constructed on top of the existing natural subgrade. Each layer was constructed by mixing the clayey silt soil with 5 percent of cement by volume using a tiller. After mixing and leveling, the two sub-layers were compacted together for six passes of the wheel roller (see figure 28).



Figure 27

Conducting tests on cement-soil and crushed limestone sections at PRF site



Figure 28

Construction of PRF sections

Cement- Soil Section (2). This section was also constructed by compacting of two sub-layers, 150 mm (6 in.) each. The two sub-layers were constructed in the same way and from the same material as the previous section. However, unlike the previous section, the first sub-layer was compacted and tested before constructing the second sub-layer.

Lime-Treated Soil Section. This section was constructed by compacting two 150 mm (6 in.) sub-layers of lime-treated soil. In each sub-layer, the clayey silt soil was mixed with 8.5 percent

lime by volume using a tiller. This section was constructed following the procedure in previous cement soil section (2).

Crushed Limestone. This section consisted of two 150 mm (6 in.) sub-layers that were constructed by mixing crushed limestone with 10 percent of clayey silt soil by volume using a tiller. The silt was required to bring it within the acceptable specification. The tested material had the gradation shown in figure 29. The Standard Proctor test showed that the maximum dry unit weight and the optimum moisture content for this material were 21.46 kN/m³ (137.8 lb/ft³) and 5.94 percent, respectively.

Blended Calcium Sulfate (BCS) Section. This section was also constructed by compacting two BCS sub-layers. The BCS is a chemical by-product of agriculture industry; it consists of 39.2 percent Calcium Oxide, 51.15 percent Sulfur Trioxide, 0.6 percent Silicon dioxide, 0.75 percent Phosphorous Pent oxide, 0.38 percent Potassium, and 0.81 percent Aluminum Oxide (Sorrento Companies Inc. DBA Louisiana Stone & Aggregates, 2003). The BCS material used in this study has the gradation shown in figure 30. The maximum dry unit weight and optimum moisture content were 17.2 kN/m³ (109.2 lb/ft³) and 10.1 percent, respectively, as measured by the standard proctor test. This section had dimensions of 1.8 m × 3 m (6 ft. × 10 ft.).

Trench Sections. Trench sections were also built at the PRF site as a joint effort with another project for controlling trench backfill construction. For this purpose, three trenches were excavated in the ground with the dimensions of 1.3 × 5 × 1 m (4 × 15 × 3 ft.) (see figures 31 and 32). Each trench consisted of three layers, each of which had a thickness 300 mm (12 in.). Each trench was divided into three equal sections compacted at different compaction efforts: light, moderate, and heavy. The light compaction was achieved by one compaction pass using a vibratory plate compactor (Wacker Packer, Model Number WP1550 AW, 200 lb.); the medium compaction was achieved by four compaction passes using the vibratory plate compactor; and the heavy compaction was achieved by four compaction passes using a Wacker Packer compactor (Model BS45Y 53 kg, 117lb.) in addition to four vibratory plate compaction passes (figure 33).

After constructing each layer, Geogauge, LFWD, DCP, and dry unit weight measurements were taken for each section (figure 34). The PLT and FWD tests were conducted only after completing the compaction of the top layer. The first trench was constructed from crushed

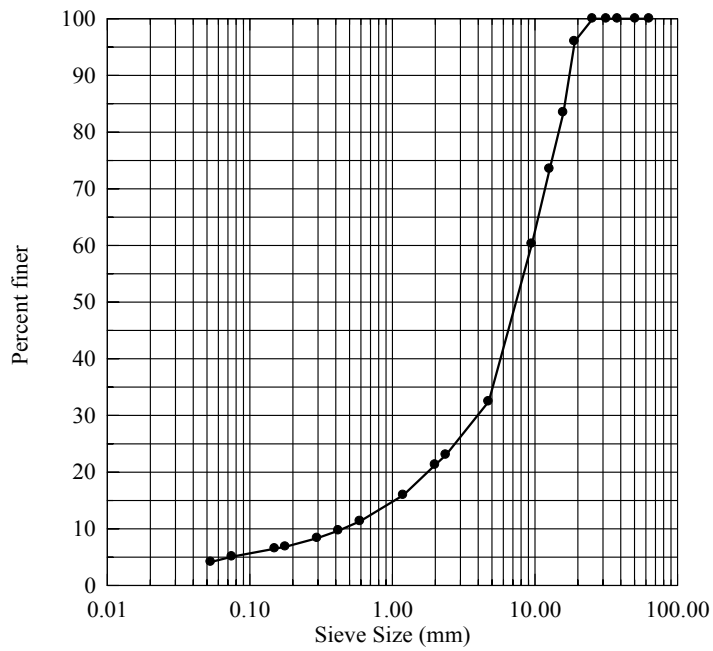


Figure 29

Gradation of tested material at the crushed limestone section

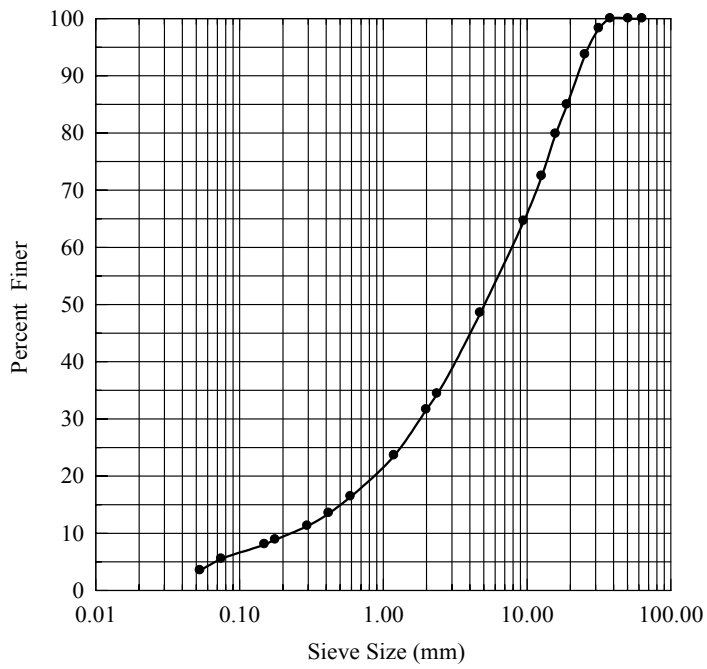


Figure 30
Gradation of BCS

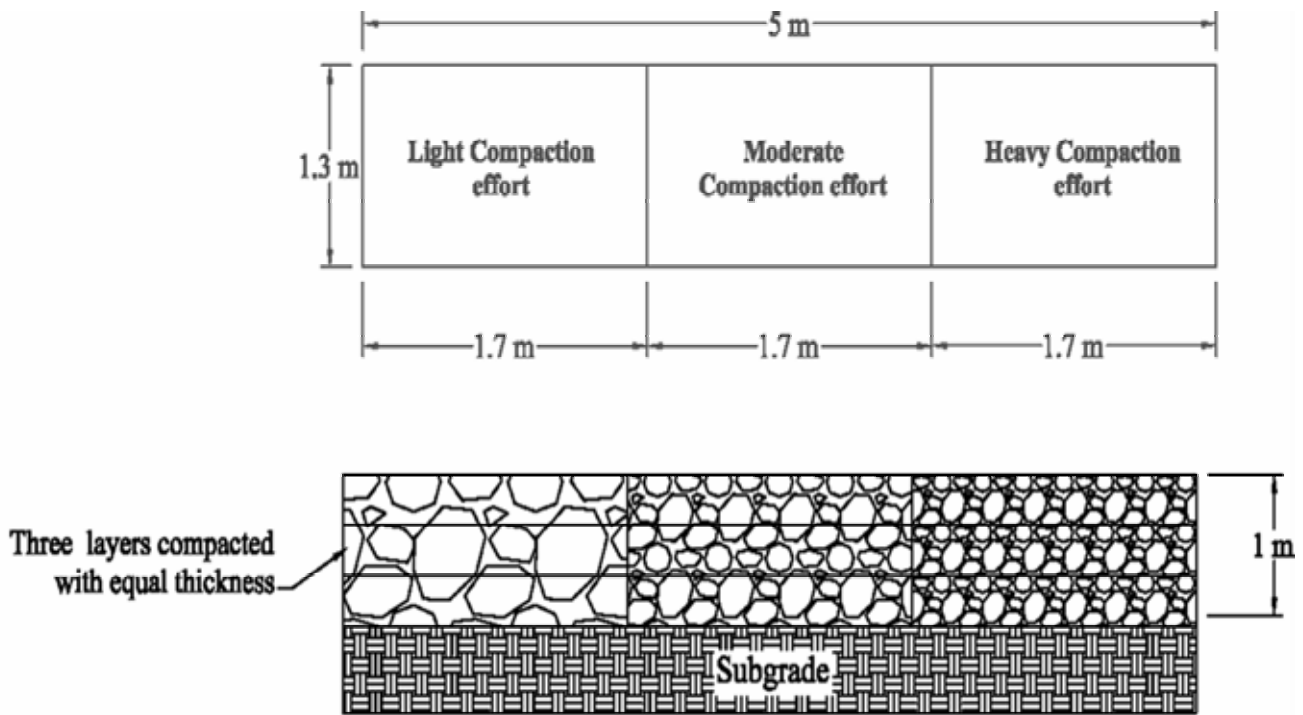


Figure 31
Layout and cross-section for PRF trench sections

limestone that was classified as A1-a and GP-GM, according to the AASHTO classification system and USCS, respectively, and had the gradation shown in figure 35.

The optimum moisture content and the maximum dry unit weight were 6.2 percent and 21.37 kN/m^3 (135.95 lb/ft^3), respectively. The second trench was constructed from sand that was classified as A-1-b and SP according to the AASHTO classification system and USCS, respectively, and had the gradation shown in figure 36. The sand also has a maximum dry unit weight of 16.8 kN/m^3 (107.86 lb/ft^3) and an optimum moisture content of 4.2 percent, measured in the standard proctor test. The third trench was constructed from Recycled Asphalt Pavement (RAP). This material is the product of milling the asphalt pavement of an existing roadway. The RAP material was classified as A-1-a and GP, according to the AASHTO classification system and USCS, respectively. The gradation of RAP material used is shown in figure 37. The RAP also has a maximum dry unit weight of 18.41 kN/m^3 (117.1 lb/ft^3) and an optimum moisture content of 8.6 percent as measured in the standard proctor test.



Figure 32
Construction of trenches at PRF site



Figure 33
Compaction of trenches at PRF site



Figure 34
Testing RAP and sand trenches at PRF site

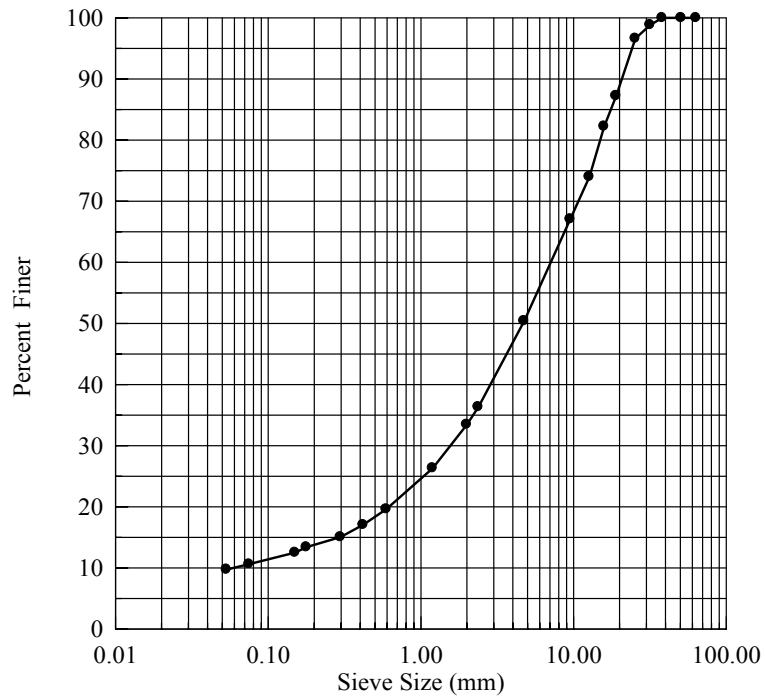


Figure 35
Gradation of crushed limestone

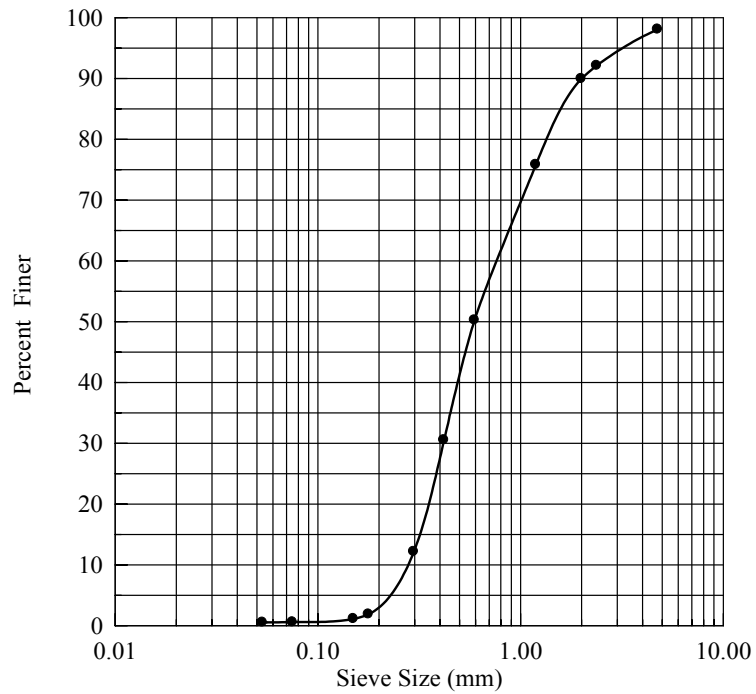


Figure 36
Gradation of sand

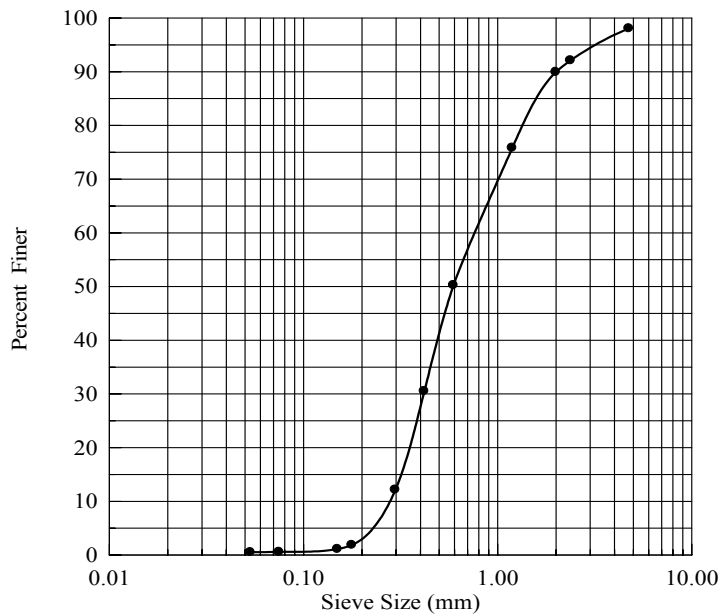


Figure 37
Gradation of RAP



Figure 38

United machine used to conduct CBR test

CBR Tests. CBR laboratory tests were also conducted on samples collected from field projects and test sections. All samples were prepared in accordance with ASTM D1883-99 without soaking them to replicate same field conditions. For unstabilized soils, all samples were prepared at the moisture content that was measured in the field; for stabilized soils, samples were prepared at the moisture content during construction.

Samples of lime-treated and cement-treated soil were tested in the same sequence as they were tested in the field. For example, if the field tests were conducted on these soils after one day of construction, then the laboratory samples were prepared in a CBR mold, placed in plastic bags (to isolate them from the surrounding environment) and then kept in the LTRC humidity room for one day before testing. The United machine (figure 38) at the LTRC soil lab performed the tests. This machine is fully automated with a piston that penetrates the prepared samples and has a load cell that records the resistance of the soil to penetration. The results of the CBR tests are presented later in this report.

Laboratory Test Results

Geogauge Laboratory Results. The Geogauge stiffness moduli for each test conducted in the laboratory testing program case are summarized in table 10 with their corresponding standard deviations and coefficients of variation (CV) for each test case. A default Poisson's ratio of 0.35 was used for all test samples. However, the data presented in this section were corrected by using the suitable Poisson's ratio for each sample, as presented in table 10. For each test case, the Geogauge tests were conducted at several locations concentrated at the center of the test box. Several modulus readings were recorded and averaged to get a single stiffness modulus value for each location on the test layer. The mean of successful measurements, which represent the stiffness modulus of each location, was then averaged to obtain the representative Geogauge stiffness moduli of each test layer. Standard deviations of moduli values for different test locations are also corrected for Poisson's ratio variations and summarized in table 10 together with the representative Geogauge stiffness modulus values for each test layer. The lowest CV was obtained in the sand layer and the highest CV was obtained in the cement-soil layers. The average CV during the testing program with the Geogauge device was found to be 12.5 percent.

A total of 28 test cases were conducted in which each one was represented by the average Geogauge stiffness modulus value (E_G). The maximum Geogauge stiffness modulus value was obtained after 11 days for 2 percent cement soil, which is 291.7 MPa. The minimum Geogauge modulus value was obtained for clayey silt-3 (w.c. = 20.1 percent), which is 16.3 MPa. Although 16.3 MPa is below the measurement range of the Geogauge as stated in the Geogauge User Guide Version 3.8, which is from 26.2 MPa to 610 MPa, the Geogauge readings for the clayey silt-3 layer were consistent and all were below the range.

The Geogauge values for the different types of materials given in table 10 were considered as one data set in the analysis. Possible correlations of the Geogauge modulus with the PLT, DCP, and CBR test results were investigated and will be presented later in this report. Dividing the data set into several soil groups would lead to insufficient data and would decrease the reliability of correlations even if there were any individual correlations for each type of material. In table 10 and throughout all of the laboratory experiments, the layers were grouped into five types for simplicity. The first group was the clay soil; the second group included the cement-soil layers, which may be denoted as CC2, CC4 (2 percent, 4 percent cement by weight, respectively) or CC (cement soil); the third group was the coarse grained material (stone), which can be denoted as

Table 10
Geogauge test results

Sample Id	Time (day)	Poisson's Ratio	Geogauge Stiffness Modulus (MPa)	Std. Deviation (MPa)	CV (%)
Clay 1		0.3	173.3	15.5	8.9
Clay 2		0.3	179.4	19.8	11.1
Clay 3		0.4	136.7	13.2	9.7
Clay 4		0.3	154.1	13.5	8.7
Clay 5		0.4	80.0	4.6	5.7
Clay 6		0.25	240.8	20.6	8.6
Clay 7		0.3	162.3	34.1	21.0
Clay 8		0.4	68.2	6.4	9.4
Clay 9		0.3	162.3	30.4	18.7
2%Cem+Clay	0	0.25	240.6	20.4	8.5
	4		266.2	24.5	9.2
	7		282.3	30.3	10.7
	11		291.7	40.5	13.9
	13		267.2	28.8	10.8
4%Cem+Clay	1	0.25	186.4	46.3	24.8
	6		222.2	63.7	28.7
	14		251.0	97.4	38.8
	20		218.5	68.1	31.2
Sand clay gravel		0.35	217.1	20.4	9.4
Crushed Limestone-1		0.35	155.3	4.9	3.1
Crushed Limestone-2		0.35	124.7	9.5	7.6
RAP		0.35	98.3	3.7	3.8
Clayey Silt-1 (opt.)		0.4	56.4	8.7	15.5
Clayey Silt-2 (dry)		0.4	67.0	2.9	4.3
Clayey Silt-3 (wet)		0.4	16.3	1.9	11.4
Sand-1		0.3	56.4	4.8	8.5
Sand-2		0.3	49.7	2.7	5.4
Sand-3		0.3	49.7	1.1	2.3
				Avg.	12.5

Table 11
Descriptive statistics of the geogauge results

Geogauge Modulus (MPa)	Number of tests	Mean value (MPa)	Min. value (MPa)	Max. value (MPa)	Lower CL*.(90%)	Upper CL*.(90%)
Clay	9	150.8	68.2	240.8	118.5	183.1
Cement-soil	9	247.3	186.4	291.7	226.4	268.3
Stones	4	148.8	98.3	217.1	88.7	209.0
Clayey Silt	3	46.6	16.3	67.0	1.5	91.6
Sand	3	51.9	49.7	56.4	45.4	58.5
ALL	28	159.7	16.3	291.7	133.2	186.3

- CL: Confidence Limit.

ST; the fourth group included the clayey silt layers, which can be denoted as CS; and the fifth group included the sand layers. Table 11 lists a summarized descriptive statistics of Geogauge modulus values for each group of layers.

LFWD Laboratory Results. The LFWD dynamic modulus values for all test layers are summarized in table 12 with their corresponding standard deviations and coefficients of variation (CV) values for each layer. There were a total of 28 test cases and each case was represented by an average LFWD dynamic modulus value. However, the LFWD data for the clay-2 layer was questionable and will be excluded from the data and discussion. The LFWD dynamic modulus readings for clay-2 layer were highly inconsistent and ranged from 400 MPa to 700 MPa, which is also too high compared to strength results obtained from other tests.

After excluding the LFWD value for the clay 2 layer from analysis, the maximum LFWD modulus value was obtained for the 20-day old CC2 layer, which was 541.6 MPa. The minimum LFWD modulus value was obtained for the sand-1 layer, which was 18.0 MPa. Table 13 lists a summary of descriptive statistics of LFWD modulus values for each group of layers. The highest average LFWD modulus was obtained in cement-treated clay layers. The highest coefficient of variation was up to 55.8 percent for the sand-1 layer.

Table 12
LFWD test results

Layer Id	Time (day)	LFWD (MPa)	SD (MPa).	CV (%)
Clay 1		182.3	19.0	10.4
Clay 2		-	-	-
Clay 3		52.5	10.3	19.7
Clay 4		134.9	63.0	46.7
Clay 5		48.6	9.4	19.4
Clay 6		314.9	39.5	12.5
Clay 7		228.6	72.3	33.5
Clay 8		34.2	0.8	2.4
Clay 9		171.4	2.0	1.2
2%Cem+Clay	0	294.2	112.9	38.4
	4	412.2	53.8	13.0
	7	442.7	61.7	13.9
	11	435.9	54.1	12.4
	13	412.4	98.0	23.8
4%Cem+Clay	1	500.0	94.7	18.9
	6	530.6	79.7	15.0
	14	477.5	236.4	49.5
	20	541.6	160.3	29.6
Sand clay gravel		300.4	92.2	30.7
Crushed Limestone-1		74.4	12.7	17.2
Crushed Limestone-2		131.2	3.9	3.0
RAP		138.3	33.9	24.5
Clayey Silt-1 (opt.)		31.4	4.4	13.9
Clayey Silt-2 (dry)		49.8	8.5	17.1
Clayey Silt-3 (wet)		28.5	13.2	46.3
Sand-1		18.0	5.7	55.8
Sand-2		40.7	3.8	13.9
Sand-3		20.6	5.3	27.6
			Average CV	23.1

Table 13
Descriptive Statistics of the LFWD Results

LFWD Dynamic	Number	Mean	Min.	Max.	Lower	Upper
Clay	8	145.9	34.2	314.9	79.8	212.0
Cement + Clay	9	449.7	294.7	541.6	402.9	496.4
Stones	4	161.1	74.4	300.4	46.7	275.4
Clayey Silt	3	36.6	28.5	49.8	17.1	56.1
Sand	3	26.4	18.0	40.7	5.5	47.4
ALL	27	224.0	18.0	541.6	163.3	284.7

*CL: Confidence Limit

DCP Laboratory Results. The DCP penetration rates (mm/blow) representing each tested layer were calculated at 8 in. and 12 in. depths and are listed in table 14. The reason for averaging the DCP readings at two different depths was to use the appropriate average PR when correlating the DCP with other devices. Since the influence depth of the Geogauge is about 8 to 9 in. as seen in the parametric study, the average PR values for 8 in. depth were used to correlate the DCP- PR with values. However, the average PR values for 12 in. depth are used to correlate with PLT and LFWD. DCP tests were conducted on 26 laboratory test cases. The reason for not conducting the DCP tests in 4-and 11-day old CC2 layers was to minimize the destruction of the layers without additional holes and cracks from DCP tests.

PLT and CBR Laboratory Results. The plate load and the CBR test results are given in table 15. Both PLT and CBR tests are considered reliable tests that have a long history in soil strength determination. In base layers that were tested with time, the PLT for each cement content was limited to two tests due to the destructive nature of the test and the space limitation of the test boxes. Twenty-three PLTs were conducted. The CBR experiments were conducted on all materials other than cement-soil layers. Nineteen CBR tests were conducted in the laboratory research, each with three or four different compaction efforts needed to obtain the corresponding CBR value for the desired density.

Table 14
DCP test results

LAYER ID	Time (day)	DCP - 8 inch (mm/blow)	DCP - 12 inch (mm/blow)
Clay 1		12.0	13.3
Clay 2		16.7	19.0
Clay 3		41.5	32.8
Clay 4		36.1	28.8
Clay 5		18.4	11.2
Clay 6		10.6	9.2
Clay 7		22.5	23.5
Clay 8		30.7	33.1
Clay 9		8.4	9.6
2%Cem+Clay	0	13.8	11.8
	4	-	-
	7	10.5	9.8
	11	-	-
	13	8.3	7.4
4%Cem+Clay	1	6.4	5.9
	6	5.0	4.8
	14	4.4	4.3
	20	4.0	3.7
Sand clay gravel		7.5	7.5
Crushed Limestone-2		13.7	12.1
Crushed Limestone-2		8.8	7.2
RAP		9.0	8.4
Clayey Silt-1 (opt.)		26.1	25.5
Clayey Silt-2 (dry)		18.8	17.6
Clayey Silt-3 (wet)		49.3	46.5
Sand-1		25.5	20.9
Sand-2		27.4	24.7
Sand-3		61.0	53.4

Table 15
Plate Load Test and CBR test results

LAYER ID	Time (day)	E_{PLT(i)} (MPa)	E_{PLT(R2)} (MPa)	CBR (%)
Clay 1		143.4	80.5	24.2
Clay 2		75.3	89.4	25.5
Clay 3		40.6	36.4	8.0
Clay 4		62.7	42.6	12.2
Clay 5		42.1	40.4	10.5
Clay 6		228.1	173.1	19.6
Clay 7		87.1	58.7	9.7
Clay 8		39.7	30.3	12.0
Clay 9		91.8	113.7	18.7
2%Cem+Clay	0	329.1	129.3	
	4			
	7			
	11			
	13	546.7	250.4	
4%Cem+Clay	1	375.3	481.0	
	6			
	14	454.6	649.8	
	20			
Sand clay gravel B.C.		268.9	217.2	19.0
Limestone		133.5	79.6	28.3
Crushed Limestone		121.0	123.2	45.2
RAP		93.8	95.0	10.5
Clayey Silt-1 (opt.)		67.6	24.3	4.6
Clayey Silt-2 (dry)		45.1	25.5	10.6
Clayey Silt-3 (wet)		6.8	8.4	1.9
Sand-1		37.6	48.0	15.7
Sand-2		33.0	51.9	4.4
Sand-3		53.8	34.2	3.5

Field Tests Results

Results of Highway Test Sections

Table 16 summarizes test results for the Geogauge, LFWD, and DCP tests conducted on all highway sections.

Table 16
Summary of test results on highway sections

Project	Station	E _G (MPa)	C _V %	E _{LFWD} (MPa)	C _V %*	DCP-PR (mm/blow)
US Highway 190						
Crushed limestone base	15+800	155.90	3.6	240	4.8	4.8
	12+530	128.5	3.2	106.13	5.6	6.9
	12+650	119.6	3.6	104.70	6.1	5.7
Highway LA 182						
Untreated subgrade	47+10	54.56	2.4	37.1	20.6	53.8
Lime-treated subgrade	47+10	63.90	4.0	28.04	28.0	36.0
Cement-treated base	173+68	238.15	7.1	366.9	3.2	3.3
Cement-treated subbase	319+00	113.55	6.0	56.0	11.4	12.8
	319+10	99.68	6.1	50.9	11.5	14.3
Lime-treated subbase	503+90	105.31	6.6	70.64	8.2	12.5
	504+00	107.64	5.8	71.56	9.2	12.2
Highway US 61						
Subbase	1	69.39	6.8	46.54	17.1	14.5
	4	80.05	4.2	69.26	15.8	10.3

PRF Site Test Results

The results for the Geogauge, LFWD, DCP, and nuclear density gauge tests that were conducted both during and after constructing sections at the PRF site are summarized in tables 17 through 36. The results of tests conducted on the trench sections constructed at the PRF site are presented in Tables 37 through 39.

Table 17**Geogauge, LFWD, and nuclear density gauge test results for PRF clayey silt section**

Sub-layer	Pass No.	E_G (MPa)	C_V %	E_{LFWD} (MPa)	C_V %	γ_d (kN/m ³)	mc %
Subgrade		34.50	--	--	--	--	--
First sub-layer	1	42.87	4.8	6.89	15.1	15.0	17.7
	2	41.88	6.4	8.10	14.8	15.8	18.4
	4	48.45	8.9	6.9	13.9	15.9	18.4
Second sub-layer	1	54.81	1.7	23.64	13.3	--	--
	2	66.05	3.4	24.66	11.1	--	--
Third sub-layer	1	56.07	1.6	20.77	12.0	--	--
	4	65.44	2.6	25.76	9.0	--	--
	6	77.78	4.3	35.5	12.1	16.5	16.6

Table 18**Summary of DCP result for three layers after six passes**

Layer	DCP-PR (mm/blow)
Constructed layers	29.0
Subgrade	12.4

Table 19**Geogauge, LFWD, and nuclear gauge test results with number of passes for cement-soil section (1)**

Pass No.	E_G (MPa)	C_V %	E_{LFWD} (MPa)	C_V %	γ_d (kN/m ³)	mc %
1	37.72	6.1	11.51	20.3	14.8	14.4
2	56.77	7.6	15.31	15.4	15.0	15.3
3	64.41	6.6	16.22	14.8	15.1	15.5
4	67.14	11.4	18.11	14.0	15.6	15.7
6	66.85	6.6	21.25	12.7	15.7	16.2

Table 20**DCP Test results with number of passes for cement-soil section (1)**

Pass No.	Layer	DCP
First	Constructed layer	43.5
	Subgrade	17.7
Sixth	Constructed layer	24.7
	Subgrade	21.6

Table 21**Geogauge and LFWD rest results with time for cement-soil section (1)**

Days After Construction	E _G	C _V	E _{LFWD}	C _V
2	108.57	7.6	--	--
3	133.37	8.0	76.37	6.5
6	136.54	4.5	99.15	5.0
13	137.90	7.1	102.07	7.9
23	146.14	6.6	116.39	4.0
31	124.85	7.8	129.18	4.2
37	118.58	7.0	127.1	7.4

Table 22**DCP test results with time for cement-soil section (1)**

Days after construction	Layer	DCP
2	Constructed layer	13.8
	Subgrade	17.2
6	Constructed layer	7.6
	Subgrade	21.3
13	Constructed layer	8.1
	Subgrade	14.1
23	Constructed layer	7.8
	Subgrade	13.7
31	Constructed layer	7.8
	Subgrade	16.9
37	Constructed layer	8.7
	Subgrade	13.3

Table 23**DCP test results with number of passes for cement-soil section (2)**

Pass No.	Layer	DCP-PR (mm/blow)
Fifth	First layer	23.6
	Subgrade	22.2
Sixth	Second layer	15.4
	Subgrade	21.6

Table 24**Test results with number of passes for cement-soil section (2)**

Sub-layer	Pass No.	E_G (MPa)	C_V %	E_{LFWD} (MPa)	C_V %	γ_d (kN/m ³)	mc %
Subgrade		26.87	--	--	--	--	--
First Layer	1	44.02	2.5	--	--	--	--
	2	57.16	5.6	--	--	--	--
	4	61.65	6.1	--	--	--	--
	5	66.19	7.7	20.84	10.1	15.4	15.1
Second Layer	1	73.34	5.1	--	--	--	--
	2	79.93	3.4	--	--	--	--
	4	84.10	5.8	--	--	--	--
	6	97.23	3.9	42.09	10.4	15.2	13.5

Table 25**Geogauge and LFWD test results with time for cement-soil section (2)**

Days After Construction	E_G (MPa)	C_V %	E_{LFWD} (MPa)	C_V %
3	194.39	6.5	228.48	2.4
10	196.70	6.4	189.1	6.1
20	186.87	6.1	184.2	6.0
28	160.09	3.9	--	--
34	150.85	6.6	169.72	5.8

Table 26
DCP test results with time for cement-soil section (2)

Days after construction	Layer	DCP-PR (mm/blow)
3	Constructed layer	5.7
	Subgrade	19.9
10	Constructed layer	5.4
	Subgrade	13.2
20	Constructed layer	6.0
	Subgrade	13.0
28	Constructed layer	6.1
	Subgrade	18.2
34	Constructed layer	6.9
	Subgrade	19.6

Table 27
DCP test results after six passes for lime-treated soil section

Layer	DCP-PR (mm/blow)
lime-treated layer	21.4
Subgrade	17.8

Table 28
Geogauge, LFWD, and nuclear gauge test results with number of passes for lime-treated soil section

Sub-layer	Pass No.	E _G (MPa)	C _V %	E _{LFWD} (MPa)	C _V %	γ_d (kN/m ³)	mc %
Subgrade		38.46	5.8	7.76	12.8	--	--
First Layer	2	72.90	4.7	--	--	--	--
	4	79.28	6.1	14.60	6.6	14.9	18.0
Second Layer	1	64.8	6.9	--	--	--	--
	2	79.66	6.1	--	--	--	--
	4	80.50	5.6	--	--	--	--
	6	83.3	4.0	30.02	12.5	15.2	16.2

Table 29
Geogauge, LFWD test results with time for lime-treated soil section

Days After Construction	E _G (MPa)	C _V %	E _{LFWD} (MPa)	C _V %
3	113.86	3.3	83.15	5.8
20	82.8	0.5	42.44	10.5
28	101.87	3.0	--	--
34	99.42	5.7	54.50	14.9

Table 30
DCP Test results with time for lime-treated soil section

Days after construction	Layer	DCP-PR (mm/blow)
3	Constructed layer	15.4
	Subgrade	16.5
20	Constructed layer	17.7
	Subgrade	18.2
28	Constructed layer	16.6
	Subgrade	16.3
34	Constructed layer	16.6
	Subgrade	23.9

Table 31
Geogauge, LFWD, and nuclear gauge test results with number of passes for crushed limestone section

Sub-layer	Pass No.	E _G (MPa)	C _V %	E _{LFWD} (MPa)	C _V %	γ_d (kN/m ³)	mc %
Subgrade	--	30.15	7.3	--	--	--	--
First Layer	2	57.65	1.7	23.33	12.7	--	--
	4	58.73	0.9			--	--
Second Layer	1	64.43	8.1	23.46	16.1	--	--
	2	72.11	5.5	45.35	17.2	--	--
	4	77.76	6.9	--	--	--	--
	6	91.78	3.9	81.47	10.9	19.2	7.5

Table 32
DCP results after construction of crushed limestone section

Layer	DCP-PR (mm/blow)
Constructed layer	12.1
Subgrade	15.1

Table 33
DCP test results after six passes for BCS section

Layer	DCP-PR (mm/blow)
Constructed layer	6.9
Subgrade	14.3

Table 34
Geogauge, LFWD, and nuclear gauge test results with number of passes for BCS section

Sub-layer	Pass No.	E _G (MPa)	C _V %	E _{LFWD} (MPa)	C _V %	γ_d (kN/m ³)	mc %
Subgrade		36.7	--	--	--	--	--
First Layer	1	146.7	7.6	8.38	17.3	14.5	30.3
	2	150.55	0.4	8.93	18.6	--	--
	4	136.92	3.7	33.01	14.7	--	--
Second Layer	1	186.69	3.1	--	--	--	--
	4	212.45	3.1	105.6	3.5	14.9	30.6

Table 35
Geogauge and LFWD with time for BCS section

Days After Construction	E _G (MPa)	C _V %	E _{LFWD} (MPa)	C _V %
1	294.72	--	214.55	--
5	394.23	1.7	249.43	4.1
12	348.57	5.5	228.34	5.1
22	335.35		224.92	
30	312.92	7.4	226.43	3.0
36	334.46	4.5	238.02	3.3

Table 36
DCP test results with time for BCS section

Days after construction	Layer	DCP-PR (mm/blow)
5	Constructed layer	5.5
	Subgrade	10.9
12	Constructed layer	5.7
	Subgrade	10.3
22	Constructed layer	5.9
	Subgrade	10.4
29	Constructed layer	6.6
	Subgrade	11.3
36	Constructed layer	6.5
	Subgrade	11.4

Table 37
Geogauge, LFWD, DCP, and nuclear gauge test results for crushed limestone trench

Layer	Compaction	E _G (MPa)	C _V %	E _{LFWD} (MPa)	C _V %	DCP-PR (mm/blow)	γ_d (kN/m ³)	mc %
First Layer	light	-	--	7.60	--	45.9	--	--
	Moderate	68.00	--	24.40	--	26.5	--	--
	Heavy	91.79	--	30.00	--	10.5	--	--
Second Layer	Light	57.4	2.8	34.5	13.5	43.8	18.7	4.8
	Moderate	72.7	4.1	49.0	12.4	23	19.0	5.1
	Heavy	99.6	4.8	79.0	2.1	9.5	21.8	5.2
Third layer	Light	51.93	2.8	30.25	13.5	37.8	18.9	4.9
	Moderate	73.06	4.0	57.28	9.3	23.1	19.1	5.2
	Heavy	95.6	3.8	82.69	3.8	9.8	21.1	5.6

Table 38**Geogauge, LFWD, DCP and nuclear gauge test results for sand trench**

Layer	Compaction	E _G (MPa)	C _V %	E _{LFWD} (MPa)	C _V %	DCP-PR (mm/blow)	γ_d (kN/m ³)	mc %
First layer	Light	67.83	--		--	68.5	16.4	4.0
	Moderate	77.00	--	--	--	27.2	16.6	3.2
	Heavy	66.39	--	--	--	18.1	16.0	5.5
Second Layer	Light	61.66	--	--	--	69.2	16.2	3.3
	Moderate	74.58	--	--	--	28.1	17.0	2.9
	Heavy	62.67	--	--	--	18.9	17.2	4.0
Third layer	Light	40.8	5.4	12.50	18.0	66.7	16.1	3.3
	Moderate	54.25	2.9	25.55	15.8	23.4	17.2	2.9
	Heavy	58.28	7.5	41.83	2.3	18.8	17.3	2.7

Table 39**Geogauge, LFWD, DCP, and nuclear gauge test results for RAP trench**

Layer	Compaction	E _G (MPa)	C _V %	E _{LFWD} (MPa)	C _V %	DCP-PR (mm/blow)	γ_d (kN/m ³)	mc %
First layer	Light	55.8	6.1	9.2	22.7	54.2	15.2	11.9
	Moderate	86.2	--	21.0	13.9	20	15.7	13.6
	Heavy	96.0	1.3	25.2	14	14.7	16.0	14.3
Second Layer	Light	66.7	6.1	27.0	12.7	42.5	15.8	11.8
	Moderate	87.2	3.1	50.8	9.5	18.8	16.6	11.5
	Heavy	134.2	1.2	71.3	6.8	9.5	18.0	11.1
Third layer	Light	57.00	4.2	29.00	15.9	30.3	15.8	11.9
	Moderate	77.00	2.3	52.00	13.1	16.1	16.9	11.4
	Heavy	126.20	5.1	116.2	4.4	9.97	18.0	11.6

ANALYSIS OF RESULTS

Analysis of Laboratory Test Results

Analysis of the Cement-soil

Analyzing the data for the cement-treated clay with special attention was necessary to monitor the improvement in the strength of these layers over time. Figure 39 illustrates the change in the Geogauge stiffness modulus, E_G , with time for the cement-soil layers. This figure shows that the Geogauge detected an increase in stiffness with time for 2 percent CC and 4 percent CC. A decrease in the Geogauge stiffness modulus was observed after 11 and 14 days for 2 percent CC and 4 percent CC layers, respectively. The reason for these results (figure 39) is most likely due to the presence of minor shrinkage cracks in cement-soil layers. The cement-treated clay layers were more brittle than the other materials tested during this research program. With the increasing percentage of the cement ratio, cement-soils were observed to be more brittle. The presence of minor cracks due to shrinkage of cement-soil with time also reduced the Geogauge stiffness modulus values and decreased the uniformity of the test layer.

As illustrated in figure 40, the DCP average PRs for CC layers decreased with time, which supports the fact that the cement-treated clay layers gain strength with time. This figure is based on the average PR of 8 in. depths. The DCP average PRs for the cement soil suggest that the 2 percent CC layer's lower stiffness than the 4 percent CC layer does not support the Geogauge results for these test cases. The DCP test results were not affected by the presence of shrinkage cracks, since it involves intrusion of a 20 mm diameter cone into the soil.

The LFWD dynamic modulus, E_{LFWD} , values with time for cement-soil layers are presented in figure 41. In accordance with the DCP results, this figure indicates that the 2 percent cement had the lower dynamic modulus than the 4 percent cement soil. However, there is no clear increase in E_{LFWD} with time for the 4 percent CC layer. This is mainly due to high standard deviation of the measurements as presented by the error bars in figure 41. The highest E_{LFWD} was obtained for the 4 percent cement-soil layer. This is comparable to the PLT results, where the highest value of $E_{PLT(i)}$ and $E_{PLT(R2)}$ were obtained for the 4 percent cement-soil layer (table 15). The results discussed above suggest that the Geogauge is very sensitive to the presence of cracks that are usually close to surface. The LFWD and PLT results were not affected by the presence of the cracks as much as the Geogauge stiffness modulus values were affected. The cracks had either a minimal or no effect on the DCP test results due the intrusion of the 20 mm cone during testing.

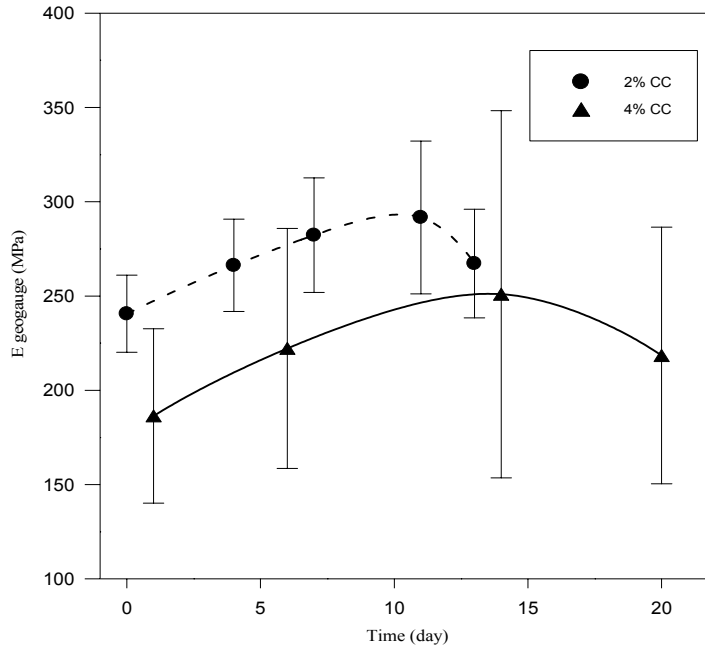


Figure 39
 E_G with time for cement-soil

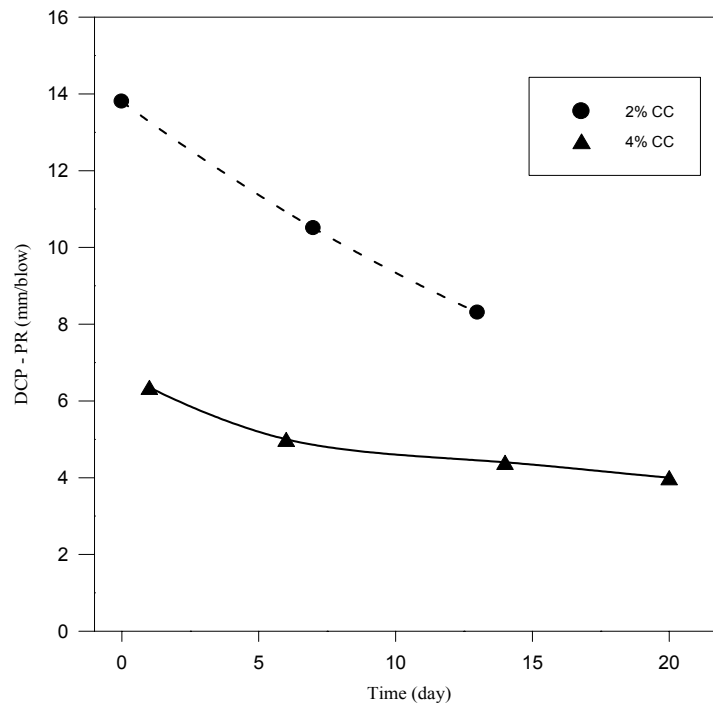


Figure 40
DCP average PR (8 inch) with time for cement-soil

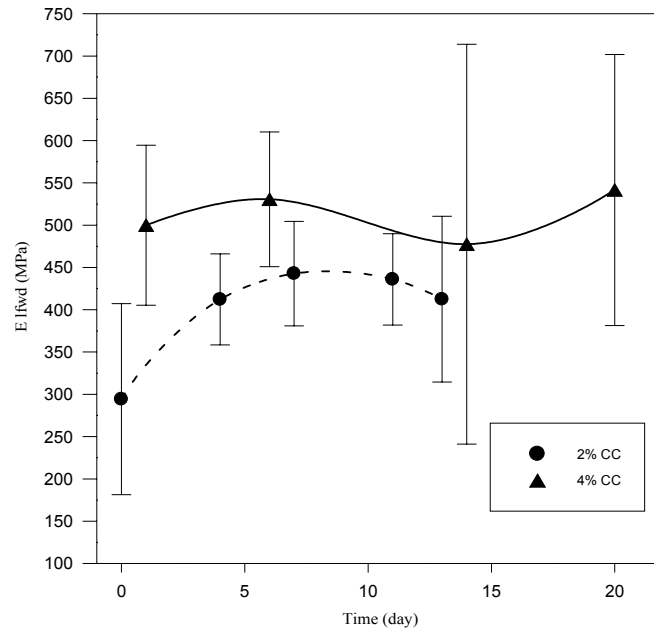


Figure 41
 E_{LFWD} with time for cement-soil

Moisture Effect Test Results

The results of the Geogauge tests conducted on the two cohesive soils and the corresponding dry densities and moisture contents are presented in tables 40 and 41. It should be noted that the Geogauge values reported in these tables represent the average of the four Geogauge measurements taken for each test. The results are also illustrated in figures 42 and 43, which show the dry density and Geogauge stiffness modulus curves versus moisture content.

Table 40
Results for test on clayey silt soil

Geogauge (MPa)	γ_d (kN/m ³)	mc %
0	14.36	24
95.75	15.04	18.3
108.68	14.50	16.2
110	14.40	15
128.88	14.33	13
132	14.28	12
100	14.11	10

Table 41
Results for tests on sandy lean clay soil

Geogauge (MPa)	γ_d (kN/m ³)	mc %
81.93	15.17	8.8
143.3	15.34	11.2
137.95	16.34	14.3
139.38	16.58	14.9
116.85	16.75	15.5
77.89	16.03	18.1

The Geogauge stiffness modulus and dry unit weight did not peak at the same time for the two soils tested. On the contrary, the stiffness modulus always peaked on the dry side of the soils' optimum moisture content. An important reason for this phenomenon is the structure of the cohesive soils particles, since for a given compaction effort, cohesive soils tend to be more flocculated for compaction on the dry side of their optimum moisture content.

However, as the water content increases, the soil inter-particle repulsions increases; thus the soil structure becomes more dispersed. The soil particles tend to orient themselves in an edge-to-face configuration in a flocculated structure, since the edges are positively charged and the faces are negatively charged. The resulting electrostatic attractive forces bond the soil particles together resulting in a higher stiffness on the dry side [40]. Another factor that can affect the strength properties of soils is suction. In a partially saturated soil, suction increases the inter-particle forces and changes the small-strain stiffness.

The current construction procedure requires compacting at the optimum moisture content ± 2 percent as obtained from the laboratory standard Proctor test. Figure 42 shows that the Geogauge stiffness variation within this range is 40 percent of the maximum stiffness value in this figure, while the dry density variation is only 2.5 percent of maximum dry density obtained from the standard Proctor curve. This suggests that the variation in the Geogauge stiffness within this range is much larger than that in the dry density. Consequently, with current construction procedures, the use of soil stiffness as acceptance criteria will be difficult to implement due to its sensitivity to the moisture content variation during compaction.

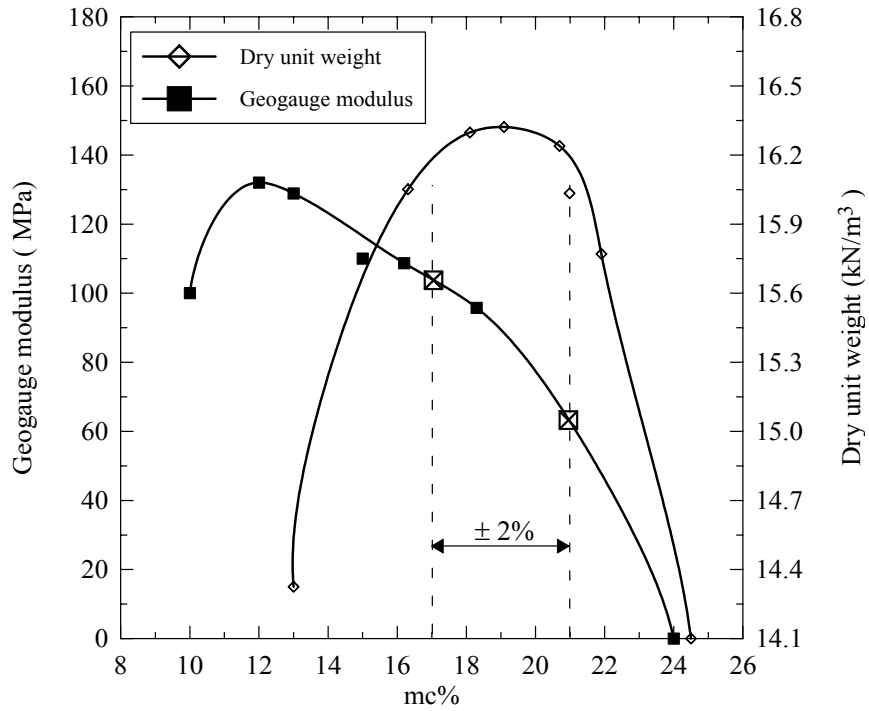


Figure 42

Geogauge stiffness modulus and dry unit weight curves (clayey silt soil)

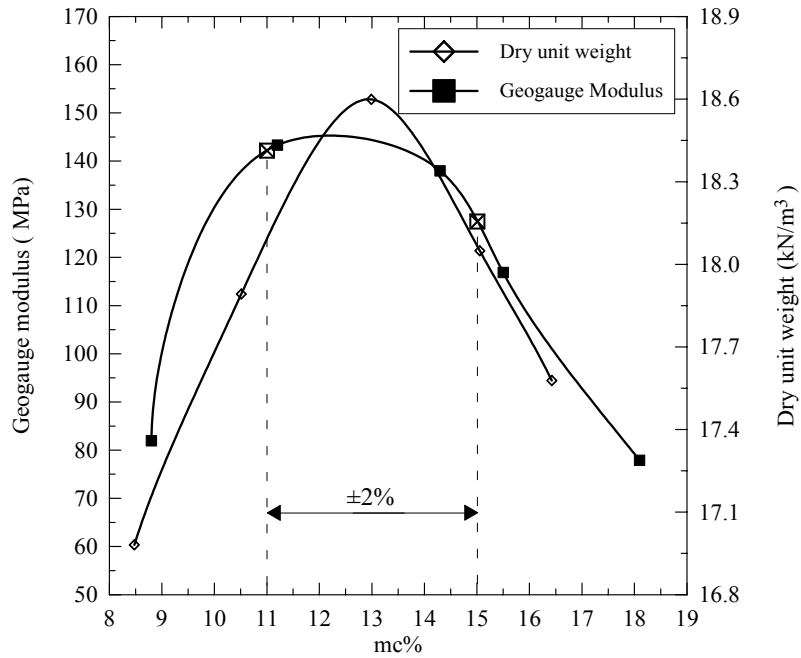


Figure 43

Geogauge stiffness modulus and dry unit weight curves (sandy lean clay)

The results of the tests conducted on BCS, clayey silt soil, and sand to investigate the influence depth of Geogauge and LFWD are presented in figures 44 through 48. In these figures, the average Geogauge and LFWD moduli for the compacted soil layer are plotted against the thickness of this layer. In tests conducted in the first box, the stiff BCS was constructed on top of the softer clay soil. The Geogauge and LFWD subsequent measurements increased with increasing depth, as shown in figures 44 and 45, and gradually stabilized at the depths that correspond to the influence depths of the investigated devices. Figures 44 and 45 indicate the influence depths for the Geogauge and LFWD were 190 mm (7.5 in.) and 267 mm (10.5 in.), respectively.

In tests conducted in the second box, clayey silt and sand soils were built on top of a BCS stiff layer. Results showed that the Geogauge and LFWD stiffness moduli values decreased with increasing thickness until they approached an asymptote at a certain thickness that corresponded to the influence depth of these devices, as shown in figures 46 through 48. For the Geogauge, this thickness was about 205 mm (8.0 in.) for the sand and the clayey silt soil. For the LFWD, the thickness at which the stiffness modulus curve stabilized was about 280 mm (11 in.). The results of these tests indicated, that in general, the influence depth for Geogauge ranged between 190 and 200 mm (7.5 and 8 in.), while it ranged between 267 and 280 mm (10.5 and 11 in.) for the LFWD. This result also suggested that the influence zone of each device depended on the stiffness of the tested layer, such that the influence depth decreased with increasing this stiffness.

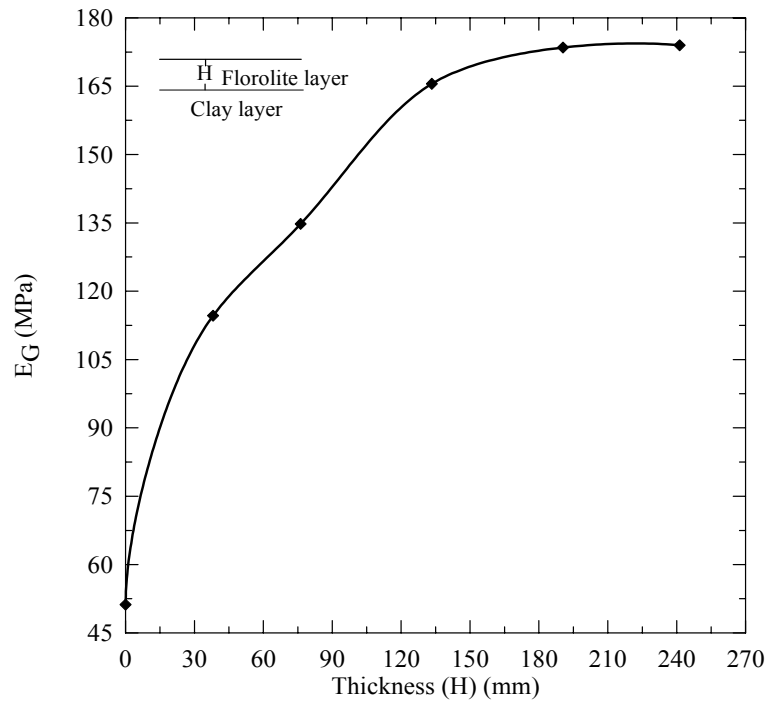


Figure 44
Geogauge stiffness modulus curve for BCS layer versus thickness

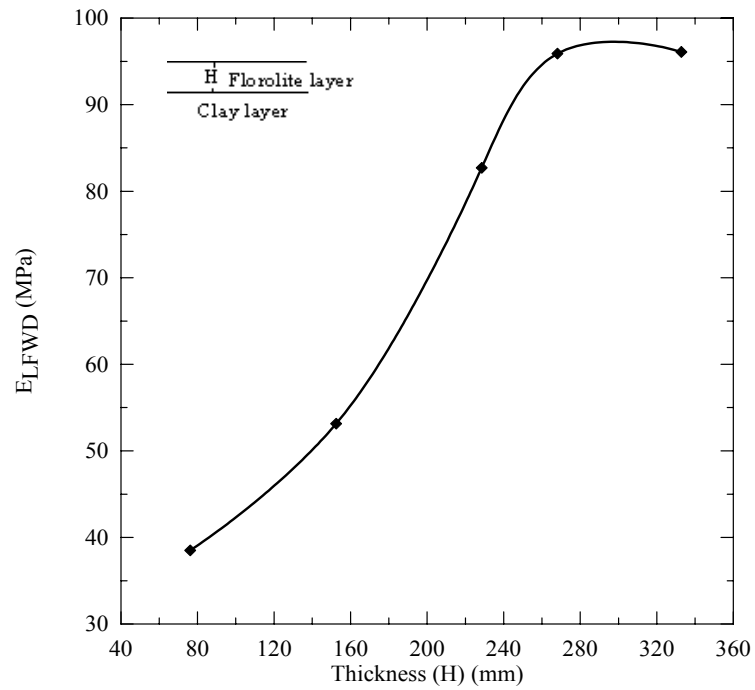


Figure 45
LFWD stiffness modulus curve for BCS layer versus thickness

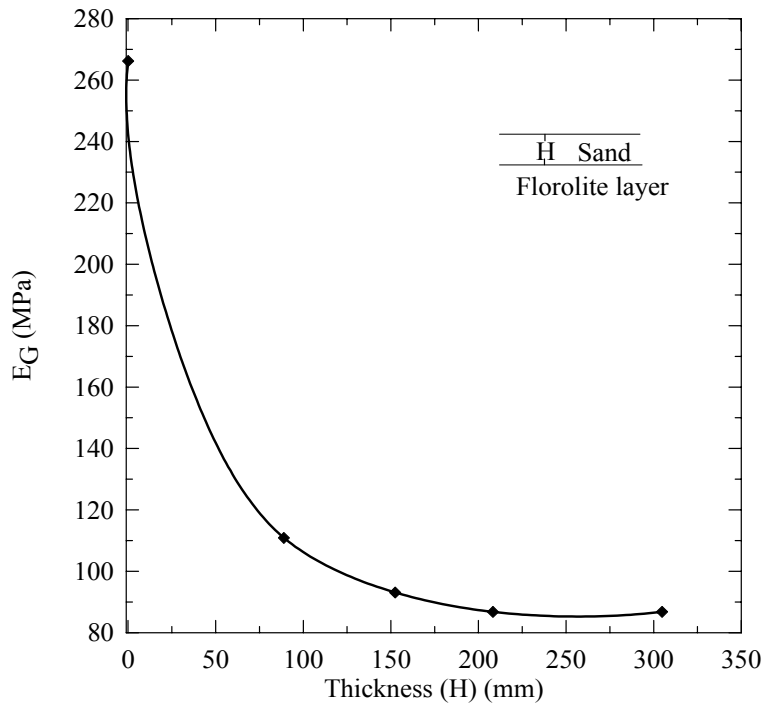


Figure 46

Geogauge stiffness modulus curve for sand layer versus thickness

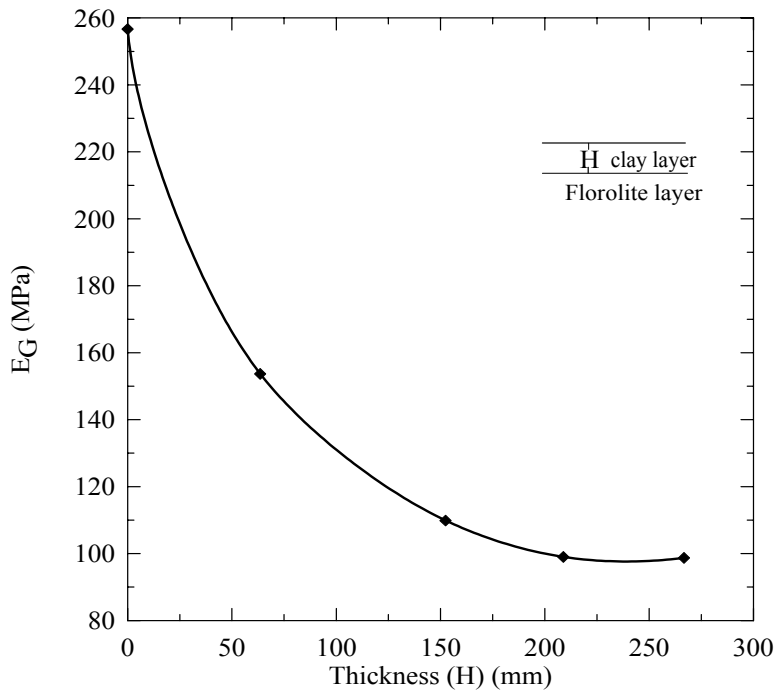


Figure 47

Geogauge stiffness modulus curve for clay layer versus thickness

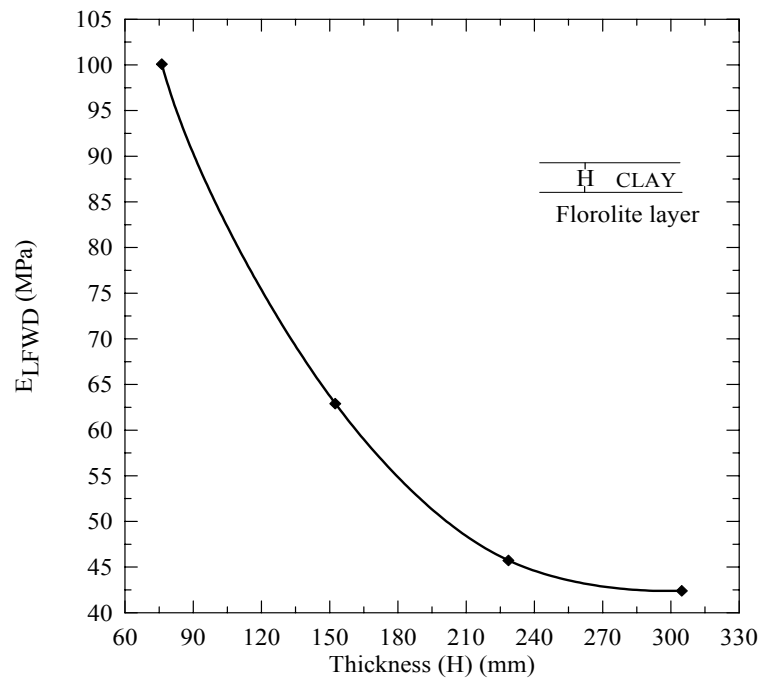


Figure 48
LFWD stiffness modulus curve for clay layer versus thickness

Analysis of Field Test Results

Analysis of Base Test Sections at PRF Site

The variation of the Geogauge modulus with the number of passes during the construction of different test sections is shown in figures 49 and 50. It is clear that for all tests, the Geogauge stiffness modulus increased with the number of passes. For the lime-treated soil and cement soil (1) sections in figure 50, the Geogauge stiffness modulus approached an asymptote and hence became stable after four passes, indicating that it reached the maximum stiffness modulus for this compaction effort. However, for the other sections in figure 51, it was not clear whether the Geogauge modulus reached a peak value.

The Geogauge stiffness modulus variations with time for four different sections are presented in figure 51. The Geogauge measurements increased with time for the first three days after construction; however, they then reached a stable value for the two cement-soil sections, while they decreased for the BCS and lime-treated soil sections. The strength of these soils is expected to increase with time due to the chemical reactions that occur in cement and lime-treated soils after mixing; these reactions can last for weeks after mixing. However, the lack of moisture affected the strength gain with time for these sections.

In addition, the lack of moisture resulted in shrinkage cracks which significantly affected the results of the Geogauge tests and thus reduced the stiffness modulus. On the other hand, the lime-treated soil and BCS sections were not covered. Considering figure 52, the Geogauge measurements for the lime section were significantly reduced by the rainfall during the testing period. BCS material has a high stiffness modulus and can be a strong supportive pavement layer. However, figure 52, shows that this material is very sensitive to moisture; the Geogauge measurements taken on the BCS section were lower than those taken on dry days. Consequently, the results suggested that the measurements on BCS were influenced by the rain that occurred during the testing period. The error in Geogauge measurement that is presented in figure 51 shows that these measurements had relatively small variability, suggesting that the variability did not affect the stiffness modulus trend with time.

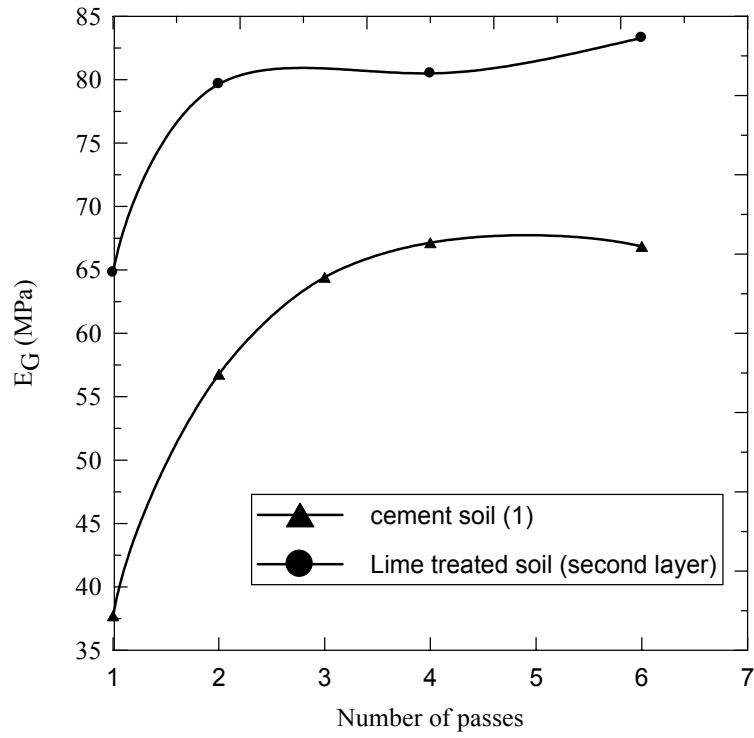


Figure 49
Geogauge modulus variation with number of passes

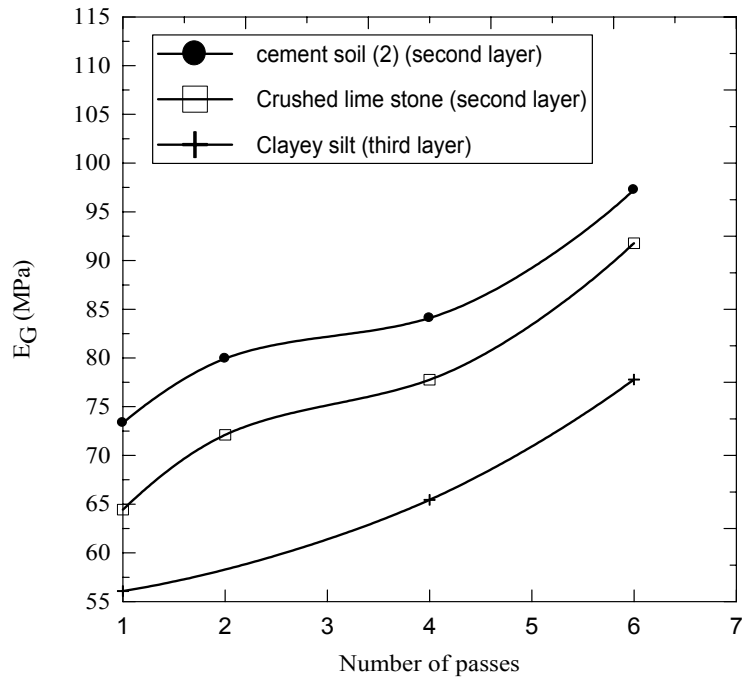


Figure 50
Geogauge modulus variation with number of passes

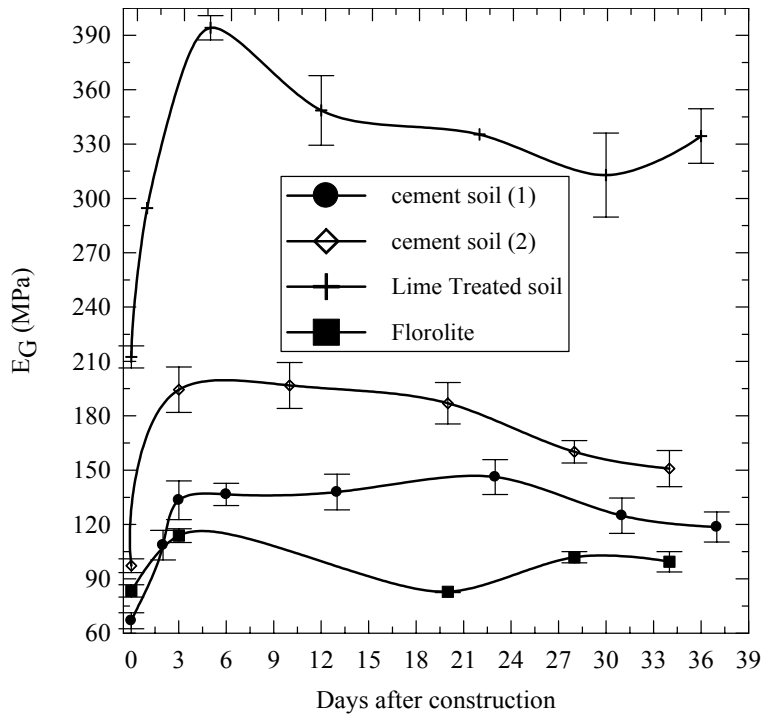


Figure 51
Geogauge modulus variations with time

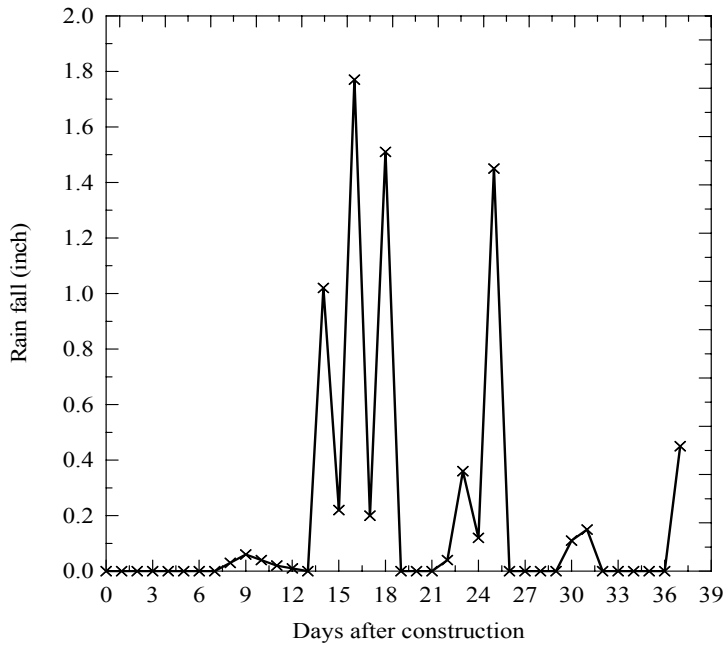


Figure 52
Rainfall record during testing time [41]

The variations of LFW D measurements with the number of passes for three different sections are presented in figure 53. The LFW D modulus increased with the number of passes. The variation of LFW D measurements with time for different sections is also presented in figure 54. For the cement soil section (1), the LFW D values increased with time until they reached a stable value; however, for the other sections shown in the same figure, the LFW D values increased with the number of passes until they reached a maximum value before slightly decreasing.

Again, the error bars for the LFW D measurements that are presented in figure 54 show that these measurements did not have much variability, suggesting that variability of the test measurements did not have much influence on the stiffness modulus trend with time.

By comparing the LFW D results in figures 53 and 54 with the Geogauge results in figures 50 through 51, it can be seen that for the tests done on the same sections the moduli measured by both devices have similar trends.

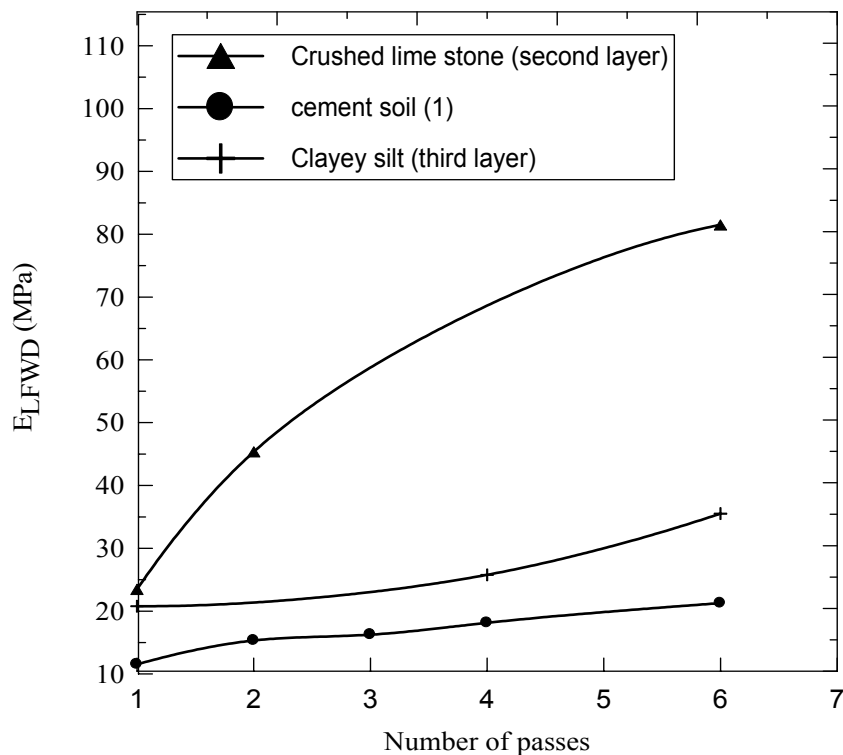


Figure 53
 $E_{LFW D}$ variation with number of passes

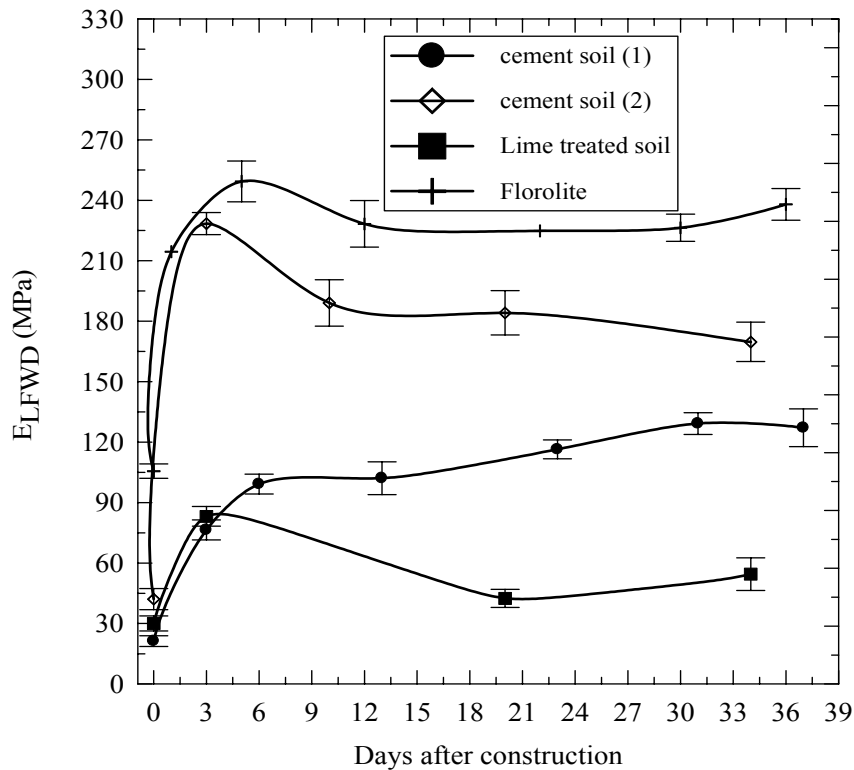


Figure 54
 E_{LFWD} variation with time

Figures 55 through 58 show the variation in the DCP-PR profile with depth for the four different sections obtained immediately at construction and one month later. It is clear that for both cement-treated soil sections, the DCP profile of the top 300 mm (12 in.) for tests conducted 37 days after construction, had lower PRs compared to those for tests conducted immediately after construction. This data indicated that both cement-soil sections gained strength with time. On the other hand, DCP profiles for both the BCS and lime-treated sections showed a slight reduction in PR between tests conducted directly after construction and those done after about one month. These results matched those from the Geogauge and LFWD; therefore, the stiffness trend was the same for all three test devices.

Trench Test Sections

The variations of Geogauge modulus with dry unit weight for the three trenches constructed at the PRF site are presented in figure 59. This figure shows that, as expected, both the dry unit weight and Geogauge modulus increased as the compaction effort increased. Figure 60 shows the LFWD modulus variation with dry unit weight for the three trenches constructed at the PRF

site. As for the Geogauge, both the unit weight and LFW D modulus increased as compactive effort increased. These figures show that both the LFW D and Geogauge stiffness moduli increased in the same trend, which confirms the fact that the stiffness increased with the increase in the dry unit weight as a result of increasing compaction. The results suggested that there is a general relation between the stiffness moduli and the dry unit weight at the same moisture content. However, this kind of relation depends primarily on the tested material and its behavior.

The variations in DCP-PR profiles with depth, for the different sections in the three trenches, are illustrated in figures 61 through 63. Each figure plots the DCP-PR profile for the heavily and lightly compacted sections. The DCP-PRs for the lightly compacted material are higher than they are for the heavily compacted material, which indicates that the penetration for a certain material is affected by the compaction effort; therefore, this rate can be correlated to the dry unit weight of this material. The DCP profiles for heavily compacted sections in all three trenches indicated that there was a sudden increase in DCP-PR values at depths greater than the thickness of the constructed trenches (3 ft). This increase indicated that the DCP was able to detect the existing weak natural soil layer underlying the constructed trenches.

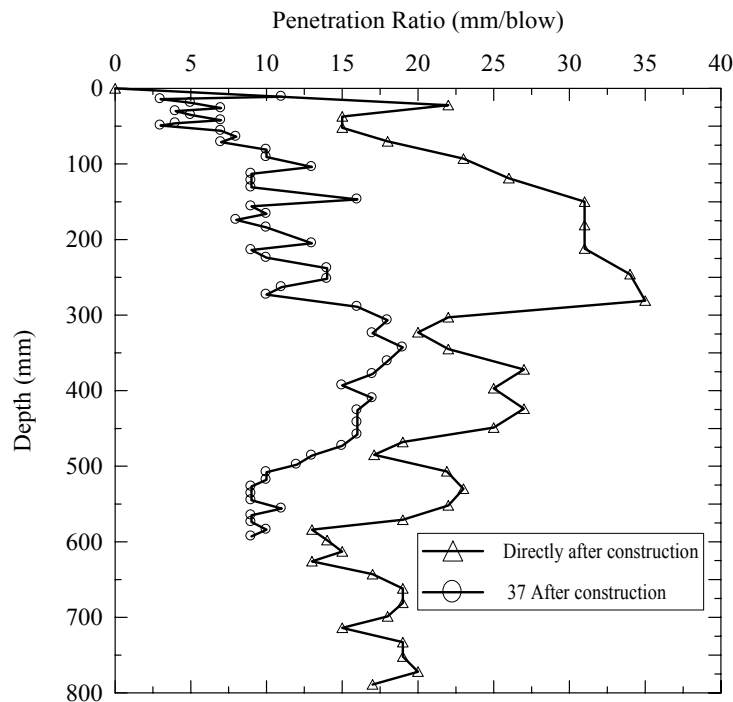


Figure 55
DCP-PR with time for cement soil section (1)

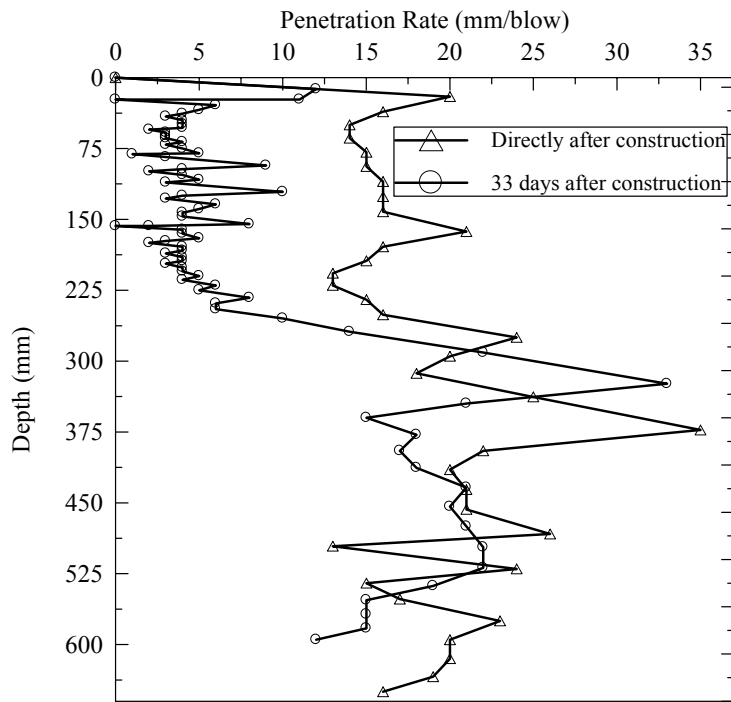


Figure 56
DCP-PR with time for cement soil section (2)

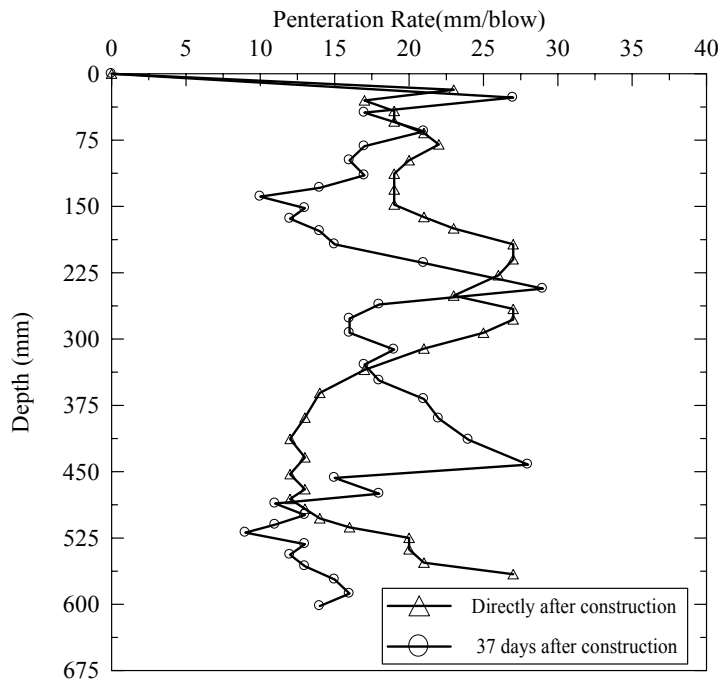


Figure 57
DCP-PR with time for lime-treated soil section

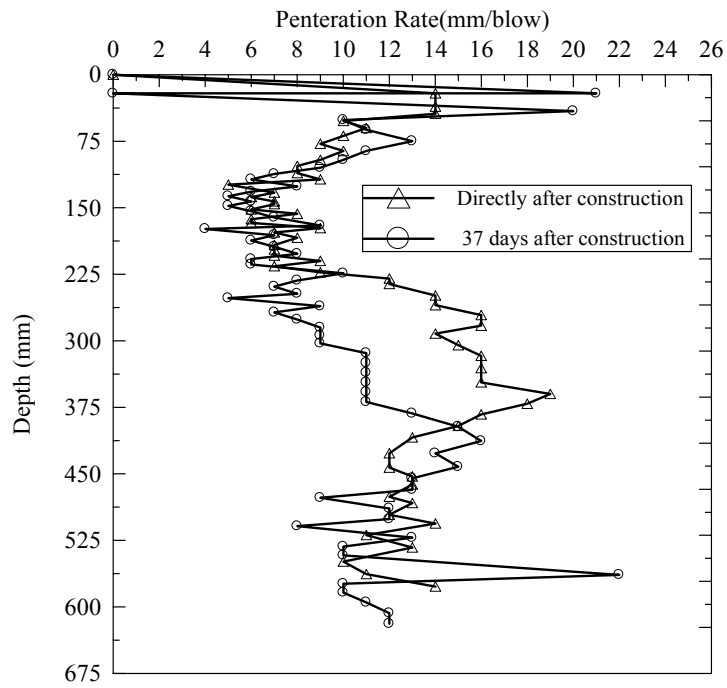


Figure 58
DCP-PR with time for BCS section

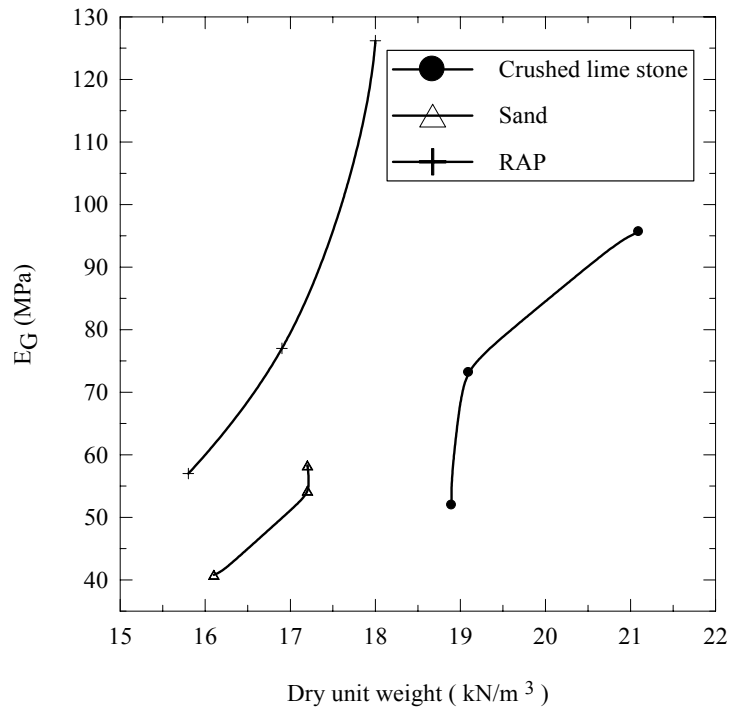


Figure 59
 E_G and dry unit weight for different trenches

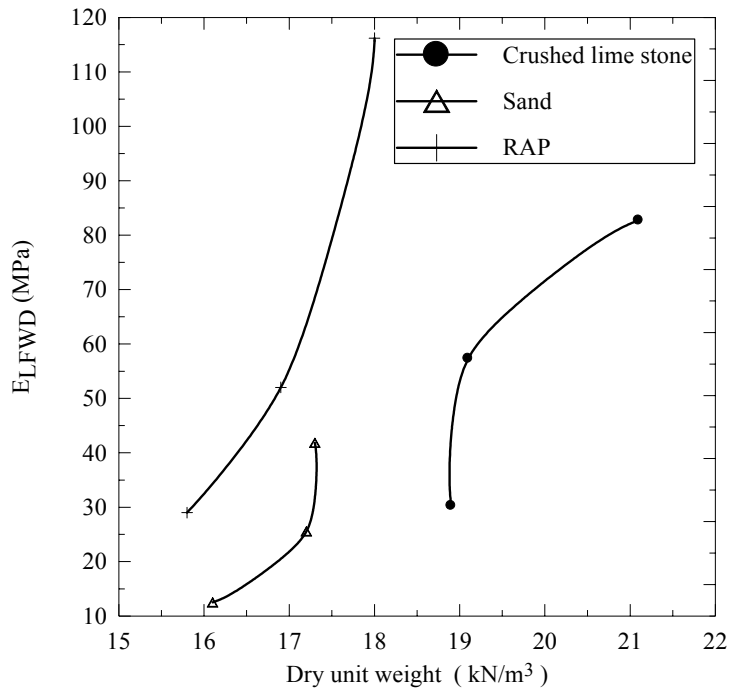


Figure 60
 $E_{LFW D}$ and dry unit weight for different trenches

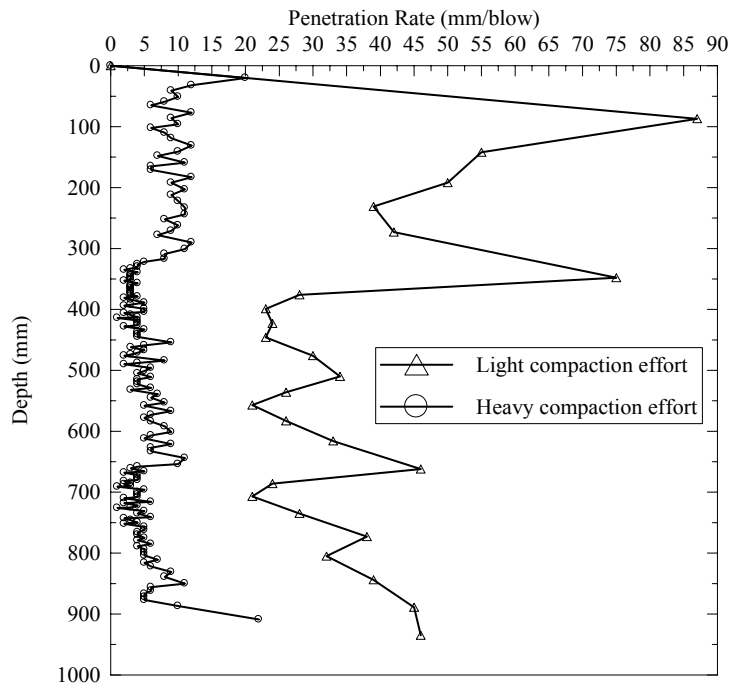


Figure 61
DCP-PR profiles for crushed limestone trench sections

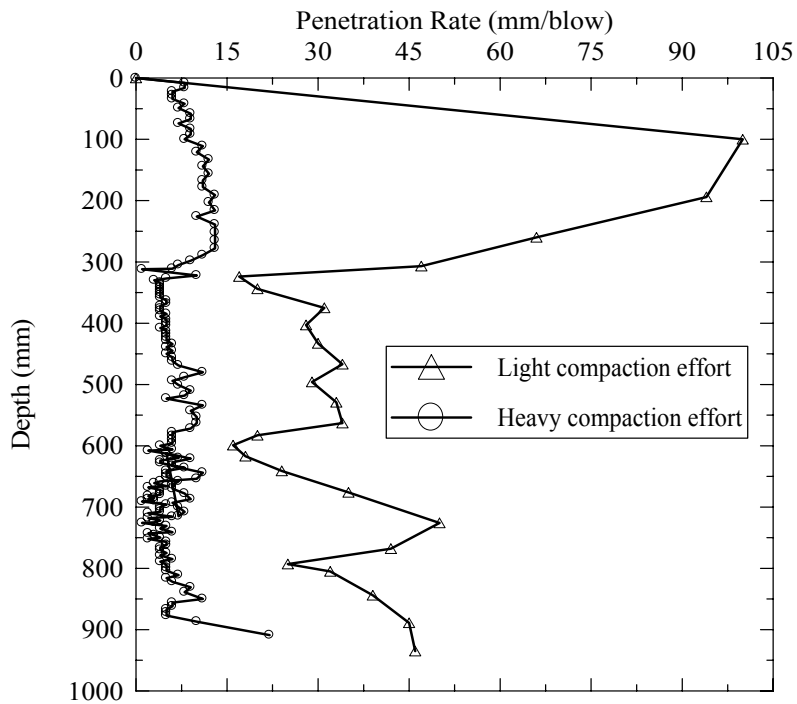


Figure 62
DCP-PR profiles for RAP trench sections

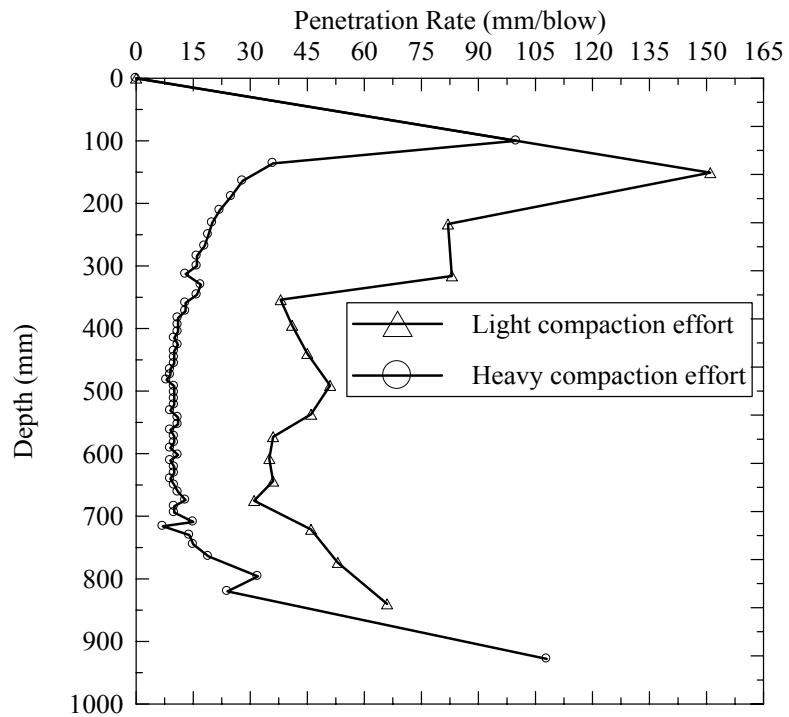


Figure 63
DCP-PR profiles for sand trench sections

Figures 61 through 63 show that the DCP profiles for lightly compacted sections suddenly increased at a depth of 300 mm (1 ft), which coincides with the thickness of the first layer. These results not only indicate that the DCP-PR can indicate the strength of a material, but also demonstrate the DCP device's ability to detect the thickness of the tested layer. Although the three layers in each trench section were evenly compacted, it was obvious that the DCP-PR values for the second and third layer for the three trenches were lower than those for the upper layer. This might be related to the effect of confinement due to the overlaying layer for soils.

Repeatability of Geogauge and LFWD for Field Tests

To assess the performance of any in-situ test device, the repeatability of the device's measurements has to be considered. As mentioned earlier, the Geogauge and LFWD values reported in this study for each field test represent the average of the five measurements taken at different spots within the tested section. The repeatability of both devices was evaluated using the coefficient of variation, C_v , of the five measurements taken at each test section.

Geogauge Repeatability. The coefficients of variation, C_v , for the Geogauge measurements of all field tests ranged from 0.37 percent to 11.39 percent, with most of the C_v values between 1 percent to 7 percent. The repeatability of the Geogauge was also evaluated in the field tests conducted as part of FHWA study SPR-2(212) for the validation of Humboldt's suggested seating procedure for the Geogauge. These tests were conducted on cement-treated soil section (2) in the PRF site 60 days after construction. Three operators performed the tests using three different Geogauge devices that were verified using the procedure suggested in the Humboldt's manual for using the Geogauge. Tests were conducted at three different locations within the cement-treated soil section (2). Each of the three operators performed six sequential Geogauge measurements within the boundaries of each location three times; therefore, a total of 54 measurements were taken at each location.

The mean stiffness, standard deviation, and coefficient of variation were calculated for all measurements made by all Geogauges and all operators for each test location. The coefficient of variation for measurements made by all Geogauges ranged from 6.1 percent to 9.5 percent. In their report, Humboldt indicated that the precision demonstrated for these tests, using the suggested seating procedure, appears to be as reliable as most geotechnical field measurements [42].

Repeatability of LFWD. The statistical analysis shows that the coefficient of variation, C_v , for LFWD measurements for all field tests ranged from 2.1 percent to 28.1 percent, with most of the C_v values between 4.5 percent and 17.5 percent. Figure 64 shows the variation of the C_v with its corresponding average LFWD stiffness moduli. The general trend for the points in this figure indicates that the C_v value decreases with the increasing in the stiffness moduli. This trend was also noted during LFWD field tests, because it was difficult to conduct the LFWD test on very weak material. On the other hand, the LFWD performance was enhanced for the more compacted and stiff materials. Fleming has reached similar findings [27]. The results of his study suggested that field tests conducted with the LFWD and FWD had a greater variation in subgrade materials when compared to those conducted on stiffer sub-base and base course materials.

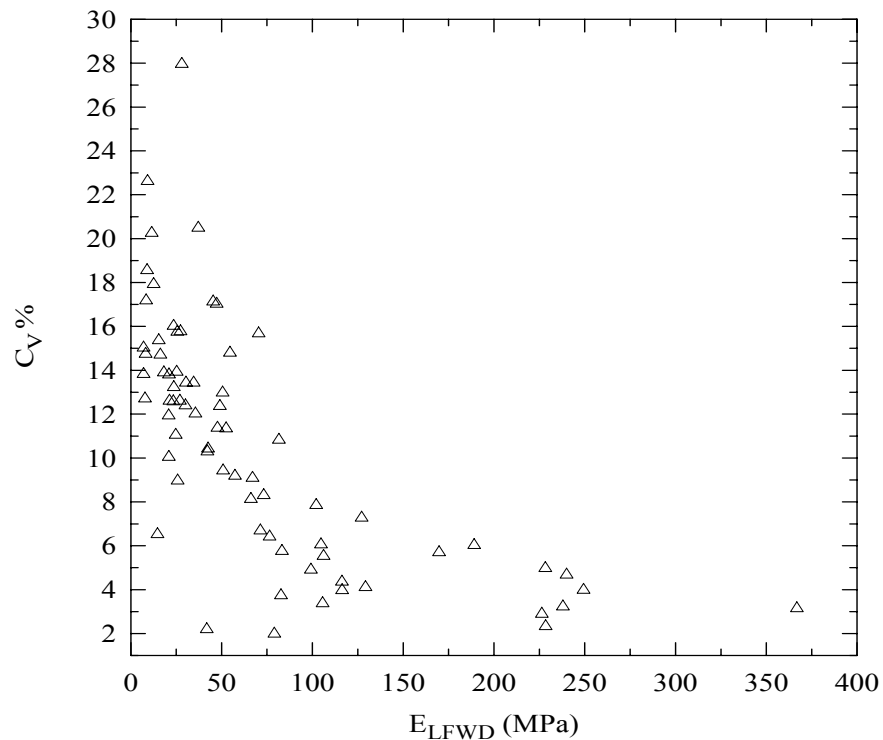


Figure 64
 C_v variation with LFWD modulus

Moduli Correlations

Geogauge Correlations

Geogauge versus Plate Load Test. Both the Geogauge stiffness modulus (E_G) and the initial ($E_{PLT(i)}$) and reloading ($E_{PLT(R2)}$) moduli obtained from the PLT data are measures of layer stiffness. Therefore, a correlation between the Geogauge and the PLT results are sought. A strong correlation between the soil modulus values obtained by these two methods can increase the credibility of the Geogauge for future use.

Two possible correlations between the Geogauge and the PLT were investigated. Equations 26 and 27 present the correlations between the Geogauge stiffness modulus (E_G) and the initial PLT modulus ($E_{PLT(i)}$) and reloading modulus, $E_{PLT(R2)}$, respectively, obtained from laboratory tests. These results are illustrated in figures 65 and 66.

$$E_{PLT(i)} = 15.5 * e^{0.013(E_G)} \quad (R^2 = 0.83) \quad (26)$$

$$E_{PLT(R2)} = 15.8 * e^{0.011(E_G)} \quad (R^2 = 0.69) \quad (27)$$

The results of the statistical regression analysis between the Geogauge stiffness modulus (E_G) and the back-calculated PLT initial and reloading elastic modulus, obtained from field tests, yielded the correlations shown in equations 28 and 29. The results of the regression analysis are shown in figures 67 and 68.

$$E_{PLT(i)} = -75.58 + 1.62 (E_G) \quad (R^2 = 0.87) \quad (28)$$

$$E_{PLT(R2)} = -65.37 + 1.50 (E_G) \quad (R^2 = 0.90) \quad (29)$$

A regression analysis was also conducted using both laboratory and field data to correlate the Geogauge modulus, E_G , with PLT moduli, $E_{PLT(i)}$ and $E_{PLT(R2)}$. The following regression models were obtained:

$$E_{PLT(i)} = 1.168 (E_G) - 37.42 \quad (R^2 = 0.72) \quad (30)$$

$$E_{PLT(R2)} = 10^{(1.2 (\log (E_G)) - 1.39)} \quad (R^2 = 0.59) \quad (31)$$

Figures 69 and 70 present the models obtained from the field and laboratory along with the combined data. The Geogauge–PLT relation was linear for field models while it was exponential for the lab model. In both figures, the data points from both the laboratory and field tests are

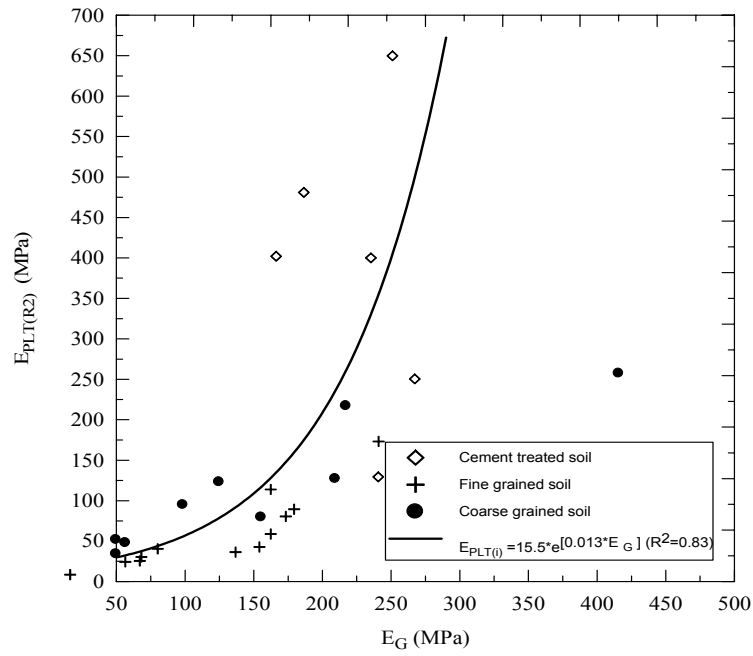


Figure 65
Correlation between E_G and the $E_{PLT(i)}$ (laboratory test)

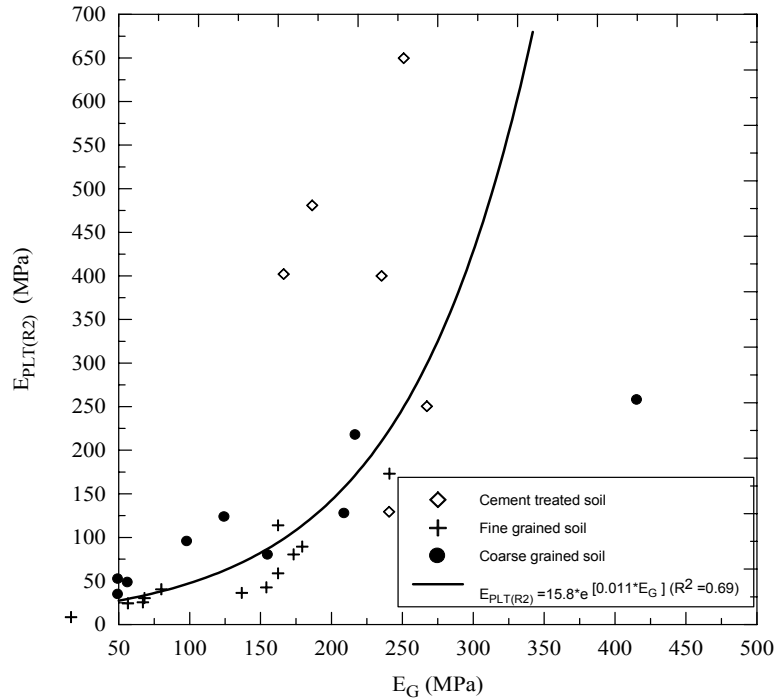


Figure 66
Correlation between E_G and the $E_{PLT(R2)}$ (laboratory test)

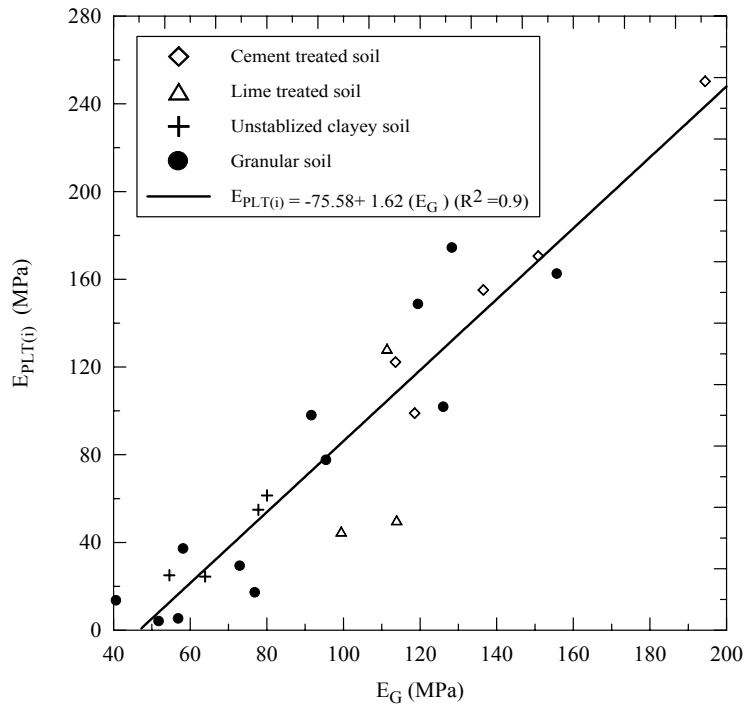


Figure 67
Correlation between E_G and the $E_{PLT(i)}$ (field test)

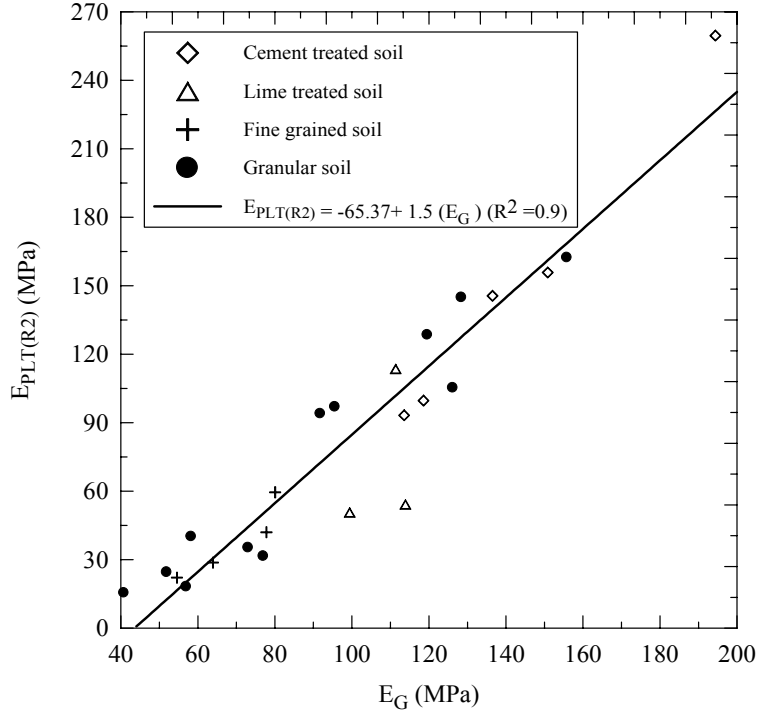


Figure 68
Correlation between E_G and the $E_{PLT(R2)}$ (field test)

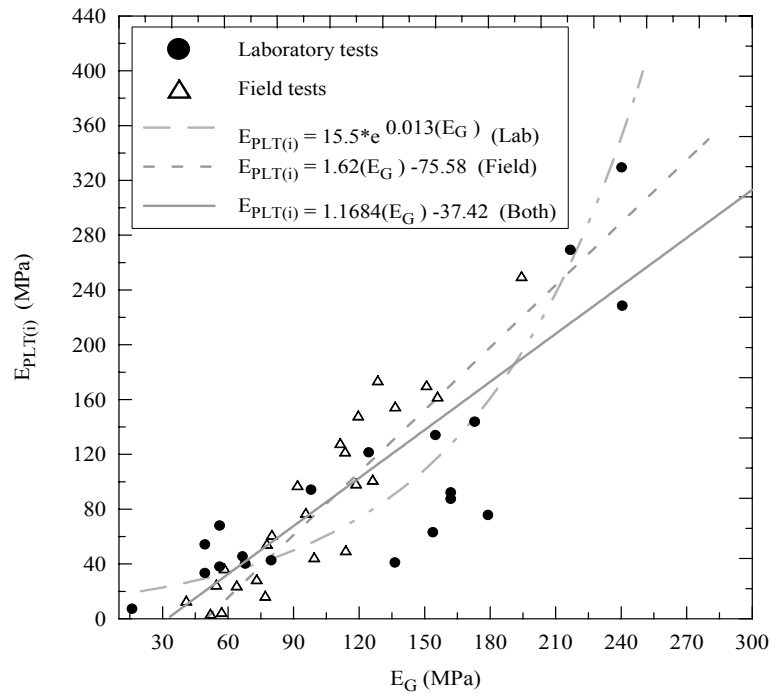


Figure 69

Comparison between laboratory and field for $E_G - E_{PLT(i)}$ correlation

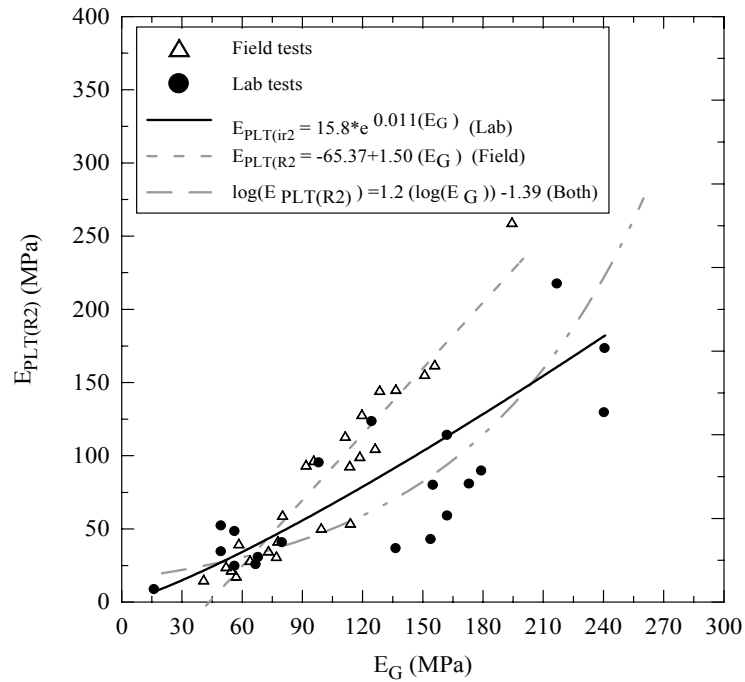


Figure 70

Comparison between laboratory and field for $E_G - E_{PLT(R2)}$ correlation

scattered, and the unexplained error for best fit line is great; consequently, the coefficient of determination was relatively low. However, it is clear that field data for the Geogauge has better correlation and should be adopted. The great variation in laboratory data is believed to be the result of the construction difficulties and the compaction inconsistency when samples were prepared.

Geogauge versus FWD. A regression analysis was conducted to determine the best correlation between the FWD back-calculated resilient moduli, M_{FWD} , and the Geogauge stiffness modulus, E_G , for all tests conducted in the field (figure 71). The results of this analysis yielded the regression model presented in equation 32.

$$M_{FWD} = -20.07 + 1.17 (E_G) \quad (R^2=0.81) \quad (32)$$

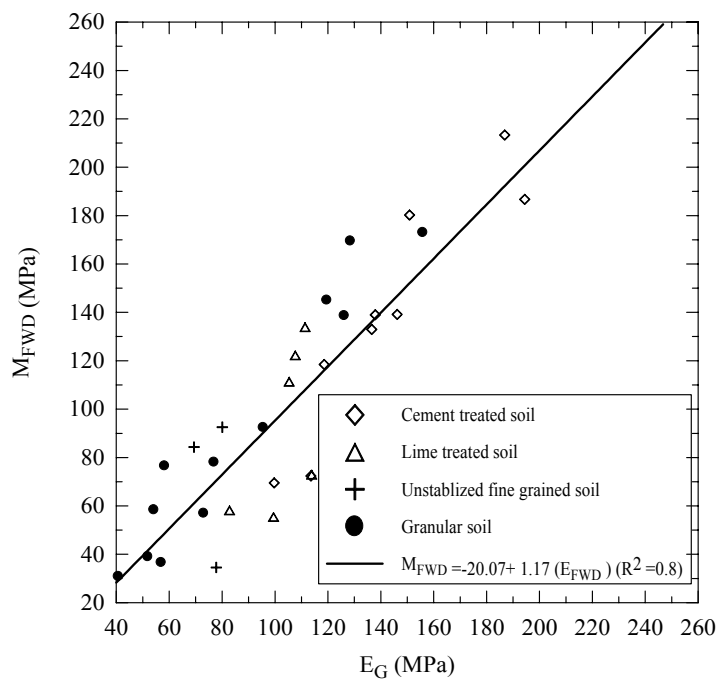


Figure 71

Correlation between E_G and the M_{FWD}

Geogauge versus California Bearing Ratio. The stiffness modulus values (E_G) obtained from laboratory tests are plotted versus the CBR (%) of corresponding material properties in figure 72. The recommended correlation is a log-log relation as defined by equation 33.

$$\log (E_G) = 1.89 + 1.48 \log (CBR) \quad (R^2 = 0.62) \quad (33)$$

A correlation between the Geogauge stiffness modulus and CBR values for field tests was also developed. Based on the results of the regression analysis, the model shown in equation 34 was recommended. Figure 73 illustrates the results of the regression analysis.

$$CBR = 0.00392 (E_G)^2 - 5.75 \quad (R^2 = 0.84) \quad (34)$$

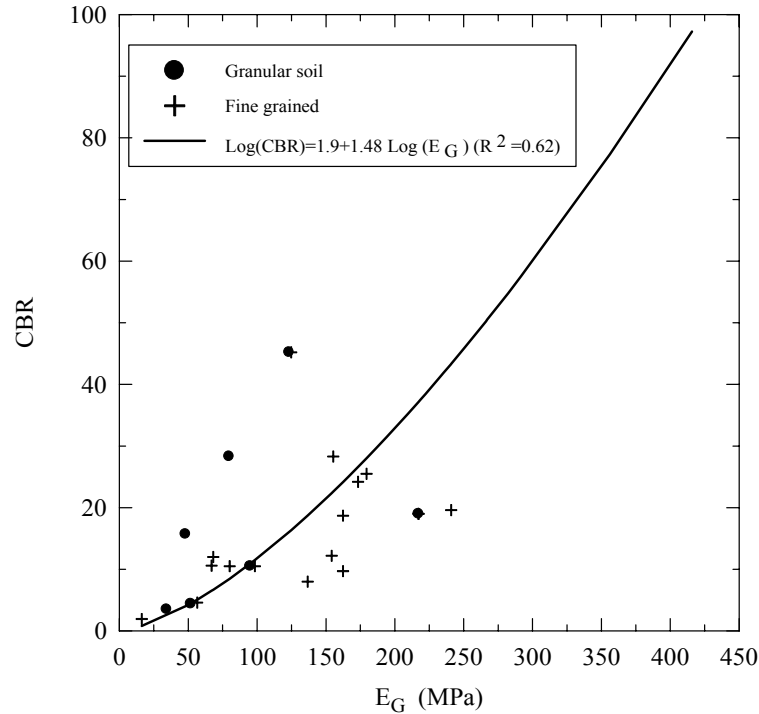


Figure 72

Correlation between E_G and CBR (laboratory test)

LFWD Correlations

LFWD versus Plate Load Test. A better correlation of the LFWD dynamic modulus (E_{LFWD}) and both the PLT initial elastic loading modulus ($E_{PLT(i)}$) and the PLT reloading elastic modulus ($E_{PLT(R2)}$) is expected. Although the LFWD is a dynamic loading test that is different than the static loading of bearing plates in the PLT procedure, a good correlation between two tests will increase the credibility of the LFWD. Correlation between the LFWD dynamic modulus (MPa) and $E_{PLT(i)}$ or $E_{PLT(R2)}$ are illustrated by figures 74 and 75, respectively. In all the analyses, the LFWD data representing Clay-2 layer was excluded since the LFWD dynamic modulus for this layer was too high compared to all other test results.

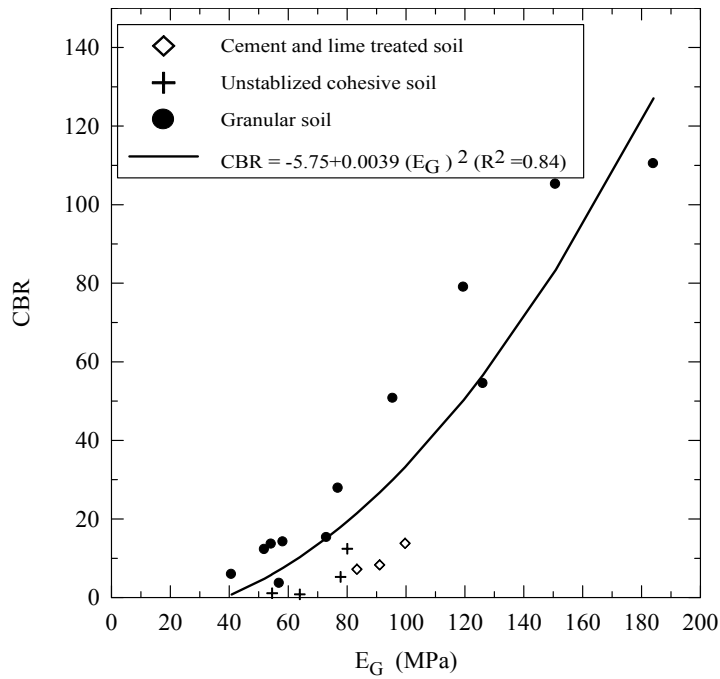


Figure 73
Correlation between E_G and CBR (field test)

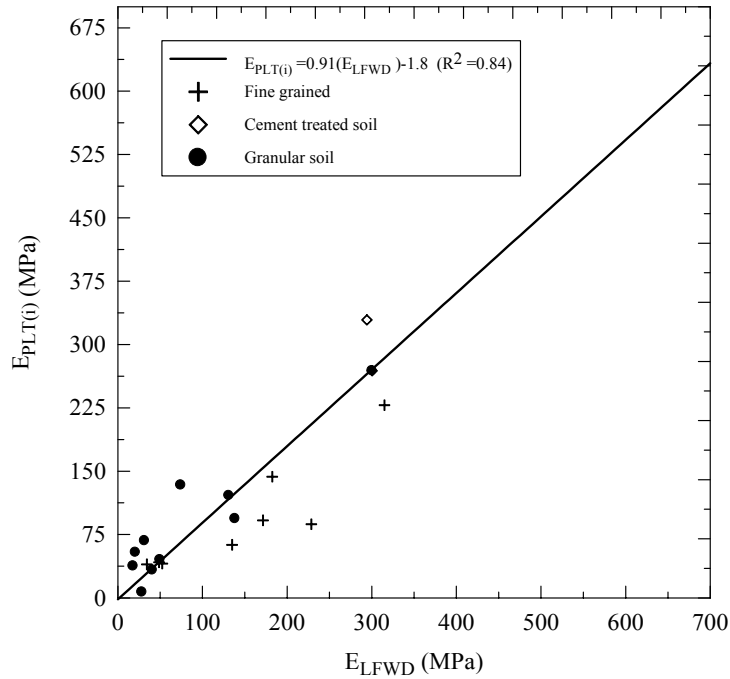


Figure 74
Correlation between E_{LFWD} and the $E_{PLT(i)}$ (laboratory test)

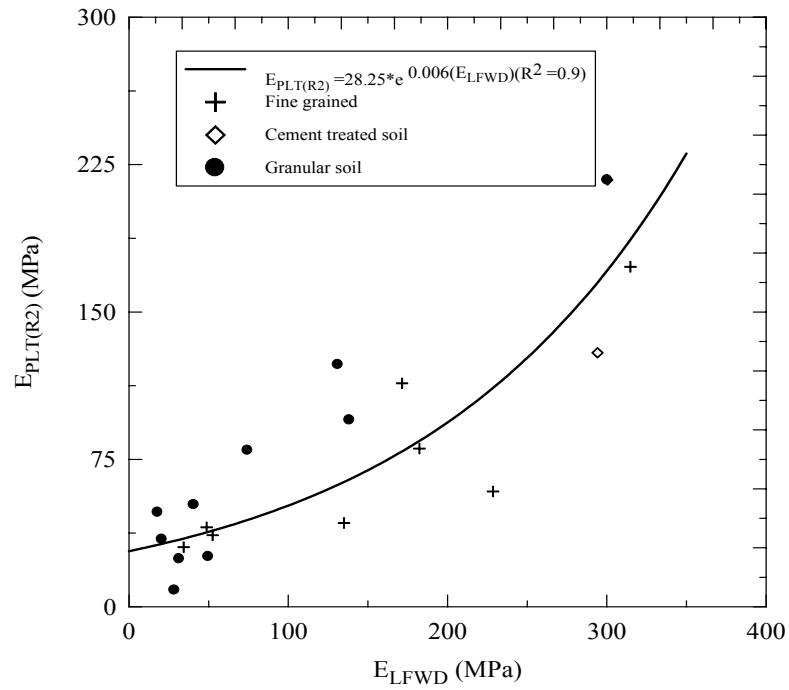


Figure 75
Correlation between E_{LFWD} and the $E_{PLT(R2)}$ (laboratory test)

The suggested correlation between the LFWD dynamic modulus (E_{LFWD}) and the initial and reloading moduli obtained from the PLT ($E_{PLT(i)}$, $E_{PLT(R2)}$) is:

$$E_{PLT(i)} = 0.907 * (E_{LFWD}) - 1.8 \quad (R^2 = 0.84) \quad (35)$$

And

$$E_{PLT(R2)} = 28.25 * e^{0.006(E_G)} \quad (R^2 = 0.90) \quad (36)$$

The modulus obtained from LFWD, E_{LFWD} , was also correlated to $E_{PLT(i)}$ and $E_{PLT(R2)}$ for all field data. The obtained regression models are shown in equations below. These regression models are illustrated in figures 76 and 77.

$$E_{PLT(i)} = 22 + 0.7 (E_{LFWD}) \quad (R^2 = 0.92) \quad (37)$$

And

$$E_{PLT(R2)} = 20.9 + 0.69 (E_{LFWD}) \quad (R^2 = 0.94) \quad (38)$$

The elastic modulus obtained from LFWD, E_{LFWD} , was also correlated to $E_{PLT(i)}$ and $E_{PLT(R2)}$ based on combined field and lab data. Based on the results of the regression analysis, the following linear correlations were obtained:

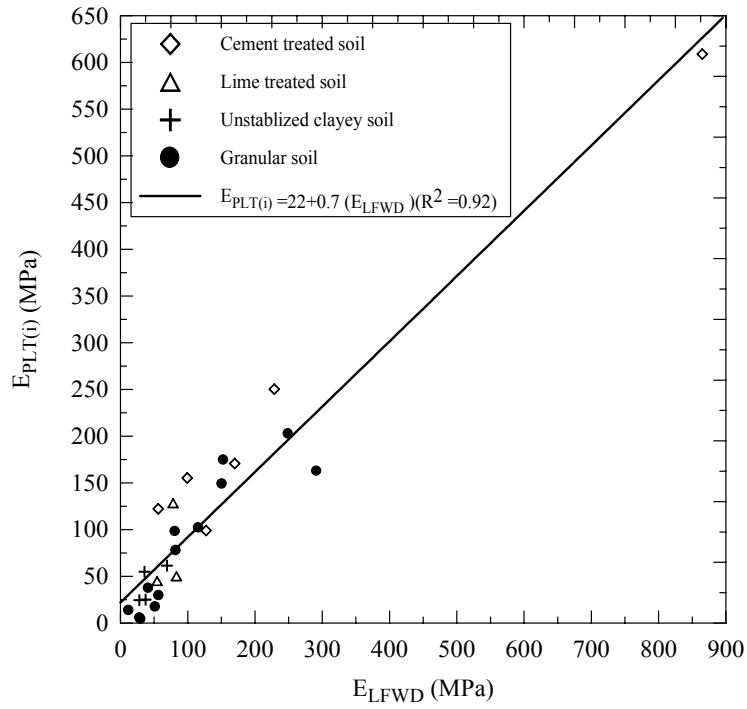


Figure 76

Correlation between E_{LFWD} and the $E_{PLT(i)}$ (field test)

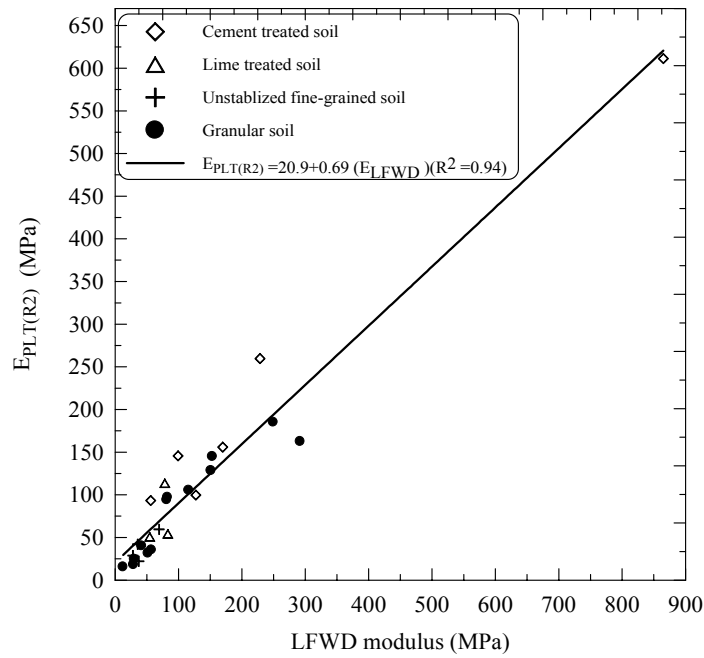


Figure 77

Correlation between E_{LFWD} and the $E_{PLT(R2)}$ (field test)

$$E_{PLT(i)} = 0.71 (E_{LFWD}) + 18.63 \quad (R^2 = 0.87) \quad (39)$$

And

$$E_{PLT(R2)} = 0.65 (E_{LFWD}) + 13.8 \quad (R^2 = 0.87) \quad (40)$$

These regression models are illustrated in figures 78 and 79. It can be observed that models obtained in this regression analysis are almost the same as the models obtained from field data. Based on that, the field or the combined correlations for the LFWD are acceptable and can be adopted.

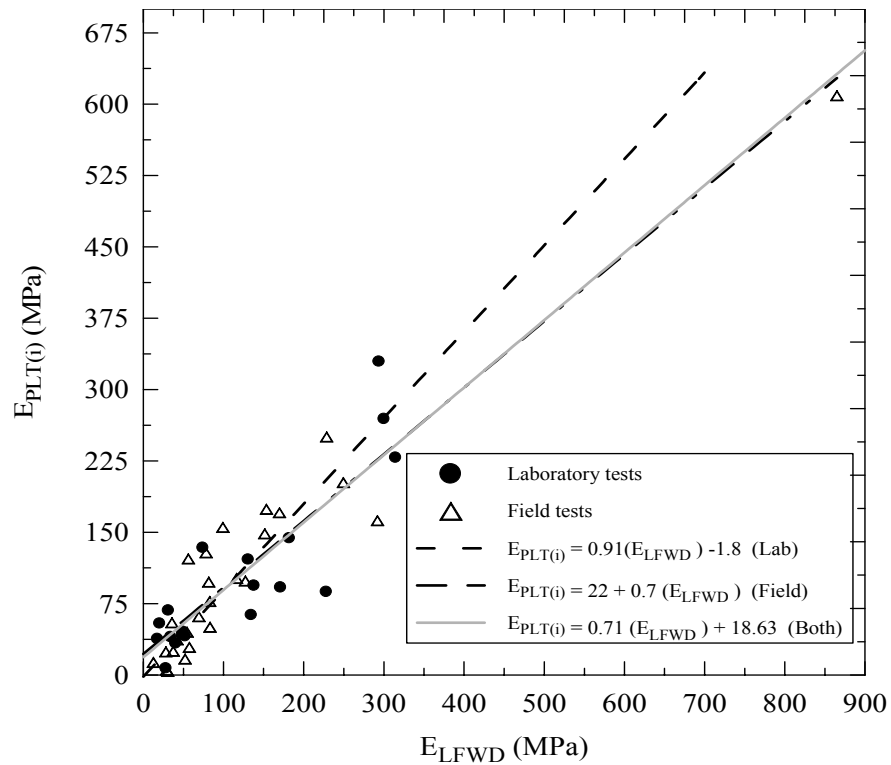


Figure 78

Comparison between laboratory and field for $E_{LFWD} - E_{PLT(i)}$ correlation

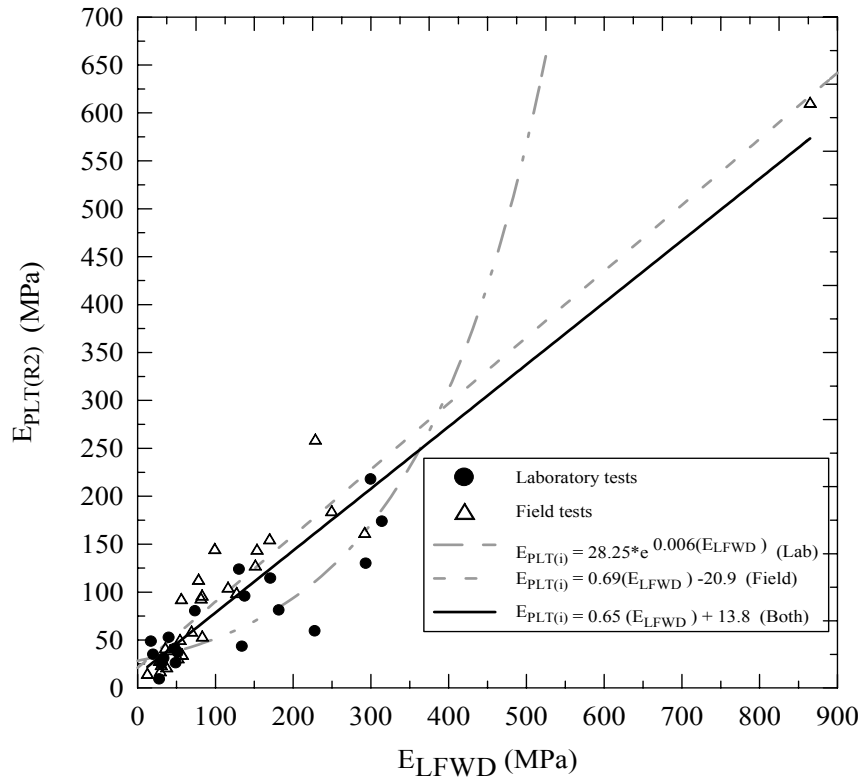


Figure 79

Comparison between laboratory and field for $E_{LFWD} - E_{PLT(R2)}$ correlation

LFWD versus FWD Correlation. The results of the regression analysis have shown that the best model to predict the FWD back-calculated resilient moduli, M_{FWD} , in (MPa) from the LFWD modulus, E_{LFWD} , in (MPa) is as follows:

$$M_{FWD} = 0.97 (E_{LFWD}) \quad (R^2=0.94) \quad (41)$$

The results of the FWD-LFWD correlation are presented in figure 80. The figure also compares the suggested FWD-LFWD prediction model to that proposed by Fleming et al. [24]. The suggested model is comparable to that proposed by Fleming et al. [24].

LFWD versus California Bearing Ratio. The LFWD dynamic modulus values are compared with *CBR* values in figure 81. There is no clear correlation between the LFWD dynamic modulus and the *CBR* (%), with wide scatter in the data as shown in this figure. As shown in equation 42, the suggested correlation is a log-log relation with a low R^2 value, which follows the trend more closely than the alternative correlations.

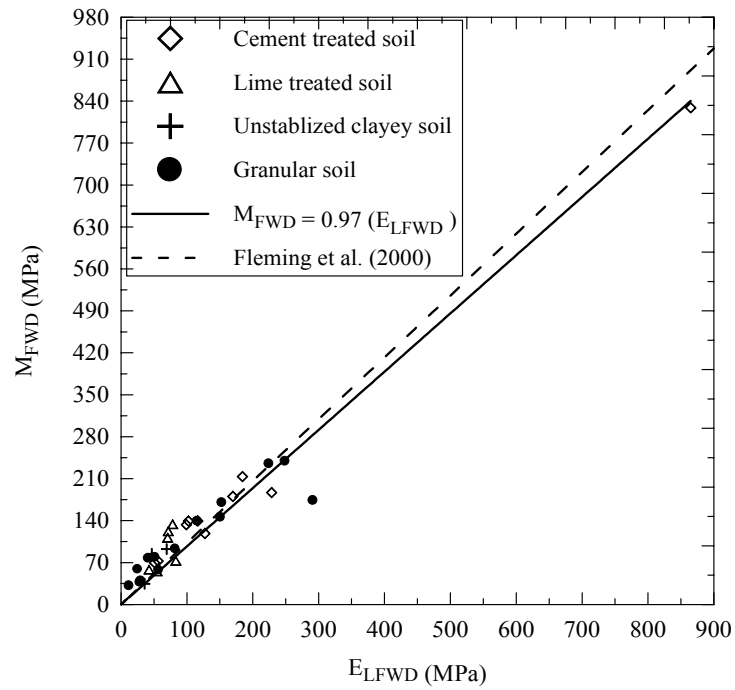


Figure 80

M_{FWD} versus E_{LFWD} correlation, and comparison to Fleming et al. [24]

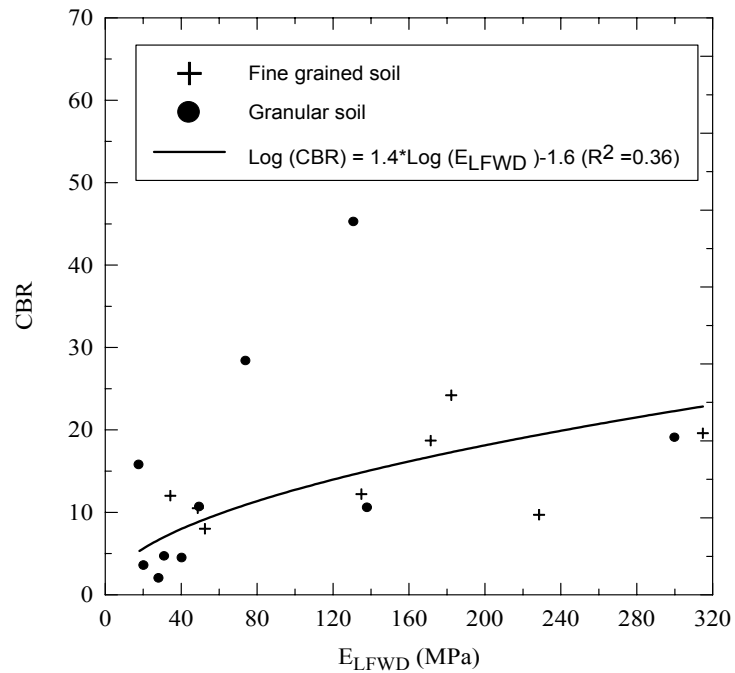


Figure 81

Correlation between (E_{LFWD}) and CBR (%) (laboratory test)

$$\text{Log}(E_{LFWD}) = 1.149 + 0.702 \log(CBR) \quad (R^2 = 0.36) \quad (42)$$

A regression analysis was also performed on field data to find the best correlation between the CBR values and E_{LFWD} . The analysis yielded the regression model shown in equation 43. Figure 82 presents the results of this correlation.

$$CBR = -14.0 + 0.66 (E_{LFWD}) \quad (R^2 = 0.83) \quad (43)$$

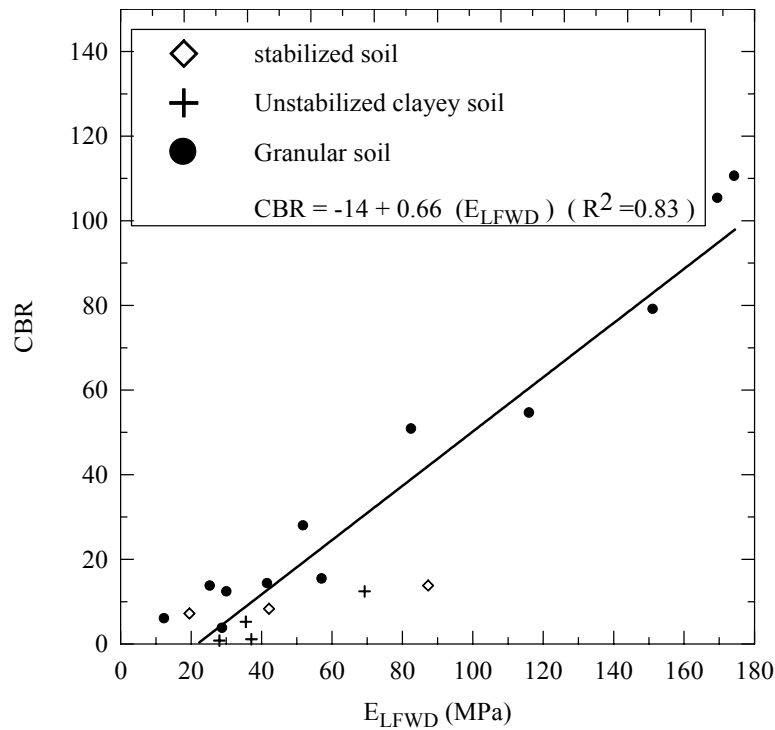


Figure 82

Correlation between (E_{LFWD}) and CBR (%) (field test)

DCP Correlations

DCP versus Plate Load Test. Several correlations between the average DCP penetration rate versus the PLT initial and reloading moduli ($E_{PLT(i)}$, $E_{PLT(R2)}$) were investigated. The DCP has already proven to be an effective tool for in-situ strength evaluation. A strong correlation between the DCP and the PLT will enhance the credibility of both devices. The average DCP penetration rates for the top 12 in. depth were used to investigate a possible relation between the DCP penetration rates and the moduli obtained from PLT, ($E_{PLT(i)}$, $E_{PLT(R2)}$). The best correlation

between the average DCP penetration rates and $E_{PLT(i)}$ is presented in figure 83 (equation 44). Figure 84 shows that there is a better correlation (equation 45) between the average DCP penetration rates and the PLT reloading modulus ($E_{PLT(R2)}$) compared to the correlation with $E_{PLT(i)}$.

$$E_{PLT(i)} = 7000 / (6.1 + PR^{1.5}) \quad (R^2 = 0.62) \quad (44)$$

$$E_{PLT(R2)} = 2460 * PR^{-1.285} \quad (R^2 = 0.77) \quad (45)$$

A correlation was also made between the DCP-PR (mm/blow) and both the $E_{PLT(i)}$ and $E_{PLT(R2)}$ in (MPa) for the data collected in the field. The results of the regression analysis yielded the following non-linear regression models:

$$E_{PLT(i)} = \frac{17421.2}{(PR)^{2.05} + 62.53} - 5.71 \quad (R^2 = 0.94) \quad (46)$$

$$E_{PLT(R2)} = \frac{5142.61}{(PR)^{1.57} - 14.8} - 3.49 \quad (R^2 = 0.95) \quad (47)$$

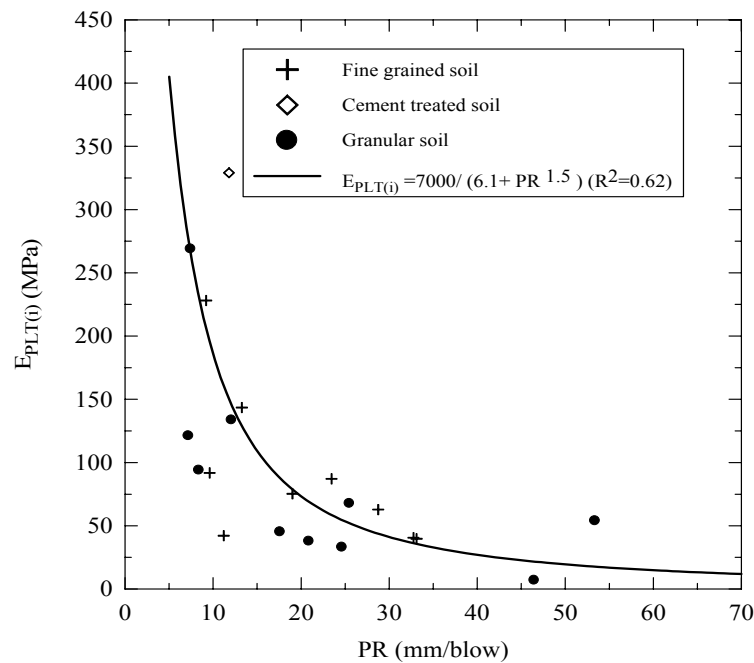


Figure 83

Correlation between DCP- PR and $E_{PLT(i)}$ (laboratory test)

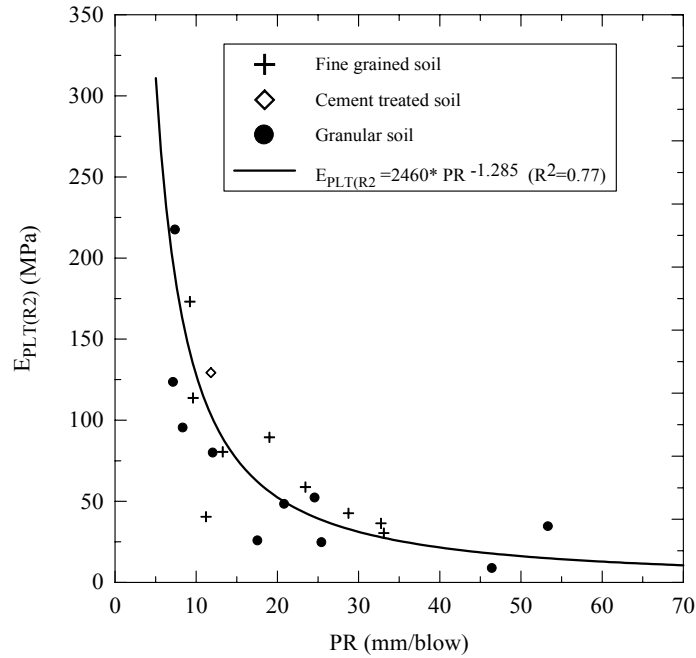


Figure 84

Correlation between DCP- PR and $E_{PLT(R2)}$ (laboratory test)

The results of these correlations are illustrated in figures 85 and 86. Comparison between the DCP- E_{PLT} relations proposed in equations 46 and 47 and the work done by Konard and Lachance is also presented in the figures [22]. These figures show that the correlations suggested by Konard and Lachance are very close to those suggested in this study at DCP- PR values less than 10 mm/blow [22].

Correlation was also made between the DCP- PR (mm/blow) and both the $E_{PLT(i)}$ and $E_{PLT(R2)}$ in (MPa) for the data collected from field and laboratory tests. The results of the regression analysis yielded the following non-linear regression models:

$$E_{PLT(i)} = \frac{9770}{(PR)^{1.6} + 36.9} - 0.75 \quad (R^2 = 0.67) \quad (48)$$

$$E_{PLT(R2)} = \frac{4374.5}{(PR)^{1.4} + 14.9} - 2.16 \quad (R^2 = 0.78) \quad (49)$$

The results of these correlations are illustrated in figures 87 and 88. Since the models obtained from the combined data lied between the laboratory and field models. These models are considered to be reliable and they will be adopted in this report.

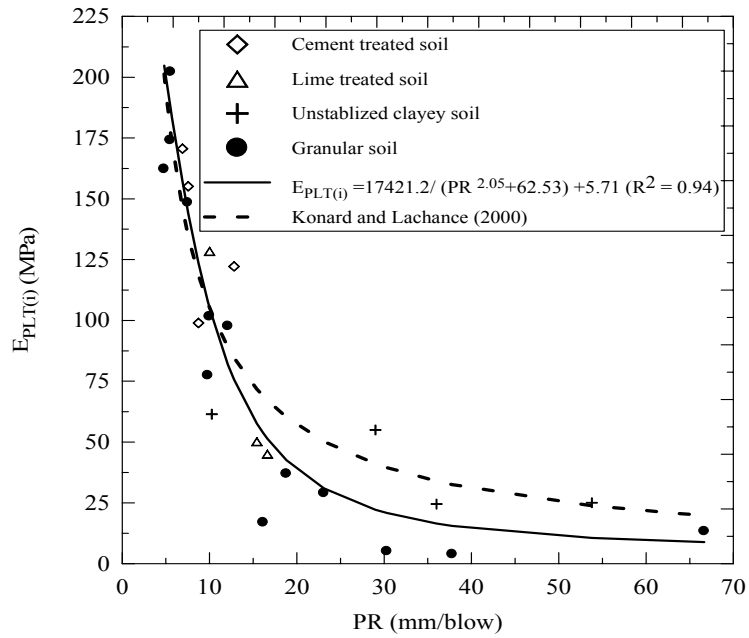


Figure 85

Correlation between DCP- PR and $E_{PLT(i)}$ (field test)

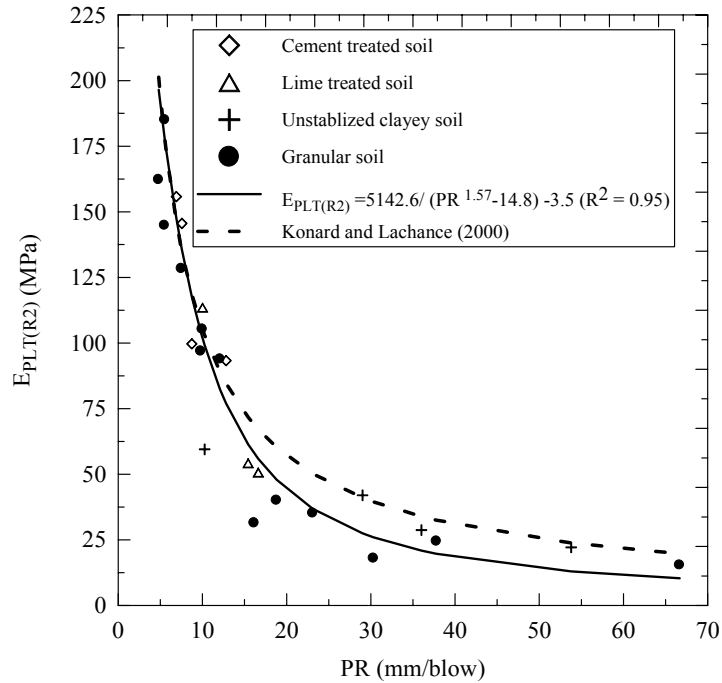


Figure 86

Correlation between DCP- PR and $E_{PLT(R2)}$ (field test)

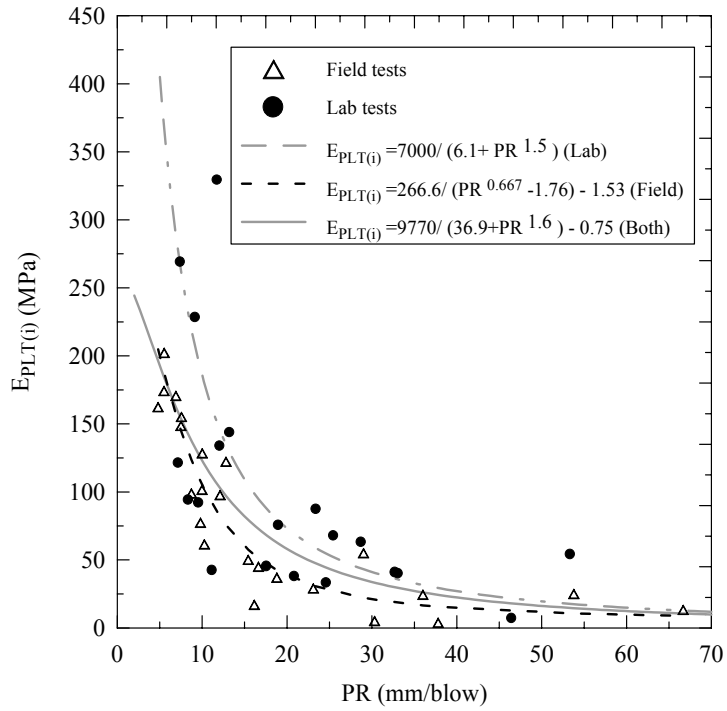


Figure 87

Comparison between laboratory and field for DCP-PR - $E_{PLT(i)}$ correlation

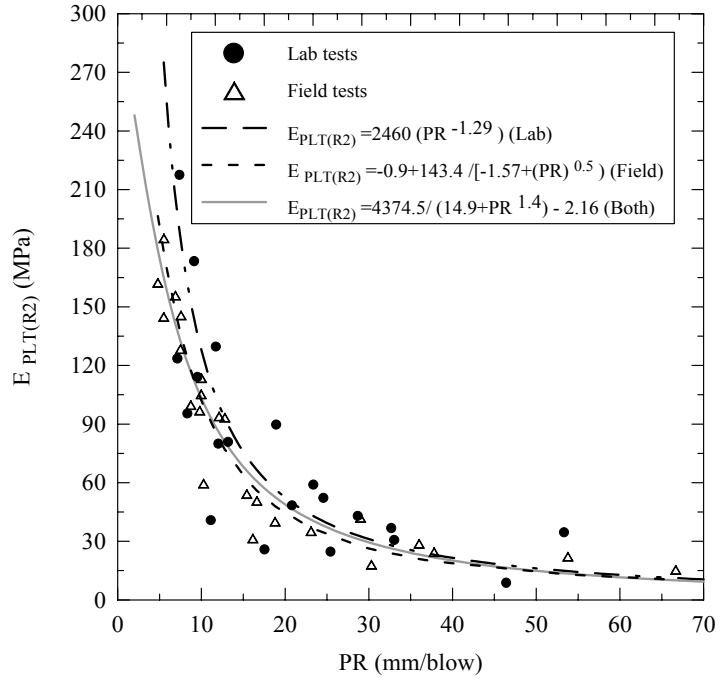


Figure 88

Comparison between laboratory and field for DCP-PR - $E_{PLT(R2)}$ correlation

DCP versus FWD. The regression analysis, which was conducted to find the best correlation between the M_{FWD} in (MPa) and the DCP- PR in (mm/blow), yielded a non-linear regression model presented in equation 50. The regression model is also presented in figure 89.

$$\ln(M_{FWD}) = 2.35 + \frac{5.21}{\ln(PR)} \quad (R^2=0.91) \quad (50)$$

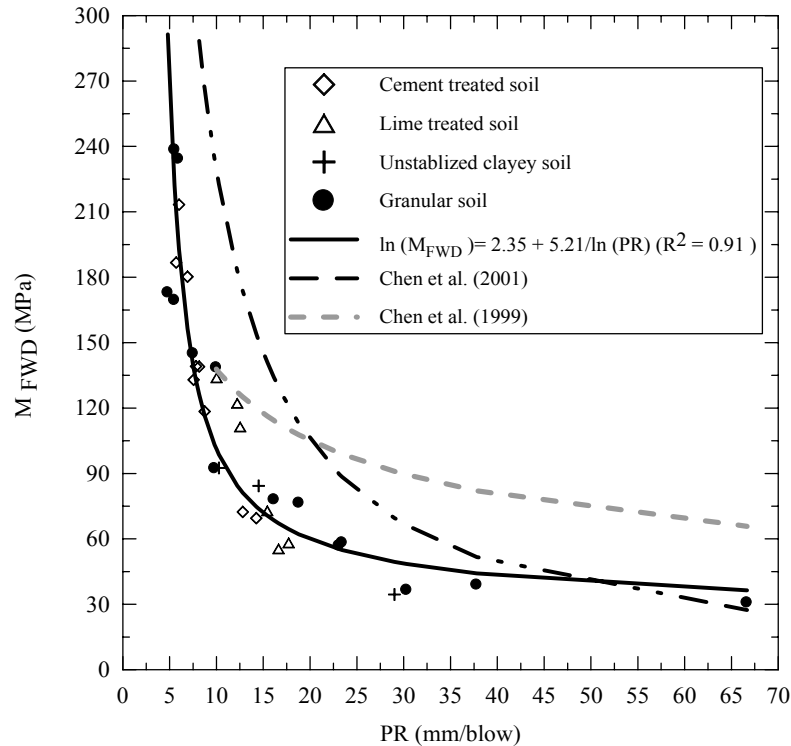


Figure 89
Correlation between DCP- PR and M_{FWD}

The DCP-FWD correlation obtained in this study was compared to those suggested by Chen et al. [8] using equation 11 [13] to compute CBR and then using equation 13 to compute FWD modulus, as shown in figure 89.

The figure also shows a comparison to the correlation suggested by Chen et al. [20]. It should be noted here that the Chen et al. correlation was suggested only for the range of $10 < PR < 60$ mm/blow [20]. As seen in figure 89, the proposed equation in this study has a better correlation with the measured data than that suggested by Chen et al. [20] and Chen et al [8].

DCP versus CBR. As mentioned earlier, the DCP penetration rate can be converted to an equivalent *CBR* value for use as a measure of stability and strength. The use of DCP tests to predict the *CBR* is preferred because it is simple and inexpensive and it enables rapid measurements of the in-situ strength of pavement layers and subgrades. Several correlations developed between the DCP penetration rates and *CBR* values are available in literature. One of the objectives of this research was to enhance the level of confidence of the DCP's usage for *CBR* determination. The average DCP penetration rates of the top 12 in. depth were used to investigate the possible correlation between the DCP penetration rate and *CBR* value. As shown in figure 90, the best fit between the DCP penetration rate and *CBR* value is a log-log correlation, which is similar to the ones available in the literature:

$$\text{Log } CBR = 2.256 - 0.954 \log PR \quad (R^2 = 0.56) \quad (51)$$

A regression analysis was performed to correlate the *CBR* and the DCP-PR obtained from field tests. The following non-linear regression model was obtained:

$$CBR = \frac{5.1}{PR^{0.2} - 1.41} \quad (R^2 = 0.93) \quad (52)$$

The results are presented in figure 91. The model obtained from the combined field and laboratory data (figure 92) lied between the lab and field model. However, figure 92 shows that field models are better than the other two models. Thus, the field models will be adopted.

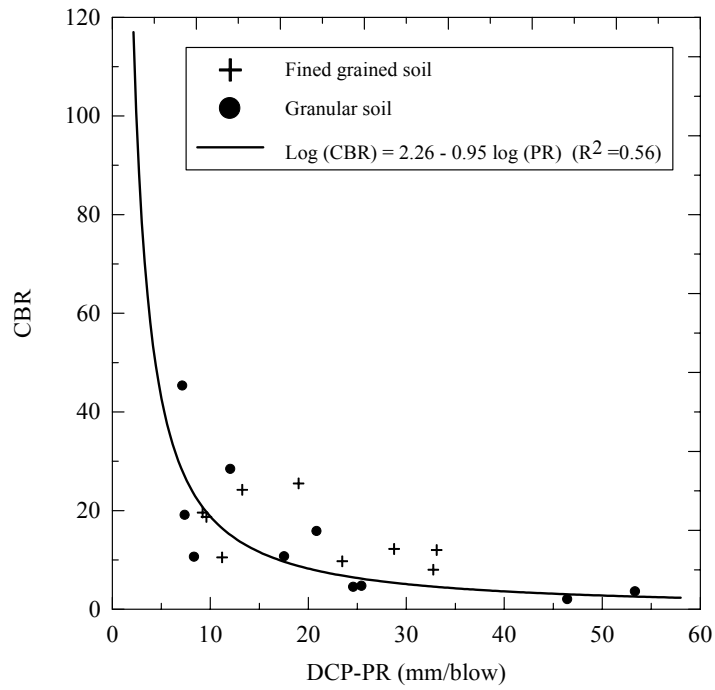


Figure 90

Correlation between DCP- PR and CBR (laboratory test)

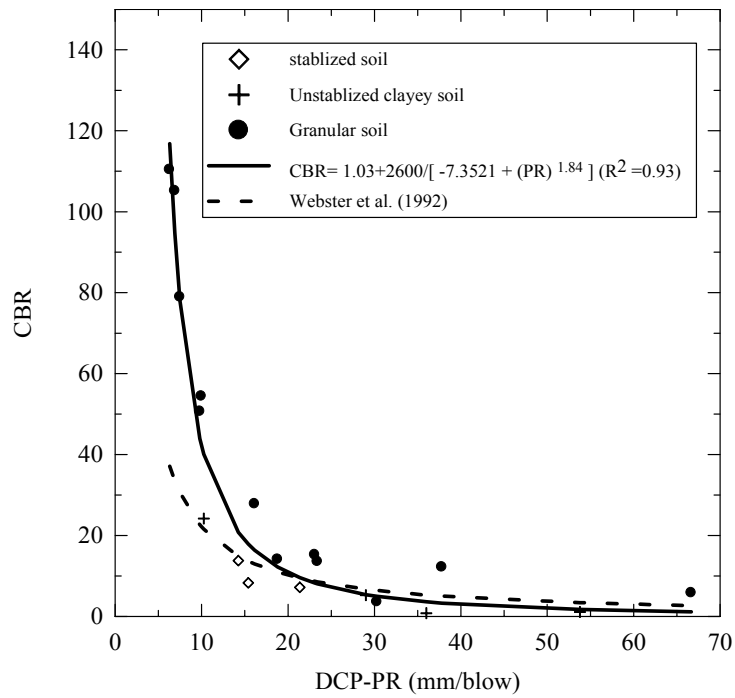


Figure 91

Correlation between DCP- PR and CBR (field test)

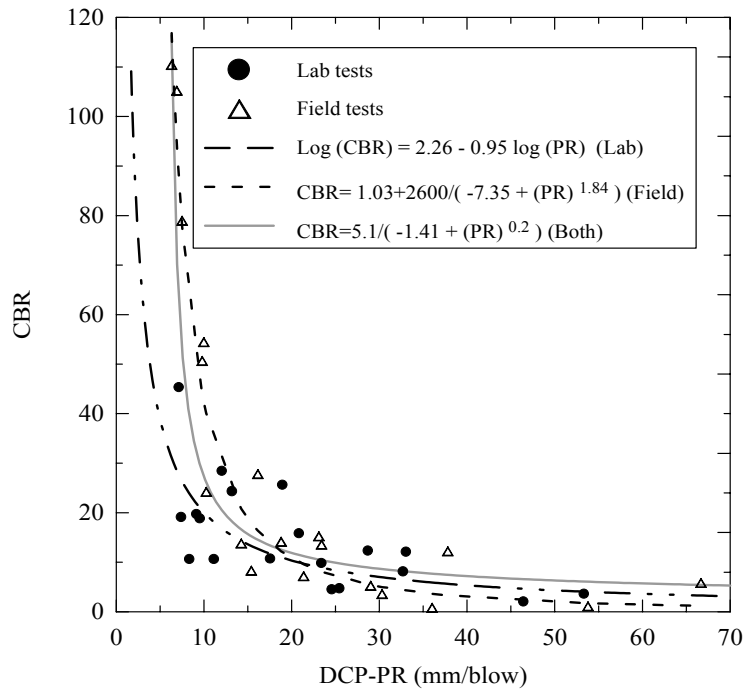


Figure 92

Comparison between laboratory and field for DCP-PR- $E_{PLT(R2)}$ correlation

CONCLUSIONS

The results of the statistical analyses indicated that there are good correlations between the measurements of the investigated devices (Geogauge, DCP, and LFWD) and the results of standard tests (FWD, PLT, and CBR). The relations obtained from statistical analyses were linear for some models and non-linear for other models, depending on the test and whether it was conducted in the laboratory or the field. However, the field test data in general showed better correlations than the laboratory test data in which the coefficient of determination (R^2) ranged from 0.81 to 0.95. The R^2 for the laboratory correlations ranged from 0.36 to 0.9. The high variation in the laboratory results was mainly due to the difficulties associated with the preparation of test layers inside the laboratory test boxes and the possibility of getting a non-homogenous layer due to inconsistency in compaction. Therefore, in most cases, the field-based correlations are recommended.

Geogauge

The main advantage of the Geogauge device is its size and compact design. It is very easy to operate, and it can give rapid results. The Geogauge is durable and has a long battery life. With these properties, it is the most user-friendly tool among the three devices. Good correlations were obtained between the Geogauge stiffness modulus, E_G , and the FWD back-calculated resilient modulus (M_{FWD}), the initial and reloading PLT moduli, ($E_{PLT(i)}$, $E_{PLT(R)}$) and the CBR values, especially for field test data. The results of laboratory tests showed more scatter and have lower correlation coefficients than the field tests. The coefficient of determination (R^2) for field tests ranged from 0.81 to 0.90; it ranged from 0.52 (with CBR) to 0.83 for laboratory tests. The Geogauge tests were also found to be more repeatable for field tests than laboratory tests, since the coefficient of variations (CV) for the Geogauge ranged from 0.2 percent to 11.38 percent for field tests and from 2.3 percent to 38.8 percent for laboratory tests.

Tests conducted on cement-treated and lime-treated soils showed that the Geogauge measurements are very sensitive to the presence of minor shrinkage cracks that might develop with time close to the surface of the layer. Therefore, when using the Geogauge, careful consideration must be given to measure the stiffness of cement-treated and lime-treated layers. Moreover, it was also noticed that Geogauge stiffness measurements are very sensitive to the moisture content and can give zero stiffness at high moisture content (m.c.), as can be seen in figure 42 at m.c. = 24 percent.

The results of the laboratory parametric study showed that the Geogauge influence depth ranged between 7.5 and 8.0 in. (190 to 200 mm). So this device is suitable for in-situ evaluation of the stiffness of pavement layers, since these layers are usually constructed in lifts of 6 to 12 in. each. These measurements can be used as input parameters in the mechanistic design method.

The results of the parametric study also indicated that for cohesive soils, the dry unit weight and stiffness modulus did not peak simultaneously, in fact, the Geogauge stiffness modulus peaked dry of optimum. This result suggests that compaction of these soils should be on the dry side of optimum to provide higher support and stability. However, while this conclusion might be appropriate immediately after compaction, it neglects the fact that any moisture gain after compaction can significantly decrease the stiffness and strength of moisture-sensitive soils.

LFWD

The LFWD is a convenient in-situ testing device compared to the regular FWD. However, it is not as handy as the Geogauge or the DCP. The LFWD as well as the DCP showed better correlations than the results of Geogauge correlations. Good correlations were obtained from both the field and laboratory tests, with the exception of the laboratory test data with CBR. The coefficient of determination (R^2) for field tests ranged from 0.83 to 0.94. The LFWD modulus (E_{LFWD}) was found to be very close to the FWD back-calculated resilient modulus (M_{FWD}) with a correlation ratio of 0.97 ($M_{FWD} = 0.97 E_{LFWD}$) and R^2 equal to 0.94. This correlation is close to the relation between FWD and LFWD suggested by Fleming et al. [24]. The results of this report suggest that the LFWD can serve as an alternative to the static plate load test and FWD. The developed LFWD correlations with the two devices increase the credibility of the LFWD in this sense. However, because the LFWD did have some limitations when testing weak subgrade layers, its repeatability could be reduced significantly.

The results of the laboratory parametric study results showed that the influence depth of the LFWD ranged between 10.5 and 11.0 in. (267 and 280 mm), depending on the stiffness of the tested materials. This suggests that the influence depth of the LFWD may reach beyond any tested pavement layer with a thickness less than 11.0 in. (280 mm). As a result, it is suggested that future LFWD tests should include the use of the more than one sensor in order to back calculate the true modulus of the tested layer.

Dynamic Cone Penetrometer

The DCP has a longer history and is more credible compared to both the Geogauge and LFWD devices. The device requires no electronics; it is durable, portable, and easy to operate. Some states are already using the device for different applications.

This study showed that the DCP had the most consistent results within the different layers. It is an effective tool to identify different layers when the PR (mm/blow) is plotted versus the penetration depth. Another advantage of the DCP is that it can take deeper measurements than the Geogauge and the LFWD. The DCP readings are not affected by minor shrinkage cracks associated with cement and lime-treated soils. Several good correlations were developed between the DCP - PR with the FWD, PLT, and CBR. The proposed DCP-PLT relations were compatible with the relation suggested by Konard and Lachance [22]. The results of this study showed that the DCP had better correlation with CBR than the other two devices ($R^2 = 0.93$ for field tests), which then can be used to estimate the resilient modulus of the tested material. Therefore, the DCP penetration can be used to profile the in-situ CBR values and/or the modulus for the different pavement layers and subgrades to the depth of penetration. Alternatively, the stiffness of materials can be represented by DCP penetration rates directly.

The results of this study indicated that the Geogauge, DCP, and LFWD can reliably predict the moduli obtained from PLT, FWD, and CBR values, and thus can be used to evaluate the in-situ stiffness characteristics of compacted soils, subgrades, base layers, and embankments for design purposes. However, it is too early to use these devices in the Q_C/Q_A procedures during the construction of compacted materials since the concept of using stiffness as acceptance criteria is not yet established. The stiffness of a compacted layer is sensitive to the moisture content during compaction, drying of the material, and strength gain with time for cement-treated and lime-treated soils. The current construction procedure requires compaction at the optimum moisture content ± 2 percent as obtained from laboratory standard Proctor tests. However, the results of this study indicated that the variation of stiffness within this range was greater than the variation in the dry density.

RECOMMENDATIONS

- This study showed that the Geogauge, LFWD, and DCP devices can reliably measure the in-situ stiffness modulus of base layers, subgrades, and embankments. Therefore, it is recommended to start implementing the stiffness measurements of these devices for mechanistic pavement design methods.
- At this time it is recommended to start implementing the DCP device in the quality acceptance of materials not sensitive to moisture content, particularly stone bases, with an acceptance criterion of PR < 10 mm/blow.
- Field measurements should be conducted using the investigated devices (particularly the DCP) along with dry density/water content measurements using the nuclear density gauge. These tests should include different types of materials with a wide stiffness moduli range. It is recommended to continue the comparison between the measurements of these devices and other in-situ measurements, such as the FWD, to verify the developed models and to gain enough confidence. This will ensure smooth statewide implementation of these devices.
- It is recommended to investigate the effect of moisture content variation on the stiffness measurements obtained by the Geogauge and LFWD and on the DCP penetration rates. This investigation should include laboratory and field tests to establish moisture-density and strength/stiffness relationships for materials expected to be used for construction.
- Future research should investigate the use of the Geogauge to evaluate lime and cement-treated compacted soil, and the effects of shrinkage cracks on the Geogauge's measurement.

REFERENCES

1. Fiedler, S.; Nelson, C.; Berkman, F.; and DiMillio, A. "Soil Stiffness Gauge for Soil Compaction Control." *Public Road Magazine*, Vol. 61, No. 5, April 1998, pp.5-11.
2. Lenke, L. R.; McKeen, R. G.; and Grush, M. P. "Laboratory Evaluation of Geogauge for Compaction Control." *Transportation Research Board 1849*, TRB, National Research Council, Washington, D.C., 2003, pp.20- 30.
3. Chen; D. H.; Wu, W.; He, R.; Bilyeu, J.; and Arrelano, M. *Evaluation of In situ Resilient Modulus Testing Techniques*. Texas DOTD Report, Austin, TX, 2000.
4. Huang, Yang H. *Pavement Analysis and Design*. Prentice Hall, New Jersey, 1993.
5. Chen, D. H.; Bilyeu,J.; and He , R. "Comparison of Resilient Moduli between Field and Laboratory Testing." *78th Annual Meeting of the Transportation Research Board*, Washington, D.C, January 1999.
6. Petersen, L.; Peterson, R.; and Nelson, C. "Comparison of Quasi-Static Plate Load Tests with the Humboldt Geogauge," CNA Consulting Engineers Report, 2002.
7. Kleyn, E. G. "The Use of the Dynamic Cone Penetrometer (DCP)," Report 2/74. Transvaal Roads Department, Pretoria, 1975.
8. Chen, D. H., Wang, J. N., Bilyeu, J. "Application of the DCP in Evaluation of Base and Subgrade Layers." *80th Annual Meeting of Transportation Research Board*, Washington, D.C, January 2001.
9. Livneh, M., "Validation of Correlations between a Number of Penetration Tests and In Situ California Bearing Ratio Tests," *TRRL 1219*, 1989.
10. Livneh, M., and I. Ishai. "Pavement and Material Evaluation by a Dynamic Cone Penetrometer." *Proc., Sixth International Conference on the Structural Design of Asphalt Pavement*, 1987, Vol. 1, Ann Arbor, Michigan , pp. 665-674.
11. Smith, R. B., and Pratt, D. N. "A Field Study of In Situ California Bearing Ratio and Dynamic Cone Penetrometer Testing for Road Subgrade Investigation." *Australian Road Research*, Vol. 13, No. 4, 1983, pp. 285-293.
12. Harrison, J.A. "Correlation of CBR and Dynamic Cone Penetrometer Strength Measurement of Soils." *Australian Road Research*, Vol. 16, No.2, 1986, pp130-136.
13. Webster, S.L.; Grau, R.H.; and Williams, R.P. *Description and Application of Dual Mass Dynamic Cone Penetrometer*. U.S. Army Engineer Waterways Experiment Station, Instruction Report, No. GL-92-3, 1992.

14. Livneh, M.; Ishai, I.; and Livneh, N. "Effect of Vertical Confinement on Dynamic Cone Penetrometer Strength Values in Pavement and Subgrade Evaluations." *Transportation Research Record 1473*, TRB, National Research Council, Washington, DC, 1995, pp. 1-8.
15. Siekmeier, J.A.; Young, D.; and Beberg, D. "Comparison of the Dynamic Cone Penetrometer with Other Tests During subgrade and Granular Base Characterization in Minnesota." *Nondestructive Testing of Pavements and Backcalculation of Moduli: Third Volume*, ASTM STP 1375, p175-188. S.D. Tayabji and E.O. Lukanen, Eds., American Society for Testing and Materials, 2000.
16. Heukelom, W., and Klomp, A.J.G. "Dynamic Testing as Means of Controlling Pavements During and After Construction." *Proceedings of the First International Conference on Structural Design of Asphalt Pavement*, University of Michigan, 1962.
17. Powell, W. D., Potter, J. F., Mayhew, H. C., and Nunn, M. E., "The Structural Design of Bituminous Roads," TRRL Report LR 1132, 1984, pp. 62.
18. Pen, C. K. "An Assessment of the Available Methods of Analysis for Estimating the Elastic Moduli of Road Pavements." *Proceeding of Third Int. Conf. on Bearing Capacity of Roads and Airfields*, Trondheim, 1990.
19. Chua, K. M., and Lytton, R. L. "Dynamic Analysis Using the Portable Dynamic Cone Penetrometer." *Transportation Research Record 1192*, TRB, National Research Council, Washington, DC, 1981, pp. 702-708.
20. Chen, J.; Hossain, M.; and LaTorella, T. "Use of Falling Weight Deflectometer and Dynamic Cone Penetrometer in Pavement Evaluation." *Transportation Research Record 1655*, TRB, National Research Council, Washington, DC, 1995, pp. 145-151.
21. De Beer, M., "Use of Dynamic Cone Penetrometer (DCP) in the Design of Road Structures." *Geotechnics in African Environment*, Blight et al. (Eds), Balkema, Rotterdam, 1990.
22. Konard, J-M., and Lachance, D. "Mechanical Properties of Unbound Aggregates from DCP and Plate Load Tests." *Proceedings of the Fifth International Conference on Unbound Aggregate in Roads*, Nottingham, United Kingdom, 2000.
23. Burnham, T. "Application of the Dynamic Cone Penetrometer to Mn/DOT's Pavement Assessment Procedures. Revised draft Report," Office of Minnesota Road Research, 1996.

24. Fleming, P.R.; Frost, M. W.; and Rogers, C.D.F. "A Comparison of Devices for Measuring Stiffness In- situ." *Proceedings of the Fifth International Conference on Unbound Aggregate In Roads*, Nottingham, United Kingdom, 2000.
25. Livneh, M, and Goldberg, Y. "Quality Assessment during Road Formation and Foundation Construction: Use of Falling-Weight Deflectometer and Light Drop Weight." *Transportation Research Record 1755*, TRB, National Research Council, Washington, DC, 2001, pp 69-77.
26. Fleming, P.R.; Rogers, C.D.F.; and Frost, M.W. "Performance Parameters and Target Values for Construction of UK Road Foundations." *Proceedings of the Fifth International Conference on Bearing Capacity of Roads and Airfields*, Vol. 3, Trondheim, Norway, 1988.
27. Fleming, P.R. "Field Measurement of Stiffness Modulus for Pavement Foundations." *79th Annual Meeting of the Transportation Research Board*, Washington, DC, January 2001.
28. Kamiura, M.; Sekine, E.; Abe, N.; and Meruyama, T. (2000), "Stiffness Evaluation of the Subgrade and Granular Aggregate Using the Portable FWD." *Proceedings of the Fifth International Conference on Unbound Aggregate in Roads*, Nottingham, United Kingdom, 2000.
29. Dynatest Engineering, *Dynatest 8000 FWD Test System owner's Manual*, 1995.
30. U.S. Department of Transportation FHWA. "Pavement Deflection Analysis Participant Workbook." NHI Course No. 13127.
31. Gurr, C.; Groenendijk, J.; and Beuving, E., "Experience with Various Types of Foundation Tests." *Proceedings of the Fifth International Conference on Unbound Aggregate in Roads*, Nottingham, United Kingdom, 2000.
32. Zaghoul, S.M., and Saeed, N.S. "The Use of the Falling Weight Deflectometer in Asphalt Pavement Quality Control, Quality Management of Hot-Mix Asphalt." *ASTM STP 1299*, D.S. Decker, Ed., American Society for Testing and Materials, West Conshohocken, PA, 1996.
33. Rogers, C.D.F; Fleming, P.R.; and Frost, M. W. "Stiffness Behavior of Trial Road Foundations." *Proceedings of the Fifth International Conference on Unbound Aggregate In Roads*, Nottingham, United Kingdom, 2000.
34. Holtz, R.D., and Kovacs, W.D. (1981), *An Introduction to Geotechnical Engineering*, Prentice-Hall, Englewood Cliffs, New Jersey.

35. American Society of Testing and Materials. D1195-93, "Standard Test Method for Repetitive Static Plate Load Tests of Soils and Flexible Pavement Components , for use in Evaluation and Design of Airport and Highway Pavements." *Annual Book of ASTM Standards*, Vol. 04.08, pp. 110-113, 1998.
36. Horhota, D. "Evaluation of the Spectral Analysis of Surface Waves (SAWS) Test Method For Florida Department Of Transportation (FDOT) Applications," Dissertation submitted to the University of Florida, 1996.
37. Odemark "Investigations as to the Elastic Properties of Soils and Design of Pavements according to the Theory of Elasticity." *Statens Väginstitut, Mitteilug* No. 77, Stockholm, 1949.
38. Yoder, E. J., and Witzak, M. W., *Principles of Pavement Design*, 2nd ed., John Wiley & Sons, New York, 1975.
39. American Society of Testing and Materials. D1883-94. "Standard Test Method for CBR (California Bearing Ratio) of Laboratory-Compacted Soils." *Annual Book of ASTM Standards*, Vol. 04.08, pp. 159-167, 1998.
40. Lambe, T. W., and Whitman, R. V., *Soil Mechanics*, Wiley, New York, USA, 1969.
41. Louisiana Office of State Climatology rainfall record for Baton Rouge station, <http://www.losc.lsu.edu/stations.php?Id=btr>, 2003.
42. Humboldt. "Fourth Validation Test of Geogauge Seating Procedure," Test Report, Humboldt Mfg. Co., 2002.
43. Sawangsuriya, A.; Edil, T.; and Bosscher, P. "Relationship between Soil Stiffness Gauge Modulus and Other Test Moduli for Granular Soils." *Transportation Research Record 1808*, TRB, National Research Council, Washington, D.C., 2002, pp.3- 10.

APPENDIX

Geogauge Principle of Operation

The Geogauge's principle of operation is to generate a very small dynamic force at frequencies of 100 to 196 Hz. In a laboratory study, Sawangsuriya et al. estimated the force generated by the Geogauge to be 9 N [43]. The Geogauge operation includes generating a very small displacement to the soil, which is less than 1.27×10^{-6} m (0.0005 in.), at 25 steady state frequencies between 100 and 196 Hz. The stiffness is determined at each frequency and the average is displayed. The entire process takes about one and one-half minutes. Powered by a set of 6 D-cell batteries, the Geogauge is designed so that the deflection produced from equipment operating nearby will not affect its measurements, since the frequency generated by traffic (at highway speed) is approximately 30 Hz, which is below the Geogauge operating frequency (Humboldt Mfg. Co. 1999, Geogauge guide).

The force applied by the shaker and transferred to the ground is measured by differential displacement across the flexible plate by two velocity sensors (figure A1). This can be expressed as follows

$$F_{dr} = K_{flex}(X_2 - X_1) = K_{flex}(V_2 - V_1) \quad (A1)$$

Where:

F_{dr} = force applied by shaker

K_{flex} = stiffness of the flexible plane

X_1 = displacement at rigid plate

X_2 = displacement at flexible plate

V_1 = velocity at rigid plate

V_2 = velocity at flexible plate

At frequencies of operation, the ground-input impedance will be dominantly stiffness controlled:

$$K_{soil} = \frac{F_{dr}}{X_1} \quad (A2)$$

Where

K_{soil} = stiffness of soil

Thus the soil stiffness can be calculated as:

$$\overline{K}_{soil} = K_{flex} \sum_1^n \left(\frac{(X_2 - X_1)}{X_1} \right) = K_{flex} \sum_1^n \left(\frac{(V_2 - V_1)}{V_1} \right) \quad (A3)$$

Where n is the number of test frequencies.

Using velocity measurements eliminates the need for a non-moving reference for the soil displacement and permits accurate measurement of small displacements. It is assumed that the Geogauge response is dominated by the stiffness of the underlying soil.

Based on finite element analysis and lab tests, Sawangsuriya et al. found that the Geogauge's depth of influence extends to 300 mm for loose sand [43]. However, if the sample to be tested is a multi-layered soil with different stiffness values, the Geogauge will measure the stiffness of an upper-layer of 125 mm or thicker. Depending on the relative stiffness of layer materials, the effect of the bottom layer can be present up to 275 mm. The same research indicates that the boundary effects become negligible for test boxes with widths greater than 0.6 m.

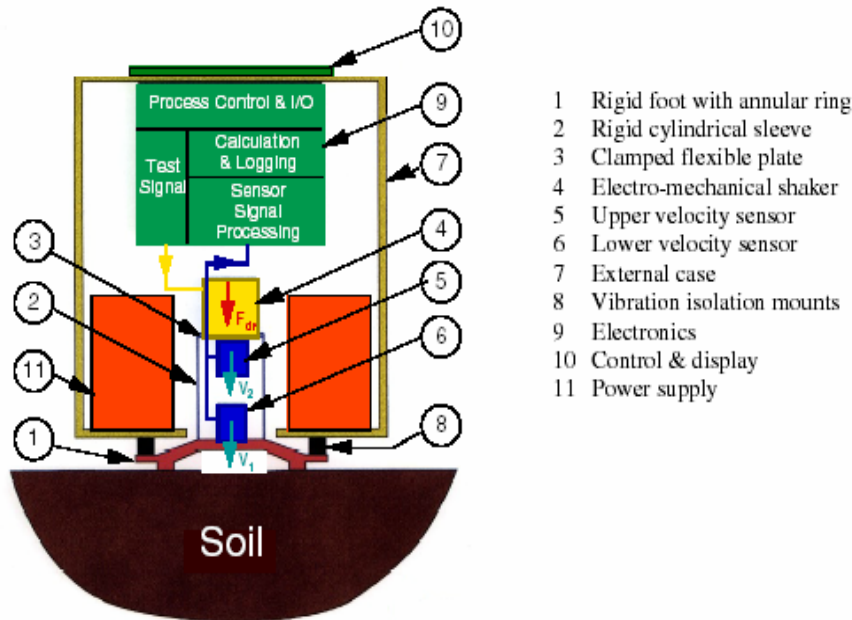


Figure A1
Schematic of the Geogauge (Humboldt, 1998)